A Chromatographic Study of
Carbon Monoxide Adsorption in Clinoptilolite

by
Güler NARİN

**A Dissertation Submitted to the
Graduate School in Partial Fulfillment of the
Requirements for the Degree of**

MASTER OF SCIENCE

**Department: Environmental Engineering
Major: Environmental Engineering
(Environmental Pollution and Control)**

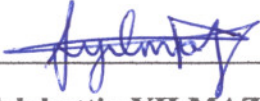**İzmir Institute of Technology
İzmir, Turkey**

January, 2001

We approve the thesis of **Güler NARİN.**

15.01.2001

Prof. Dr. Semra ÜLKÜ
Supervisor
Department of Chemical Engineering

15.01.2001

Asst. Prof. Dr. Selahattin YILMAZ
Co-Supervisor
Department of Chemical Engineering

15.01.2001

Prof. Dr. Devrim BALKÖSE
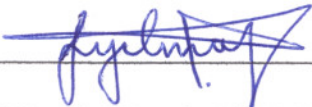Department of Chemical Engineering

15.01.2001

Prof. Dr. Muhsin ÇİFTÇİOĞLU
Department of Chemical Engineering

15.01.2001

Asst. Prof. Dr. Fehime ÖZKAN
Department of Chemical Engineering

15.01.2001

Asst. Prof. Dr. Selahattin YILMAZ
Head of Interdisciplinary
Environmental Engineering Program

ABSTRACT

Adsorption equilibrium and kinetic parameters for CO/clinoptilolite adsorbate/adsorbent pair were determined by perturbation gas chromatography. Chromatographic experiments were performed at temperatures in the 60-120°C range and at carrier gas flow rates in the range of 10.31-24.36 cm/sec. The chromatographic response peaks were obtained by concentration pulse method. A packed column of 10 cm length and 0.46 cm inlet diameter which was packed with clinoptilolite particles with narrow size distribution (500-850 μm) around mean diameter of 301.9 μm was used. The clinoptilolite particles were excavated from Gördes, Western Anatolia. The moments of the response peaks were calculated by integration of experimental chromatographic data and matched to the model parameters in order to determine the equilibrium constants and diffusion coefficients. The dynamic model (Haynes and Sarma, 1973) was applied to describe the adsorption and diffusion processes in the packed column. This model includes axial dispersion, external mass transfer resistance, micropore and mesopore diffusion resistances.

The equilibrium constants (Henry's law constants, K) were calculated in the range of 40 - 952 and were found to be in good agreement with the results in the literature. These constants were found to decrease with increasing temperature. The heats of adsorption were obtained in the range of 54.15 - 57.14 kJ/mol from the slope of van't Hoff plots and compared with those in the literature. The heats of adsorption were found to be lower than those reported in the literature obtained for the same adsorbate/adsorbent pair. The higher heats of adsorption were explained by the smaller pore size, higher cation content of the clinoptilolite and more accessibility of the cations in the clinoptilolite framework by CO molecules. Heats of adsorption remained almost constant over the carrier gas velocity range studied.

The contributions of axial dispersion and other mass transfer resistances in diffusion of CO in clinoptilolite were also determined. The total dispersion exhibited slight change (average 0.035 sec) with temperature implying that the micropore diffusional resistance was not dominant for diffusion of CO in clinoptilolite under the experimental conditions studied. The axial dispersion coefficient was determined in the range of 1.14-9.88 cm^2/sec and the total mass transfer resistances were found between 0.02-0.06 sec. The results showed that the mesopore diffusion resistance was the controlling mechanism in CO diffusion in clinoptilolite. Mesopore diffusion coefficient was estimated as 2.98x10^{-3} cm^2/sec. This value was in good agreement with the theoretically determined value.

ÖZ

Karbon monoksit/klinoptilolit adsorbat/adsorbent sistemi için adsorbsiyon denge ve kinetic parametreleri pertürbasyon gaz kromatografi yöntemi ile belirlenmiştir. Kromatografik deneyler 60-120°C sıcaklık ve 10.31-24.36 cm/sn taşıyıcı gaz hız aralığında gerçekleştirilmiştir. Kromatografik yanıt pikleri konsantrasyon atım (pulse) yöntemi ile elde edilmiştir. Çalışmada 10 cm uzunluğunda, 0.46 cm iç çaplı, 500-850 μm parçacık büyüklüğü dağılımı (ortalama çapları 301.9 μm) gösteren klinoptilolit parçacıkları ile doldurulmuş kolon kullanılmıştır. Klinoptilolit parçacıkları Batı Anadolu bölgesi, Gördes'teki zeolit yataklarından sağlanmıştır. Kromatografik yanıt piklerinin momentleri deneysel kromatografik verilerin entegrasyonu ile hesaplanmıştır ve adsorpsiyon denge ve kinetik parametrelerinin belirlenmesi için uygun dinamik modelle eşleştirilmiştir. Haynes ve Sarma'nın (1973) geliştirmiş olduğu dinamik model dolgulu kolondaki adsorbsiyon ve difüzyon olaylarının açıklamak için uygulanmıştır. Bu model eksensel yayılım, parçacık yüzeyi kütle taşınım direnci, mikrogözenek ve mezogözenek dirençlerini içermektedir.

Adsorpsiyon denge sabitleri (Henry Yasası sabitleri, K) 40-952 aralığında hesaplanmış ve literatürdeki değerlerle uygunluk gösterdiği görülmüştür. Bu sabitlerin artan sıcaklıkla azalmıştır. Adsorpsiyon ısı değerleri van't Hoff eğrilerinin eğimlerinden 54.15-57.14 kJ/mol aralığında bulunmuş ve bu değerler literatürdeki değerlerle karşılaştırılmıştır. Bu karşılaştırma sonucu bu çalışmada belirlenen adsorpsiyon ısı değerlerinin literatürdeki değerlerden daha yüksek olduğu görülmüş ve bu kullanılan klinoptilolitin daha küçük gözenek boyutuna sahip olmasına, daha fazla katyon içermesine ve katyonların karbon monoksit moleküllerince daha ulaşılabilir konumda bulunmalarıyla açıklanmıştır. Adsorpsiyon ısı değerleri çalışılan taşıyıcı gaz hızı aralığında sabit kalmıştır. Ayrıca karbon monoksitin klinoptilolit içindeki difüzyonunda etkili olan eksensel yayılım katsayısı ve diğer kütle taşınım dirençleri de belirlenmiştir. Toplam yayılımın sıcaklık ile fazla değişmemesi (ortalama 0.035 sn) çalışılan deneysel koşullarda mikrogözenek

direncinin karbon monoksitin klinoptilolit içinde difüzyonunda baskın mekanizma olmaması ile açıklanmıştır.

Toplam kütle transfer direncinin 0.02-0.06 sn, eksensel yayılım katsayısının 1,14-9,88 cm^2/sn aralığında değiştiği belirlenmiştir. Bu sonuçlar, çalışılan deneysel koşullarda mezogözenek direncinin karbon monoksitin klinoptilolit içindeki difüzyonunda etkin mekanizma olduğunu göstermiştir. Mezogözenek difüzyon katsayısı 2.98x10^{-3} cm^2/sn olarak bulunmuştur. Bu değer teorik olarak hesaplanan değerlerle uygunluk göstermektedir.

TABLE OF CONTENTS

LIST OF FIGURES

LIST OF TABLES

NOMENCLATURE

a_a	: Area occupied by a single adsorbate molecule
A	: Adsorption potential
A_s	: Surface area of the adsorbent
A_a	: Constant in Lennard-Jones potential for the adsorbent
A_{aa}	: Constant in Lennard-Jones potential for adsorbate
$B_c(q)$	: Mobility parameter.
$(Bi)_m$	: Biot number for mass transfer
$(Bi)_h$	: Biot number for heat transfer
c_o	: Initial sorbate concentration in the bulk phase
$c = c_1 + c_2$	: Total gas phase concentration
c_1	: Gas phase concentrations of component1
c_2	: Gas phase concentrations of component2
$c(t)$	: Gas phase concentration measured by the detector
$c = c(z,t)$	: Dynamic response of the column
Δc	: Concentration difference between the two faces of the pellet
C	: BET constant, related to the heat of adsorption for the first layer
d	: Diameter of the adsorbate molecule
$D_o(q)$	: Corrected intracrystalline diffusivity
$D(q)$	: Self-diffusivity
$D_c(q)$	: Intracrystalline diffusivity
D_c/r_c^2	: Micropore diffusional time constant
D_{eff}	: Effective diffusion coefficient in the porous adsorbent
D_K	: Knudsen diffusivity
D_L	: Axial disperison coefficient
D_m	: Molecular diffusivity
D_p	: Macropore diffusivity
D_p/R_p^2	: Macropore diffusional time constant

E_a	: Diffusional activation energy
f	: Dimensionless friction factor
h	: Overall heat transfer coefficient between adsorbent particle and fluid
H.E.T.P.	: Theoretical plate height
ΔH_o	: Limiting heat of adsorption (isosteric heat of adsorption) at low coverage
J	: Molar flux due to diffusive transport
k_B	: Boltzman constant
K	: Dimensionless Henry's law adsorption equilibrium constant
K_o	: Pre-exponential factor
l	: Slit width
L	: Column length
Δl	: Distance between the peak starting point and the peak maximum
m	: Mass of adsorbent in the column
m_n	: n^{th} moment of the response peak
M	: Molecular weight
N_a	: Number of atoms per unit area of adsorbent
N_{aa}	: Number of molecules per unit area of adsorbate
N_A	: Avogadro number
Nu	: Nusselt number
p	: Gas phase pressure.
p_1	: Partial pressure of component 1
p^*	: Critical condensation pressure
Δp	: Pressure drop across packed column
P	: Total pressure
p/p_o	: Relative pressure
q	: Concentration of the adsorbate in the porous zeolite medium
$\bar{q}$	: Adsorbed phase concentration averaged over a adsorbent particle
q^*	: Adsorbed sorbate concentration at equilibrium
dq_1/dc_1	: Slope of the isotherm
$\partial q/\partial x$	: Concentration gradient along the micropore distance x
$\partial q/\partial t$	: Local mass transfer rate averaged over an adsorbent particle

r_c	:	Crystal radius
R_p	:	Particle radius
$\bar{r}$	:	Mean macropore radius
r_m	:	Mean radius of curvature of the liquid meniscus
R	:	Universal gas constant
$RT \ln(p/p_O)$	:	Free energy change
Re	:	Reynolds number ($Re = 2\rho v_i \varepsilon R_p / \mu$)
Sc	:	Schmidt number ($Sc = \mu / \rho D_m$)
Sh	:	Sherwood number for packed columns
t	:	Film thickness on the pore walls
t_R	:	Mean retention time
t_p	:	Pellet thickness
$t_{R, packed}$	:	Experimentally determined first moment for the packed column
t_{empty}	:	Experimentally determined first moment for the empty column
T	:	Temperature
ΔU_o	:	Internal energy change of adsorption at low concentration
v_I	:	Interstitial velocity
V_r	:	Retention volume
Vg	:	Free gas volume
$V_{adsorbed}$	:	Adsorbed volume of the adsorbate
V_a	:	Amount adsorbed at the relative pressure p/p_o
V_m	:	Monolayer capacity
w_1	:	Specific adsorbed amount of component 1
w_2	:	Specific adsorbed amount of component 2
dw_1/dc_1	:	Slope of the individual isotherms at composition c_1
dw_2/dc_2	:	Slope of the individual isotherms at composition c_2
W	:	Quantity adsorbed at relative pressure p/p_o
W_o	:	Limiting micropore volume
X	:	Mole fraction of adsorbable component

Greek Symbols

β	: Effective molecular volume of sorbate (Å^3/ molecule)
γ	: Surface tension of the liquid condensate
$\varepsilon^{\prime}$	: Lennard-Jones force constant
κ	: Distance on the baseline between the points of tangents intersecting it
λ	: Mean free path of diffusing molecules
λ_g	: Thermal conductivity of gas phase
λ_s	: Thermal conductivity of solid
μ_o	: Standard state chemical potential
μ	: Net first moment
υ	: Volume of cavity of adsorbent (Å^3)
υ/β	: Ratio of cavity to molecular volume of the sorbate
ψ	: Affinity coefficient
σ^2	: Net second moment
σ_{ii}	: Collision diameter of the diffusing molecule
σ^2_{packed}	: Experimentally determined second moment for the packed column
σ^2_{empty}	: Experimentally determined second moment for the empty column
θ	: Contact angle between the adsorbent and condensed adsorptive
τ	: Tortuosity factor
ϖ	: Molar volume of the liquid condensate
ξ	: Distance from a surface atom at zero interaction energy

ACKNOWLEDGEMENTS

CHAPTER 1

INTRODUCTION

There are critical environmental problems associated with air pollution, including photochemical smog, acidic deposition, stratospheric ozone depletion and the most significant one the world has ever faced is the global climate change.

Global climate has warmed during the past 150 years and it was predicted that the earth's temperature will increase by about $0.9\text{-}3.5^\circ C$ by the year 2100 [2]. There is evidence that the atmospheric concentration of the greenhouse gases are increasing due to gases emitted from man's activities causing the earth's average temperature to increase. The main greenhouse gases are carbon dioxide (CO_2), methane (CH_4) and nitrous oxide (N_2O). Much of the anthropogenic impact on the atmosphere is associated with the use of fossil fuels as an energy source, for heating, transportation and electric power production.

Research on climate change focus on improvement of detection and prediction of climate change, the effects of climate change on the physical and biological environment, development of technologies and on reduction of greenhouse gas emissions. There is increasing international environmental concern regarding the control of gaseous pollutant emissions. Industry is being forced to develop economically feasible and effective methods to reduce the pollutant emissions to acceptable levels by environmental regulations.

Conventional air pollution control methods involve adsorption, absorption, condensation and combustion. Adsorption has advantages over other techniques such as low energy consumption and usefulness for low sorbate concentrations. It is based on preferential partitioning of adsorbate from the gaseous phase and accumulation on the adsorbent surface. Microporous solids are chosen as adsorbent to achieve high adsorptive capacities for economic viability. The most commonly used commercial adsorbents in gas separation and purification applications are carbon molecular sieves, activated carbons, silica, alumina, synthetic and natural zeolites.

1

Zeolites differ from the other traditional adsorbents. They have uniform pore size distributions in the range of 3-10 Å, depending on the type. These pores selectively adsorb or reject the molecule based on the relative size of the molecule and the pore. However, natural zeolites have not been examined in detail as molecular sieves due to their inconsistency of composition and purification cost. Special interest has been devoted to natural zeolites, especially on clinoptilolite in this study due to the large amount of reserves (2 billion tonnes) in the Western Anatolia region. The objective of this study is to determine the potential capacity of clinoptilolite for CO adsorption process.

The design of an effective adsorption separation process requires the determination of kinetic and equilibrium parameters for the adsorbate-adsorbent pair of interest. Adsorption equilibrium data characterizes adsorption capacity of the adsorbent which is dependent on the pressure, temperature, surface area and porosity of the adsorbent, and the nature of the adsorbate-adsorbent interactions. It gives information on how strongly the gas is adsorbed. Equilibrium data is also important for gas separation applications, since the separation factor is expressed as the ratio of Henry's Law constants for the components. Therefore, using pre-determined Henry Law constants, it is easy to select the suitable adsorbent for the specific separation process.

Most experimental studies on adsorption kinetics and equilibrium of zeolites are performed by volumetric or gravimetric method. Gas chromatography method is applicable for in a wider range of diffusivity. The concentration pulse chromatography method was used. This method involves the perturbation of the sorbate-free column that was initially brought to equilibrium with a flowing pure carrier gas by either a pulse of the pure adsorbate. Then, the detector output was monitored as a function of time. The analysis and interpretation of the experimental chromatographic data requires a mathematical model. The dynamic model developed by Haynes and Sarma (1973) offers the most suitable model to describe the diffusion and adsorption processes in a column packed with biporous adsorbent. The adsorption equilibrium and diffusion parameters can then be derived by matching the experimental parameters to the model parameters.

CHAPTER 2

AIR POLLUTION

Air pollution is an important problem for human health and the natural environment. It can be defined based on the concentration of pollutant gas in the environment. The composition of clean air used as a benchmark is given in Table 2.1.

Table 2.1. Concentration of atmospheric gases in clean air [1]

Component	Concentration (% by volume)
Nitrogen (N_2)	78.09
Oxygen (O_2)	20.95
Argon (Ar)	0.93
Carbon dioxide (CO_2)	0.032
Neon (Ne)	0.0018
Helium (He)	0.00052
Methane (CH_4)	0.00015
Krypton (Kr)	0.0001
Hydrogen (H_2)	0.00005
Dinitrogen oxide (N_2O)	0.00002
Carbon monoxide (CO)	0.00001
Xenon (Xe)	0.000008
Ozone (O_3)	0.000002
Ammonia (NH_3)	0.0000006
Nitrogen dioxide (NO_2)	0.0000001
Nitric oxide (NO)	0.00000006
Sulphur dioxide (SO_2)	0.00000002
Hydrogen sulphide (H_2S)	0.00000002

If the concentration of a constituent is higher than the concentration present in the atmosphere, it is then termed as an air pollutant. The major pollutants include sulfur dioxide, carbon monoxide, nitrogen oxides, ozone, suspended particulate matter, lead, carbon dioxide, and toxic pollutants. Although some pollutants are released by natural

sources, the effect is very small when compared to emissions from industrial sources, power and heat generation, waste disposal, and the operation of internal combustion engines. Table 2.2 gives brief information about typical sources of these pollutants.

Table 2.2. Typical sources for air pollutants

Source	Typical air pollutants emitted
Transportation	CO, Pb, NO_x, O_3
Stationary (power plants, industrial processes)	CO, Pb, NO_x, particulate matter, SO_2
Solid Waste Disposal	SO_2, CO
Miscellaneous (Forest fires, asphalt road paving, coal mining etc.)	CO, NO_x, particulate matter, SO_2

Air pollution has some potential negative impacts on natural systems, national economies, and life quality which could be destructive for human health, ecosystems, food security and water resources in some regions of the world.

Global warming is one of the most important effects of air pollution which is attributed to the increase in concentration of naturally occurring or man-made greenhouse gases in the upper atmosphere. It causes heat and radiation balance of the Earth to change significantly. Figure 2.1 shows the variation in global temperature. Global temperature has increased about 0.5°C over the last 100 years. The 20th century's 10 warmest years occurred within the last 15 years. Moreover if the gases continue to accumulate, according to the projections based on atmospheric computer models, the average global surface temperature could rise 0.9–3.5°C by 2100 [2].

The snow cover in the Northern Hemisphere and floating ice in the Arctic Ocean have decreased. Globally, sea level has risen 10-25 cm over the past century. Worldwide precipitation over land has increased by about 1 %. The frequency of extreme rainfall events has increased. Increasing concentrations of greenhouse gases are likely to accelerate the rate of climate change, thus evaporation will continue to increase as the climate warms leading average global precipitation to increase. Moreover, soil moisture is likely to decline in many regions, intense rainstorms are likely to become more frequent, and sea level is likely to increase [3].

4
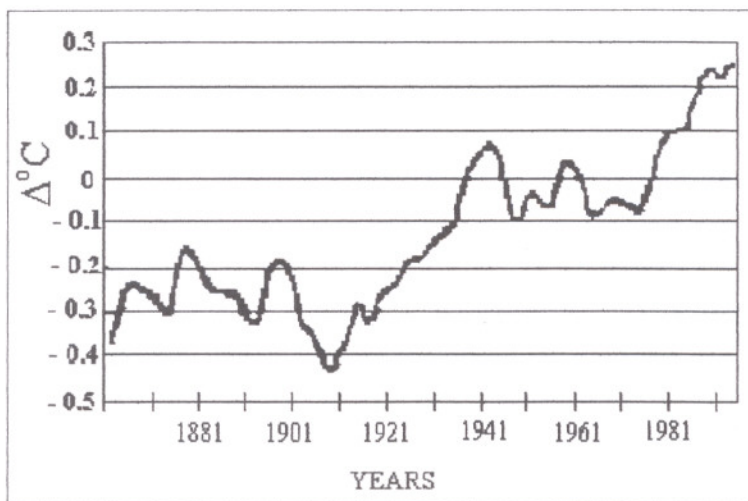
Figure 2.1. Global temperature changes (1861 – 1996)

(Intergovermental Climate Change Panel, 1995)

2.1. Carbon Monoxide

Since carbon monoxide is that of particular interest in this study, the next part is dedicated to discuss the sources, health effects, present air pollution situation based on carbon monoxide emission, standards and control methods of carbon monoxide emissions in details.

Carbon monoxide is colourless, tasteless, odourless, poisonous, flammable and chemically inert under normal conditions. It survives in the atmosphere for a period of approximately one month and eventually is oxidized to carbon dioxide (CO_2) [4]. CO is defined as an "indirect green house gas" together with NO_x, VOC and SO_2 in Intergovermental Climate Change Panel.

2.1.1. Carbon Monoxide Sources

Carbon monoxide is emitted from both natural and anthropogenic sources. According to Argonne National Laboratory reports, the major natural source is the oxidation of methane gas from decaying vegetation producing 3.5 billion tonnes of CO yearly [5].

The major anthropogenic carbon monoxide sources are mobile sources including transportation, and stationary sources like power plants, industrial processes and solid waste disposal areas. These sources and their approximate CO emissions are summarized in Table 2.3.

Table 2.3. Sources and quantities of carbon monoxide emissions [5]

Source	Emissions, 10^6 tonnes/year				
	1968	1970	1975	1977	1980
Transportation	102.5	100.6	77.2	85.7	69.1
Fuel combustion in stationary sources (power and heating)	1.8	0.7	1.5	1.2	2.1
Industrial processes	7.7	10.3	7.7	8.3	5.8
Solid-waste disposal and miscellaneous	24.8	23.3	9.8	7.5	8.4
Total	136.8	134.8	96.2	102.7	85.4

The combustion of coal, oil, and gasoline are the major sources for CO. 80 % of the carbon monoxide comes from burning gasoline and diesel fuels in vehicles. The amount of carbon dioxide produced depends on the carbon content of the fuel. The average CO emissions from transportation estimated in 1968, 1970, 1975, 1977, and 1980 were about 78.8 % of the total. In European urban areas, the produced CO is almost 90 % from traffic emissions. Elevated carbon monoxide levels are most likely to occur during the colder months in urban areas. The emissions from mobile sources are based on vehicle miles travelled (VMT) data as given in Table 2.4 [6].

Table 2.4. Unleaded gasoline exhaust products per Vehicle Mile Travelled [6]

Exhaust Products	Emissions			
	grams	percent of total	moles	percent of total
Carbon Dioxide (CO_2)	272.38	69.38	6.19	49.01
Water Vapor (H_2O)	109.42	27.88	6.08	48.14
Methane (CH_4)	0.08	0.02	<0.01	0.07
Nitrogen Oxides (NO_x) Nitrous Oxide (N_2O)	0.87	0.22	0.02	0.16
Carbon Monoxide (CO)	9.00	2.29	0.32	2.53
Nonmethane Hydrocarbons (C_nH_m)	0.86	0.21	0.01	0.09

As a result of long-term improvements in CO emission control, CO emissions decreased by 38 % between 1981 and 1991, while vehicle miles travelled increased by 35 %, as shown in Figure 2.2.
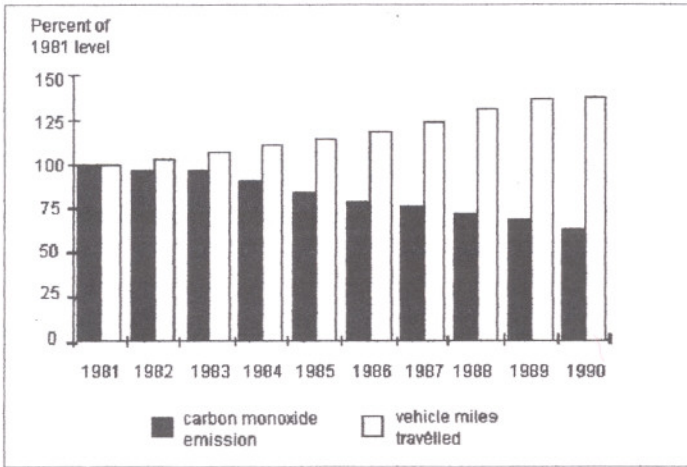
Figure 2.2. CO emission trend from vehicles

In 1997, the world fossil fuel industry produced 5.2 billion tons of coal, 26.4 billion barrels of petroleum and 81.7 trillion cubic feet of natural gas. 6.2 billion metric tons of carbon was emitted as a result of the combustion of these carbon-based fuels into the atmosphere contributing to global warming [8]. One solution to lower the CO gas emissions from the power plants is the adoption of renewable energies. These energy sources range from solar, wind, and hydro to fuel cells powered by hydrogen.

Other major anthropogenic sources of carbon monoxide emissions are chemical and metallurgical industry including iron and steel mills, zinc, lead, and copper smelters, municipal incinerators, petroleum refineries, cement plants, and nitric and sulphuric acid plants where carbon monoxide is used as an industrial chemical or as a fuel. Carbon monoxide is commonly emitted by industry as a result of incomplete combustion of carbon-containing material; for example the exhaust gases of gasoline, diesel, and propane engines. If the temperature of combustion is not sufficiently high, oxygen is not enough, or the time is not sufficient for complete burning, then the fuel will not be completely oxidized to carbon dioxide. The following reaction expresses incomplete combustion of methane:

$CH_4 + O_2 \rightarrow$ mostly $(CO_2 + H_2O)$ + traces of $[CO +$ Hydrocarbons$]$

7
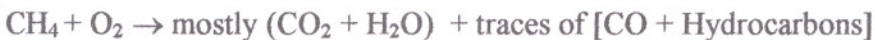
Solid-waste disposal and miscellaneous causes including forest fires, structural fires, coal refuse, and agricultural burning were reported as the second largest source of anthropogenic carbon monoxide.

2.1.2. Effects of Carbon Monoxide on Health

It was reported that CO levels in ambient air may reduce the oxygen-carrying capacity of the blood, since it has 200 times greater affinity for hemoglobin than oxygen. Table 2.5 gives the effects of different levels of CO in the air.

Table 2.5. Health effects of CO concentration in the air [5]

CO Level (ppm)	Effect
1-3	None
20-60	Reduced capacity for work exposure limits for 8-hour day
60-150	Frontal headache, shortness of breath on exertion
150-300	Throbbing headache, dizziness, nausea, lower dexterity
300-650	Severe headache, nausea, vomiting, confusion, collapse
700-1000	Coma, convulsions
1000-2000	Heart and lungs depressed, fatal if not treated
over 2000	Rapidly fatal

2.1.3. Carbon Monoxide Emission Standards

In USA, national primary and secondary ambient-air-quality standards were set and incorporated into the Clean Air Act amendments in 1970. The 1970 national ambient-air-quality standards established the threshold levels below which no adverse effects are known to occur as given in Table 2.6. Primary standards is based on air quality criteria for protection of public health, while secondary standards were established to protect public welfare, i. e., plants, animals, property and materials. Maximum 8-hour and 1-hour carbon monoxide concentration standards should not be exceeded more than once a year [7].

Table 2.6. USA national ambient air quality standards for CO

Pollutant	Primary and Secondary Standards
Maximum 8-hour concentration	10 ppm (12.5 mg/m^3)
Maximum 1-hour concentration	40 ppm (50 mg/m^3)

2.1.4. Air Quality in Turkey based on CO Emissions

CO is released to the atmosphere from fuel consumption, industrial processes and combustion of agricultural wastes. While CO emission was reported as 3,773,000 tonnes in 1990, this value was increased to 4,198,000 tonnes in 1997, in Turkey. In 1997, 87.82 % of those emissions was due to fuel consumption, 1.56 % from industrial processes, and 10.61 % from agricultural combustion facilities. Percent contribution from major sources in the 1990-1997 period is given in Table 2.7 [9].

Table 2.7. Percent CO emission contributions from the major sources in Turkey [10]

Source	Percent Contribution to CO Emission (%)							
	1990	1991	1992	1993	1994	1995	1996	1997
Fuel consumption	86.35	86.01	87.18	87.06	88.35	87.91	87.53	87.82
Industrial processes	1.59	1.48	1.46	1.47	1.48	1.56	1.58	1.56
Combustion of agricultural wastes	12.06	12.51	11.36	11.47	10.17	10.53	10.59	10.61

Trend for energy-related CO emissions are sketched in Figure 2.3. Since 1980, Turkey's energy-related carbon emissions have jumped from 18 million metric tons annually to 47.1 million metric tons in 1998. Although this is low compared to other Energy Information Administration countries, the upward trend and the rate of increase are alarming [10].
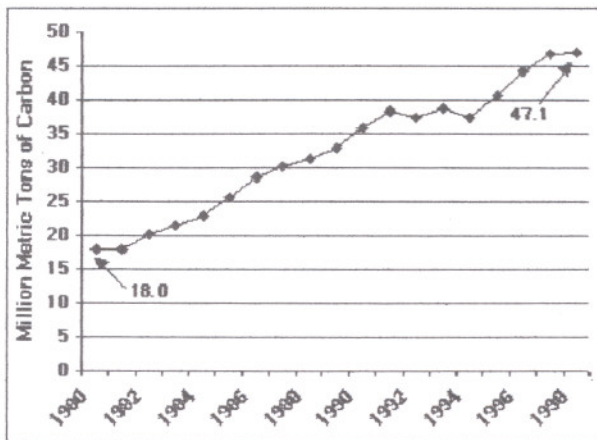
Figure 2.3. Turkey's energy related carbon (CO and CO_2) emissions
(Energy Information Administration, EIA) [10]

In Turkey, the government and municipalities have taken several measures to reduce pollution from energy sources in order to meet EU (European Union) environmental standards. Flue gas desulfurization (FGD) units are required on all newly commissioned coal power plants and retrofitting FGD onto older units. In addition, the planned "Blue Stream" natural gas pipeline from Russia should provide the necessary supplies for Turkey to rely more heavily on cleaner-burning gas rather than coal [10].

Turkey also needs to maintain and increase investments in public transport especially in urban areas and improve the implementation of existing regulations on air quality in order to reduce air pollution. Additionally, it is required to improve the quality of oil products and promote investments in the environmental control system [10]. Present air quality standards for CO are given in Table 2.8 and 2.9.

Table 2.8. Air quality limit standard for CO in Turkey [11]

Pollutant	Long-Term Limit	Short-Term Limit
Carbon Monoxide (CO)	10 mg/m^3	30 mg/m^3

Table 2.9. Long-term air quality standards proposed by WHO for Turkey [11]

Pollutant	Assessment	Long-Term Limit
Carbon Monoxide (CO)	8-hour averaged daily maximum	10 mg/m^3 40 mg/m^3

Turkey is not a signatory to the United Nations Framework Convention on Climate Change (UNFCC) or to the Kyoto Protocol, meaning the country has no binding requirements to cut carbon emissions by the 2008-2012 period as most other IEA countries have. However, Turkey has established a National Climate Coordination Group (NCCG) to carry out the national studies in line with those conducted by all countries of the UNFCC.

2.1.5. CO Emission Control Methods

Environmental regulations force industry to develop economically feasible and efficient methods to reduce the pollutant emissions to acceptable levels. Control of pollutants at the source is far more desirable than control by dilution in the ambient air. Adsorption, absorption, condensation and combustion are four basic control methods.

Adsorption is widely used in industrial processes and environmental applications, because of its low energy consumption and usefulness for low sorbate concentrations. The first step in the development of an adsorption separation process is the choice of a suitable adsorbent to maximize the adsorption capacity. Preferential affinity for specific substances and large surface area per unit volume provided by the internal pores of the solid are two key characteristics of solid adsorbents [12].

The use of solids for removing substances from gaseous mixtures accompanies by preferential partitioning of substances from the gaseous phase and accumulation on the adsorbent surface. To achieve the sufficient adsorptive capacities for economic viability, microporous solids with pore diameter ranging from a few Å to a few hundred Å and with high specific surface area about 200-2000 m^2/g are employed. The quantity of gas adsorbed by a solid depends on pressure, temperature, the nature of the gas, and the nature of the solid. The most commonly used commercial adsorbents in gas separation and purification applications are given in Table 2.10.

In the traditional adsorbents, there is a distribution of pore size. On the other hand, molecular sieve zeolites and carbon molecular sieves have a well defined bimodal pore size distribution since they are made of small particles of the microporous solids formed into macroporous particles or pellets. The dehydrated crystalline zeolites show the most important molecular sieve effects due to the uniform pore sizes (3-10 Å) which are uniquely determined by the unit structure of the crystal. These pores selectively adsorb or reject the molecule based on the relative size of the molecule and the pore [13].

Table 2.10. Commercial adsorbents for gas separation and purification applications

Bulk Gas Separations (a)	
Adsorbent	Separation
Zeolite	Normal paraffins, isoparafins, aromatics, N_2/O_2, H_2O/ethanol
Carbon molecular sieve	O_2/N_2
Zeolite, Activated carbon	CO, CH_4, CO_2, N_2, Ar, NH_3/H_2
Activated carbon	Acetone/vent streams, C_2H_4/vent streams
Gas Purifications (b)	
Adsorbent	Separation
Silica, Alumina, Zeolite	H_2O/olefin-containing cracked gas, natural gas, air, synthesis gas
Zeolite	CO_2/C_2H_4, natural gas Sulfur compounds/natural gas, H_2, liquified petroleum gas NO_x/N_2, SO_2/vent streams, Hg/chlor-alkali cell gas effluent
Activated carbon	Organics/vent streams, Solvents/air, Odors/air

(a) Adsorbate concentrations of about 10 weight % or higher in the feed

(b) Adsorbate concentrations generally less than about 3 weight % in the feed

CHAPTER 3

ZEOLITES

3.1. History, Formation and Occurrences of Zeolites

Thousands of years ago ancient people have recognized that zeolites can absorb moisture and heat, act as a natural air conditioner as well as a building material in pyramids and other ancient buildings.

It was believed that the Mayan pyramids and buildings at Chichen Itza in the Yucatan in Mexico had been built by limestone during the last century. Many scientists thought that these large limestone blocks were moved by manpower alone over 160 kilometres. In point of fact, most of the large building blocks used by the Mayans at this site were light weight zeolite blocks moved only about 48 kilometres and through the centuries dust particles and sediment from rains and floods resulted to fill the zeolite crystalline structure making them heavier [14].

Zeolites were first recognized by Cronstedt in 1756, as a new group of minerals consisting of hydrated aluminosilicates of the alkali and alkaline earths with his discovery of stilbite. Cronstedt called the mineral a "zeolite" derived from two Greek words: "zeo" and "lithos" meaning "to boil" and "a stone" [15].

The study of the adsorption of gases and vapours on solids dates from Gideon's tests on fleece in 1100 B.C. In 1840, Damour has found that zeolite crystals could be reversibly dehydrated without apparent change in their transparency or morphology. Eichhorn has discovered the reversibility of ion exchange on zeolite minerals in 1858. St. Claire Deville has reported the first hydrothermal synthesis of a zeolite, levynite, in 1862. In 1896, Friedel has noted that the structure of dehydrated zeolites consists of open spongy frameworks by observing the adsorption of alcohol, benzene and chloroform on dehydrated

zeolites. In 1909, Grandjean has observed that dehydrated chabazite adsorbs ammonia, air and hydrogen. In 1925, Weigel and Steinhoff reported the first molecular sieve effect noting that dehydrated chabazite crystals rapidly adsorbed water, methyl alcohol, ethyl alcohol and formic acid while excluding acetone, ether or benzene. Taylor and Pauling determined the first structures of zeolites in 1930. In 1932 McBain established the term "molecular sieve" to define porous solid materials that act as sieves on a molecular scale.

By the mid-1930's, the literature described the ion exchange adsorption, molecular sieve, structural properties and synthesis of zeolite minerals. However, synthesis work has not been verified due to incomplete characterization and the difficulty of experimental reproducibility. Barrer studied synthesis of zeolites and their adsorption properties in 1930's and 1940's and the first classification of zeolites based on molecular size has been presented in 1945. In 1948, he reported the first definitive synthesis of zeolites including the synthetic analogue of the zeolite mineral mordenite. Work carried out in the late 1940's by Milton and Breck et al. They synthesized the first completely determined new zeolitic structure, named Zeolite A [15].

Natural zeolites are often formed during low-temperature metamorphism of volcanic glass-like quenched molten rocks or volcanically-derived sediment that are immersed in aqueous environment. Composition and pore size depend upon the type of rock minerals involved [16]. For 200 years, natural zeolites were considered to occur typically as minor constituents of basaltic and volcanic rocks. However, geologic discoveries in the 1950s and 1960s showed that some natural zeolites might occur also in sedimentary deposits [15].

Natural zeolites are occurred in the widespread tuffaceous volcanic rocks of Arizona; Hoodoo Mountains and the Yucca Mountains in Nevada, Washington, Oregon and California, USA. Also found in Syria, Austria, Bulgaria, British Columbia, Canada, Germany; Italy, Japan, New Zealand, India and Turkey. Locations and types of the natural zeolites in Turkey are given in Table 3.1.

The deposit in Bigadiç, Western Anatolia Region was reported as about 2 billion tonnes [18, 19, 20]. Gündoğdu [21] reported that heulandite–clinoptilolite content of Bigadiç and Gördes zeolites was about 80 % and clinoptilolite was the major mineral in Bigadiç. Özkan and Ülkü [17] reported the available zeolite reserve in Balıkesir-Bigadiç region as 500.000 tonnes and total reserve as 50 billion tonnes.

Table 3.1. Natural Zeolite Deposits in Turkey [17]

Location	Type of Natural Zeolite
Balıkesir, Bigadiç	Clinoptilolite
Emet, Yukarı Yoncaağaç	Clinoptilolite
İzmir, Urla	Clinoptilolite
Kapadokya Region (Tuzköy, Karain)	Clinoptilolite
Gördes	Clinoptilolite
Bahçecik, Gülpazarı, Göynük	Analcime
Polatlı, Mülk, Oğlakçı, Ayaş	Analcime
Nalıhan, Çayırhan, Sabanözü	Analcime
Kalecik, Çandar, Hasayar	Analcime

3.2. Structure of Zeolites

Zeolites are three dimensional, microporous, hydrated crystalline aluminosilicates of group IA and group IIA elements such as sodium, magnesium, potassium, calcium, strontium, and barium. They have a regular structure of pores and chambers.

The structural formula based on the crystallographic unit cell is represented by $M_{x/n}[(AlO_2)_x(SiO_2)_y] \cdot wH_2O$, where M is Na, K, Li and/or Ca, Mg, Ba, Sr, n is the cation valance, w is the number of water molecules. The ratio y/x (Si/Al ratio) usually lies within the range of 1 to 6 depending upon the structure. The sum $(x+y)$ is the total number of tetrahedra in the unit cell. The $[(AlO_2)_x (SiO_2)_y]$ portion represents the framework composition.

The empirical oxide formula for natural zeolites is given by $M_{2/n}O \cdot Al_2O_3 \cdot ySiO_2 \cdot wH_2O$ where y is 2 to 10 since AlO_4 tetrahedra are joined only to SiO_4 tetrahedra, n is the cation valance, and w represents the water contained in the voids of the zeolite.

There are three relatively independent components in the zeolite structure: the aluminosilicate framework, exchangeable cations and zeolitic water. The aluminosilicate framework is constituted by primary building units. This unit is a tetrahedron, the centre of which is occupied by silicon or aluminium atom, with four oxygens atoms at the vertices as shown in Figure 3.1 [13].
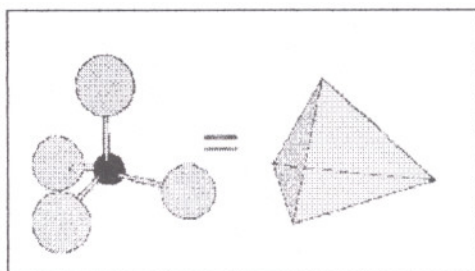
Figure 3.1. An $[AlO_4]^{5-}$ or $[SiO_4]^{4-}$ tetrahedra (primary building unit)

These SiO_4 and AlO_4 tetrahedra are linked to each other by sharing all of the oxygens and form secondary building units (SBU) as indicated in Figure 3.2 [13].
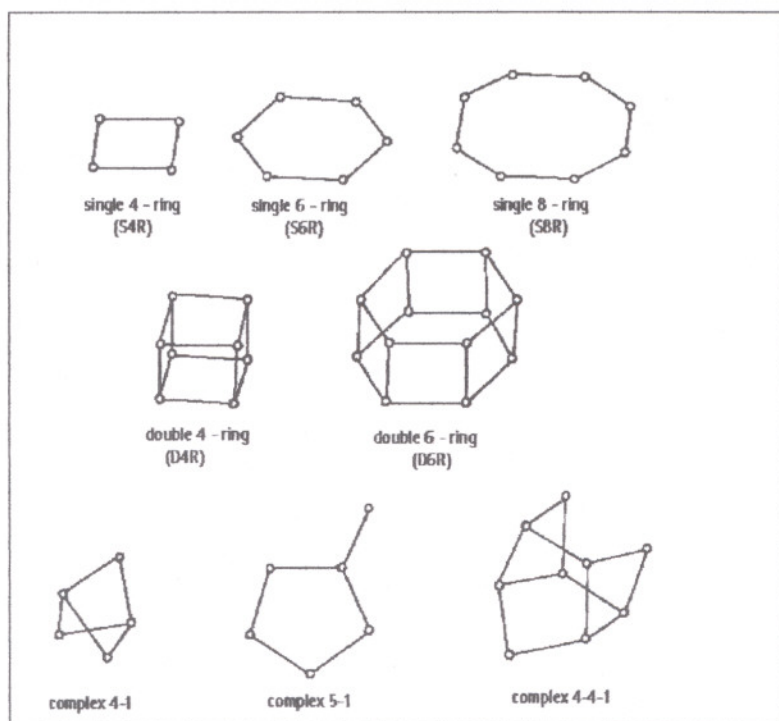
Figure 3.2. Secondary building units of zeolite framework

In this figure each vertex represents the location of a Si or Al atom while the lines represent the diameters of the oxygen atoms or ions which are very much larger than the tetrahedral Si and Al atoms. These SBU's are further interconnected and form the infinitely extended framework of the zeolitic crystal structures with interconnecting channels that range in size from 2 to 4.3 Å (Figure 3.3).

16
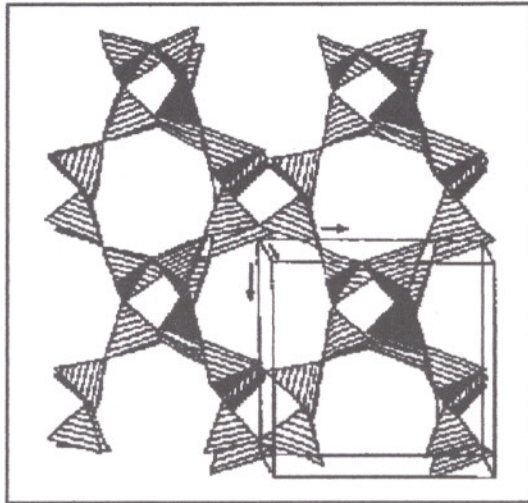
Figure 3.3. The primary building units combine
to form the secondary building units

Si and Al which are not exchanged under ordinary conditions are termed as tetrahedral (T) or framework cations. The substitution of aluminium ion for silicon ion results in a net negative charge on the framework, which is balanced by monovalent or divalent cations. Since these cations are loosely bound to the lattice, they can be substituted by other cations to varying degrees, thus they are referred as exchangeable or extra-framework cations. They are located at specific sites within the void spaces and interconnected channels of the framework together with water molecules.

The water content depends on the character of those cations. Under ordinary conditions water molecules completely fill the free volume of channels and voids in the zeolite structure. The intracrystalline volume occupied by water may amount to as much as 50% of the volume of the crystal. This intracrystalline "zeolitic" water can be removed continuously and reversibly. Then, the free inner volume of the zeolite can be calculated by measuring the volume of the water released under heating in vacuum. The capacity of the zeolite for adsorption is usually related to this free space or void volume [22].

This framework structure containing channels or interconnected voids that are occupied by the cations and water molecules allows some molecules to pass through, and causes others to be excluded.

3.2.1. Internal Channel Structures and Apertures in Zeolites

Zeolites have various internal channels and void spaces, which gives zeolites the ability to separate mixtures of molecules on the basis of their effective sizes. Three types of channel systems are identified for zeolites as: one-dimensional system in which the channels do not intersect as that of anaclime, two-dimensional systems, as found in clinoptilolite and three-dimensional channels. The free diameter of all three-dimensional channels is equal as in chabazite, faujasite, erionite or channels are not equidimensional as in gmelinite and offretite. The preferred type has 2 or 3 dimensional channels to provide rapid intracrystalline diffusion in adsorption and catalytic applications.

The nature of the void spaces and the interconnecting channels in dehydrated and hydrated zeolite crystals and the interaction of molecular species with cations within the channel openings are important in determining the physical and chemical properties. These internal channels and void spaces are accessed through oxygen windows which are formed by oxygen atoms of connected tetrahedra. In general, these windows involve 6, 8, 10, or 12 oxygen atoms. If these oxygen windows are assumed to be planar and assuming oxygen to have diameter of 2.7 Å, the free diameter of the windows can be calculated as given in Table 3.2, where "n" represents the number of oxygen atoms [15].

Table 3.2. Estimated diameters of planar configuration

n	Diameter (Å)
4	1.1
5	1.9
6	2.7
8	4.3
10	6.0
12	7.7

On the other hand, temperature is an important factor in determining the aperture size, the effective size increases with increasing temperature due to thermal vibration of the oxygens in the aperture rings.

The free diameter of the windows in the intracrystalline channel structure determines the intracrystalline diffusivity and the molecular sieve properties. Molecules with critical kinetic diameters smaller than the free window diameter may penetrate these

windows. Furthermore, the interaction between the adsorbing molecules and the oxygen atoms in the windows is important. For example, the kinetic energy of the diffusing molecule determines whether it can surmount the potential energy barrier created by the window into the crystal interstices. The free diameter of these windows is reduced depending on the number and nature of the blocking cations and causes the diffusivity of the guest molecules to reduce. Therefore, it is possible to obtain molecular sieve separation between molecules by substitution of cations.

3.2.2. Adsorption Properties of Zeolites

Zeolites have a high internal surface area available for adsorption due to the channels or pores distributed throughout the entire volume of the adsorbent. The external surface area of the adsorbent particles contributes only a small amount of the total available surface area [13]. Separation of gases by zeolites depends on the structure and composition of the framework, cationic form and the zeolitic purity. Different cationic forms may lead to significant differences in the selective adsorption of a given gas, due to both the location and size of the interchangeable cations which affect the local electrostatic field, and the polarization of the adsorbates. The energetic characteristics of the adsorption of different gases in natural and synthetic zeolites have been studied extensively.

The adsorbate molecules with critical size smaller than the critical dimension for entry of the zeolite can access into the clinoptilolite channel. The adsorption capacity of zeolties was also determined by the strength of the sorbate-adsorbent interaction [23]. Moreover, the polarizability, electric dipole moments and molecular sizes of adsorbate molecules, and polarizing power of the cations and their location in the zeolite framework have also important effects on adsorption properties of zeolites. [24]. These effects were examined and it was concluded that as the polarizing power of cation increased the diffusivity decreased [25]. The size and polarizing power values for common cations in zeolite framework are given in Table 3.3.

Since the CO molecule is of interest in this study, its dimensions and kinetic properties are given in Table 3.4, based on Pauling's values of bond lengths and van der Waals radii of molecule [13]. The critical diameter value corresponding to the cross-sectional diameter of CO molecule, dumbbell-shaped molecule, is the critical dimension for penetrating the zeolite.

Table 3.3. Physical characteristics of the exchangeable cations

Cation	Ionic Radius (Å)	Polarizing Power (∅)
H^+	-	-
Na^+	0.95	1.05
K^+	1.33	0.75
Cs^+	1.69	0.59
Mg^{2+}	0.65	3.08
Ca^{2+}	0.99	2.02
Ba^{2+}	1.35	1.48

When the zeolite channels are large enough to allow the free passage of CO molecule, the retention volume is related to the electrostatic interaction of the CO molecule with the adsorption sites of the zeolite. The strength of such interaction depends mainly on the local electrostatic field resulting from the ionic nature of the zeolite framework and on the polarity (dipole and quadrupole moments) and/or polarizability (induced dipole) of the CO molecules [26]. Breck [13] and Barrer [27, 28] showed that CO exhibits high retention volume in most of the cases due to its permanent dipole moment which is the most important electrical component of the overall interaction energy.

Table 3.4. Physical characteristics of Carbon Monoxide

Dipole (Debye)	Quadrupole ($Å^3$)	Polarizability ($Å^3$)	Kinetic Diameter (Å)	Critical Diameter (Å)
0.12	0.33	1.60	3.76	4.2 x 3.7

3.3. Classification of Zeolite Structures

There are over 45 known different framework topologies for natural zeolites, and nearly 150 synthetic types have been reported. Some of the natural zeolites are:

Analcime   (Hydrated Sodium Aluminum Silicate)

Chabazite   (Hydrated Calcium Aluminum Silicate)

Clinoptilolite   (Hydrated Sodium Potassium Calcium Aluminum Silicate)

Edingtonite   (Hydrated Barium Aluminum Silicate)

Epistilbite   (Hydrated Calcium Aluminum Silicate)

Erionite   (Hydrated Sodium Potassium Calcium Aluminum Silicate)

Goosecreekite   (Hydrated Calcium Aluminum Silicate)

Gmelinite   (Hydrated Sodium Calcium Aluminum Silicate)

Harmotome   (Hydrated Barium Potassium Aluminum Silicate)

Heulandite   (Hydrated Sodium Calcium Aluminum Silicate)

Laumontite   (Hydrated Calcium Aluminum Silicate)

Levyne   (Hydrated Sodium Calcium Aluminum Silicate)

Mesolite   (Hydrated Sodium Calcium Aluminum Silicate)

Mordenite   (Hydrated Sodium Potassium Calcium Aluminum Silicate)

Natrolite   (Hydrated Sodium Aluminum Silicate)

Phillipsite   (Hydrated Potassium Sodium Calcium Aluminum Silicate)

Scolecite   (Hydrated Calcium Aluminum Silicate)

Stellerite   (Hydrated Calcium Aluminum Silicate)

Stilbite   (Hydrated Sodium Calcium Aluminum Silicate)

Thomsonite   (Hydrated Sodium Calcium Aluminum Silicate)

These natural zeolites can be classified into seven groups based on framework topology as given in Table 3.5 [13].

Table 3.5. Classification of zeolites based on framework topology

Groups	Secondary Building Units (SBU)
1	Single, 4-ring, S4R
2	Single, 6-ring, S6R
3	Double, 4-ring, D4R
4	Double, 6-ring, D6R
5	Complex 4-1, T_5O_{10} unit
6	Complex 5-1, T_8O_{16} unit
7	Complex 4-4-1, $T_{10}O_{20}$ unit

Another classification of zeolites is based on the structural variations as chain-like structures whose minerals form needle-like crystals such as natrolite, sheet-like structure where crystals are flattened with basal cleavages including heulandite, and framework structures where the crystals are more equal in dimensions such as chabazite.

3.4. Clinoptilolite

The group 7 zeolites include the morphologically lamellar zeolites; heulandite, stilbite and clinoptilolite. Samples of heulandite structure can be classified according to optical, thermal and other properties as heulandite, high-silica Heulandite, low-silica clinoptilolite (Ca-Clinoptilolite) and high-silica clinoptilolite (Clinoptilolite). The minerals with enhanced Ca, Sr and Ba content with respect to Na and K are termed as Heulandite, while the others are called as Clinoptilolite [22].

Clinoptilolite is silica-rich member of the heulandite group of minerals and it differs from heulandite only in framework and exchange ion composition, not in framework structure. The mineral occurs in extensive deposits throughout the world.

Clinoptilolite can be represented by the typical oxide formula as:

$(Na_2, K_2) O \cdot Al_2O_3 \cdot 10 SiO_2 \cdot 8 H_2O$
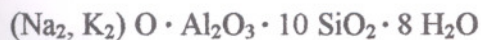
Unit cell contents of clinoptilolitie can be expressed as:

$(K_2, Na_2, Ca)_3O \cdot (AlO_2)_6 \cdot (SiO_2)_{30} \cdot 24H_2O$
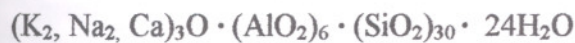
The unit cell of clinoptilolite is monoclinic (or obliquely inclined) and usually characterized on the basis of 72 oxygen atoms and 24 water molecules, with Na^+, K^+, Ca^{2+}, and Mg^{2+} as the most common charge-balancing cations. Representative unit cell parameters are a=1.762 nm, b=1.791 nm, c=0.730nm, β=2.029 rad. [29] and the corresponding unit cell volume is 2.091 nm^3. Some of the structural properties of clinoptilolite are given in Table 3.6 [13].

Because of the higher Si /Al ratio found in clinoptilolite, it exhibits thermal stability to 700°C in air. The amount of water lost below 800°C varies from 7.8 wt % for cesium containing clinoptilolite to about 15.5% for Mn, Li, and Sr containing clinoptilolite.

Table 3.6 Structural Properties of Clinoptilolite

SBU	Unit 4-4-1
Void Volume	0.34 cc/cm^3
Framework Density	1.71 g/cm^3
Dehydrated-Effect of Dehydration	Very stable in air up to 700°C
Largest Molecule Adsorbed	O$_2$
Kinetic Diameter, σ, Å	3.5
Density	2.16 g/cm^3
Si/Al	4.25 – 5.25

Clinoptilolite is assigned to the same framework (HEU) in which 4-4-1 secondary building units are joined in a layer-like array as shown in Figure 3.4 The layers are joined to create 8- and 10- membered oxygen windows. The 2-D channel system is apparent in the clinoptilolite. Channel A contains 10 - member ring, channel B of 8 - member ring is parallel to channel A and channel C of 8 - member ring lies along the crystallographic a axis and intersects both A and B channels. These channels are shown in Figure 3.5.
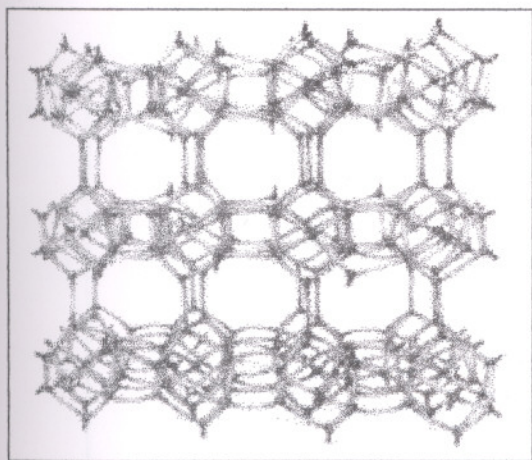
Figure 3.4. Clinoptilolite framework system
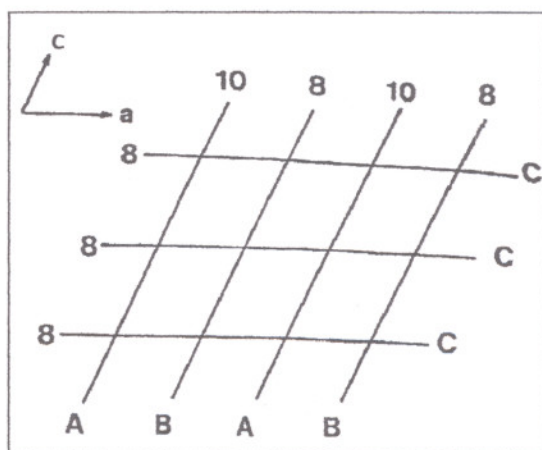
Figure 3.5. Orientation of clinoptilolite channel axes [30]

Diffusion within a pore structure is composed of inaccessible regions corresponding to the rigid framework, active sites, windows between cages and free volume within a cage. Gas penetrates the clinoptilolite structure through a series of intersecting channels along the a and c axes, not along b axis [30]. The approximate channel dimensions and cation sites where various cations can be positioned are given in Table 3.7 [31, 13] and illustrated in Figure 3.6.

Table 3.7. Channel Characteristics and Cation Sites in Clinoptilolite

Channel	Tetrahedral Ring Size/ Channel Axis	Cation Site	Major Cations	Approximate Channel Dimensions (nm x nm)
A	10 / c	M(1)	Na, Ca	0.72 x 0.44
B	8 / c	M (2)	Ca, Na	0.47 x 0.41
C	8 / a	M (3)	K	0.55 x 0.40
A	10 / c	M (4)	Mg	0.72 x 0.44
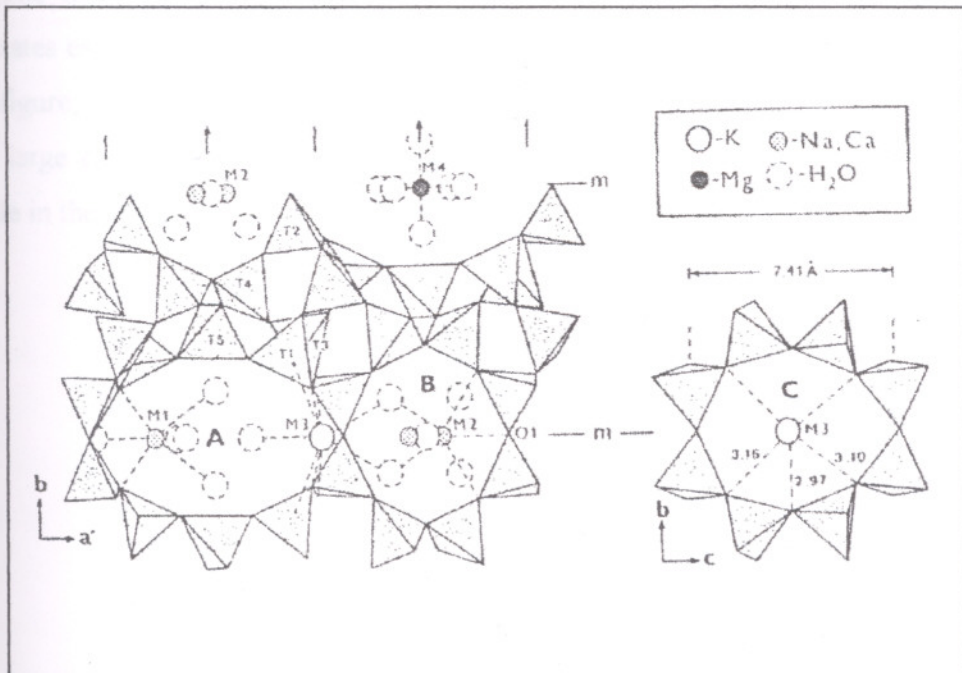
Figure 3.6 Main components in the clinoptilolite structure [22].

The type, number, location of the cations and relative size of the channels and cations may cause various degree of channel blockage as shown in Figure 3.7.
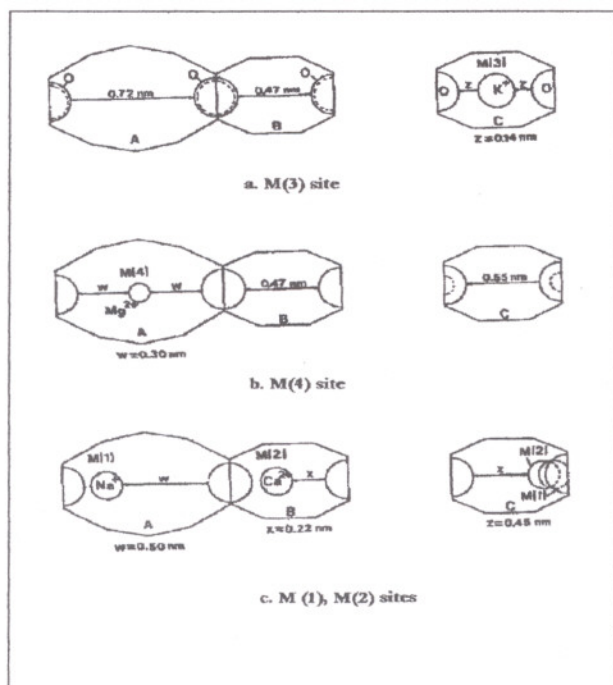
Figure 3.7. Channel blockage diagrams [30]

The channel blockage by cations affects the adsorption capacity, selectivity and uptake rates especially for a small molecule such as water vapour as shown in Figure 3.8. In this figure, the case A represents the effects of small cation molecule in the lattice, B that of large cation molecule in the lattice and case C that of intermediate size cation molecule in the lattice on molecular sieve properties of the clinoptilolite.
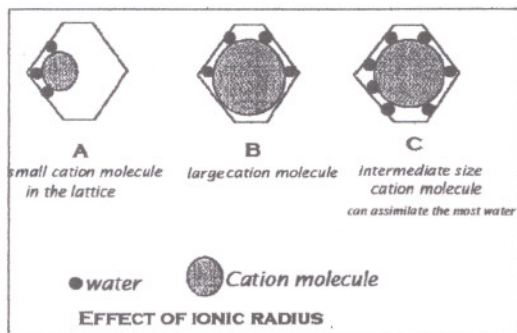
Figure 3.8. Effect of cation and molecule radius on
molecular sieve properties of clinoptilolite [32]

The windows may also be blocked by adsorbed molecules reducing the probability of passage through that window. The diffusivity is reduced more strongly by molecules within the intersections, since blockage of an intersection prohibits passage through four different channel segments.

3.5. Industrial Applications of Zeolites and Clinoptilolite

Zeolites are one of the most suitable materials in environmental pollution control, separation science and technology. Zeolites were also employed as additive to food products in order to eliminate radiation from citizens exposed to the Chernobyl disaster in the former Soviet Union [14]. Other interesting applications of zeolites include their uses as talcum powder and other health products in Hungary and as feed to animals for weight gain and health benefits, also in paper and concrete in japan due to lightweight, flexibility, excellent thermal and acoustic properties. The uses of zeolites can be categorized into four functional groups as ion exchange, catalytic applications, water adsorption and gas adsorption.

3.5.1. Ion Exchange Applications of Zeolites

The highly selective cation exchange capacity make zeolite useful in some applications such as in detergents, controlling of cations in water systems, aquaculture, agriculture and nuclear waste treatment processes. Ion exchange process occurs when water molecules pass through the channels and pores allowing cations in the solution to be exchanged for cations in the zeolite structure. Solution strength, pH, temperature and the presence of other competing cations in the solution can affect the ion exchange selectivity and capacity. Each zeolite mineral has different selectivity and capacity of exchange of internal cations for other cations depending on the ion and channel diameter.

Natural zeolites such as chabazite, mordenite, clinoptilolite have been found also suitable for the removal and recovery of cesium and strontium radioisotopes in the nuclear industry. Zeolites are preferred because of their resistance to high doses of radiation and high selectivity in contrast to resin ion exchangers that loose capacity and selectivity under irradiation. Zeolite can remove dangerous isotopes which is present even in very low concentrations.

The most important ion-exchange application of zeolites can be found in detergents. Polyphosphates were previously used as builders but they are harmful to the environment. Modern detergents use zeolites as builders removing calcium and magnesium ions from the washing water to prevent their precipitation by surfactants. The synthesized Zeolite A is mainly used for this purpose that it has no harmful effects on the environment but it is not successful at removing Mg^{+2} ions as Ca^{2+} ions so some polyphosphates are still used.

The use of natural zeolites in aquaculture includes the removal of ammonium resulted from biological processes of fish in fish farming, fish aquaria and in fish transport areas. Ammonium-based fertilizers are employed conventionally to supply nitrogen as an essential nutrient to crops. Excess amount of ammonium supplied to crops is not only toxic to the crop by burning its root systems, but also harmful to fish and aquatic life increasing the level of ammonium in agricultural wastewater. Proper use of natural zeolites may help in the solution of this problem. Zeolites improve cation exchange capacity of sandy soils resulting in lower fertilizer requirements. They reduce the need for nitrogenous fertilizers by reducing bacterial nitrification, reduce nutrient and fertilizer loss through heavy rains, leaching and irrigation, resulting in less environmental damage through water runoff.

Another most well known use of ion exchange characteristic of zeolites is in water softeners, in removal of calcium and magnesium ions causing problem of scum to occur in water treatment processes. Conventionally, quartz sand filters are used for removal of suspended particles from drinking water. However, quartz sand is expensive and has a low fine-trapping capacity. Studies have shown that quartz sand can be replaced by natural zeolites [33, 34, 35, 36]. Due to high porosity of zeolites, especially clinoptilolite, allowing operation at high flow rates, they are more appropriate for use as filter materials than quartz [36]. Table 3.8 summarizes percent porosity of some filter materials:

Table 3.8. Porosity of filter materials [33, 34, 35]

Filter material	Porosity	
	Maximum	minimum
Quartz sand	43	38
Crushed rock	60	48
Mordenite	55	45
Clinoptilolite	62	50

Clinoptilolite is commonly used in wastewater treatment plants due to its selectivity for one ion over others. The details of some wastewater treatment plants using clinoptilolite columns are given in Table 3.9 [15]. Research results have shown that clinoptilolite can remove colour and heavy metal ions such as barium, lead, cadmium, zinc and copper from dyeing and other industrial wastewater. It is also useful to remove heavy metals from mining and metallurgical wastewaters by means of zeolites. In wastewater treatment plants, the use of clinoptilolite increases the nitrogen content i. e., quality of the resultant sludge making it valuable as fertilizers. Regeneration and reuse of zeolites are also possible.

Table 3.9. Use of clinoptilolite in wastewater treatment plants

Location of plant	Zeolite used	Plant capacity	Regeneration
Rosemount, USA	Clinoptilolite	0.6 MGD[a]	Yes
Occoquan, USA	Clinoptilolite	22.5 MGD	Yes
Virginia, USA	Clinoptilolite	22.5 MGD	Yes
Tahoe-Truckee, California, USA	Clinoptilolite	6 MGD	Yes
W. Bari, Italy	Clinoptilolite Phillipsite	10 m^3/ h	Yes
Vae, Budapest, Hungary	Clinoptilolite tuff	50 m^3/ day	Yes
Toba, Japan	Clinoptilolite tuff	80 m^3/ day	Not available
Japan	Clinoptilolite tuff	500 m^3/ day	Yes

Other more general treatments using clinoptilolite are listed in Table 3.10. It seems likely that the use of clinoptilolite will continue to expand [15].

Table 3.10. Application of clinoptilolite to treat liquid effluents

Use	Species removed or treated
Boiler waters	Fe
Condensates from soda ash products	NH_4^+ and oils
Heating and power station waters	NH_4^+
Drinking water treatment	30,000 m^3/ day pilot plant
Nutrient recovery from sewage	240 m^3/ day plant
Textile waste	Caprolactam and lubricants
Wastewaters	Oil
Organochloride production clean up	Trichloroethylene
Non-ferrous metal production	Zn, Cu

3.5.2. Catalytic Applications of Zeolites

Clinoptilolite treated with acid and alkali solutions promote many chemical reactions such as hydrogenation, dehydrogenation and dealkylation. Clinoptilolite can catalyze cracking, toluene disproportionation and isomerization processes. Extremely high strength acid sites, thermal stability and molecular sieving properties of zeolites make them more superior than other catalysts for a number of chemical reactions. At present, zeolite catalysts are widely used in the old USSR, USA and Canada in oil refineries for cracking, hydrocracking and isomerization reactions [22].

3.5.3. Water Adsorption Applications of Zeolites

Natural zeolites possess a high affinity for water and they can reversibly adsorb and desorb water without chemical or physical change in their structures. This property makes them suitable materials for a low cost, efficient media for heat storage and solar refrigeration applications.

3.5.4. Gas Adsorption

Zeolites have a high internal surface area available for adsorption due to the channels or pores distributed throughout the volume of the adsorbent. The external surface area of the adsorbent particles contributes only a small amount of the total available surface area [13]. The ability of zeolites to adsorb many gases selectively is determined by the size of the channels ranging from 2.5 to 4.3 Å in diameter depending on the zeolite type. Specific channel size enables zeolites to act as molecular sieves selectively adsorbing such gases as ammonia, hydrogen sulfide, carbon monoxide, carbon dioxide, sulfur dioxide, water vapour, oxygen and nitrogen. The type of zeolites i.e., the framework structure and composition, cationic form and purity of the zeolite affects the efficiency of gas removal. The quantity of gas adsorbed also depends on the pressure, temperature and the nature of the gas.

Applications currently under study and development include air purification, adsorption of heavy metals, absorbent linings in landfills, removal of radioactive elements from water. With the expansion of molecular sieve science, more interesting uses of zeolite are awaiting to be explored. The future of zeolites certainly looks promising.

3.6. World Zeolite Demand

World synthetic zeolite capacity totaled approximately 2 million metric tons in early 1995 and the market totaled approximately $1.5 billion in 1994. Since many types of zeolites have been identified or synthesized, only a few are currently used commercially on a significant scale. Total demand level for building materials is around 2.4 million tones, for agriculture is about 800,000 tones, and for ion exchange, adsorption, and catalyst applications is around 400,000 tones per year in 1997.

The catalyst sector represents the largest sector on a value basis and detergent zeolites the largest on a volume basis in North America, West Europe and Japan in 1988 as shown in Figure 3.9.
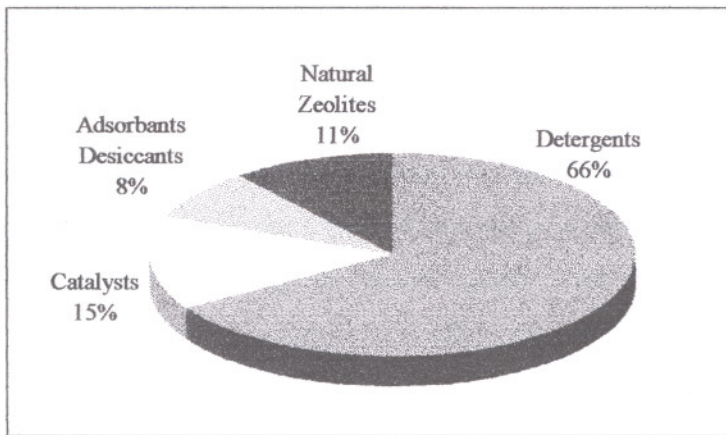
Figure 3.9. Zeolite consumption as volume distribution
over application areas in North America, West Europe and Japan in 1988

The largest market for zeolites is catalyst, totally more than $ 500M per year in the USA. However, the market increases only at 3% per year, principally for petroleum cracking. Catalyst demand has increased over the past five years as a result of the decision to produce unleaded gasoline and the consequent development of octane-enhancing catalysts. Consumption in this application reached almost 102 thousand metric tons in 1994.

Zeolite A was developed as a replacement builder for use in regions where excessive freshwater eutrophication rates restricted on the use of phosphate-built detergents in the late 1970s. Zeolite-built detergent powders are being displaced phosphate-containing detergents in both the United States and Japan and holding a major market share in Western Europe. Although detergent zeolites have not been widely commercialized due to their low bulk densities, it is expected that the trade will increase in the future in order to utilise existing capacity to supply any new growth in markets in Asia, Australia and Latin America. Total zeolite use as a detergent builder in the United States, Canada, Western Europe and Japan was reported as 906 thousand metric tons in 1994. Synthetic zeolites have been used as detergent builder market over the past 20 years but only in some regions including Western Europe, North America and Japan where strict restrictions exist to use of phosphate in detergents. Therefore, the demand for synthetic zeolites was limited. Worldwide detergents-grade zeolites capacity utilization is less than 60% of the total capacity. Zeolite manufacturers in USA are reported to be operating at around 80% of capacity, while in Asia this operation capacity is 64%.

Approximately 55 thousand metric tons of zeolite "molecular sieves" was used as adsorbents and desiccants in 1994. The anticipated significant growth in demand for adsorbent/desiccant and catalyst zeolites will be primarily in Asia-Pacific and the Middle East. Demand for natural zeolites has increased rapidly over the past decade and it is expected to grow higher than that for synthetic zeolites with forecast rate as 10 % per year [37].

CHAPTER 4

DIFFUSION IN ZEOLITES

Most adsorption separation processes depend on differences in adsorption equilibrium, but separations based on the differences in the adsorption/desorption kinetics or the micropore diffusivities are also possible.

In practical operations, maximum capacity of adsorbent cannot be completely used due to mass transfer effects, involved in fluid-solid containing processes. Therefore, it is necessary firstly to have information on adsorption equilibrium in order to estimate dynamic adsorption capacity. Then kinetic analyses are conducted based on rate processes depending on types of contacting processes.

In practical application of adsorbents, the adsorbent is usually contacted by fluid flowing through a packed bed. The overall dynamics of the packed bed control the design and determine the process efficiency.

4.1. Driving Force for Diffusion

The rates of adsorption and desorption in porous adsorbents such as zeolite crystals can be expressed mathematically by Fick's Law:

$$J = -D_c(q)\frac{\partial q}{\partial x} \tag{4.1}$$

where J is the molar flux due to diffusive transport, $\partial q/\partial x$ is the intracrystalline concentration gradient along the micropore distance x, and q is the concentration of the adsorbed diffusing species in the porous zeolite medium. $D_c(q)$ is the intracrystalline

(Fickian) diffusivity which is generally dependent on the concentration., but independent of $\partial q/\partial x$ according to Equation (4.1). From a thermodynamic point of view, a system is at equilibrium when the chemical potential, μ, is constant throughout the system. Thus, the true driving force of a transport process is the gradient of the chemical potential of the adsorbed species, $\partial \mu/\partial x$, rather than the intracrystalline concentration gradient. Then, the molar flux can be expressed as;

$$J = -B_c(q)q\frac{\partial \mu}{\partial x} \tag{4.2}$$

where $B_c(q)$ is the mobility parameter. If equilibrium with an ideal gas phase is assumed, then the chemical potential can be represented by:

$$\mu = \mu_o + RT \ln p \tag{4.3}$$

where μ_o is the standard state chemical potential, R is the universal gas constant, T is temperature and p is the gas phase pressure. Differentiating Equation (4.3) with respect to x yields:

$$\frac{\partial \mu}{\partial x} = RT \frac{d \ln p}{dq}\frac{\partial q}{\partial x} \tag{4.4}$$

Substituting this equation into Equation (4.2);

$$J = -D_o(q)\frac{d \ln p}{d \ln q}\frac{\partial q}{\partial x} \tag{4.5}$$

where $D_o(q)$ is the corrected intracrystalline diffusivity. Comparing the Equations (4.1) and (4.5);

$$D_c = D_o(q)\frac{d \ln p}{d \ln q} \tag{4.6}$$

Equation (4.6) indicates that the Fickian diffusivity approaches a limiting value, $D_o(q)$, only when Henry's law is obeyed, i.e., $d\ln p/d\ln q = 1$. However, the corrected diffusivity may still be a function of the concentration.

These expressions relate molar fluxes and concentration or chemical potential gradients, but the rates of adsorption is expressed as concentration change inside the porous medium as a function of time:

$$\frac{\partial q}{\partial t} = D_c(q)\frac{\partial^2 q}{\partial x^2} \tag{4.7}$$

This expression is known as Fick's second Law.

4.2. Resistances to Mass and Heat Transfer

There are several distinct resistances to mass and heat transfer and the determination of which resistance or resistances control mass transfer requires detailed examination of the kinetic data recorded under well-controlled conditions.

Zeolites have a well-defined bimodal pore size distribution. Most applications involve a fixed bed with adsorbent particles as shown in Figure 4.1.
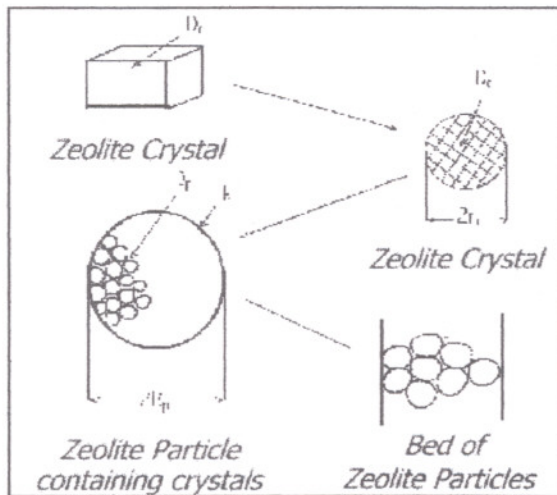
Figure 4.1. Schematic diagram of a bed of composite adsorbent pellets
containing zeolite, showing the principal resistances to mass transfer

34

These particles are formed by combining many zeolite crystals. Each crystal contains intracrystalline pores that are on the order of molecular dimensions. The intercrystalline space between the particles forms another set of pores (macropores), which are typically of dimensions of tenths of a micron (Figure 4.2). Primary porosity is defined by crystal micropores constituting the main transport channels and secondary porosity by transfer pores and macropores.
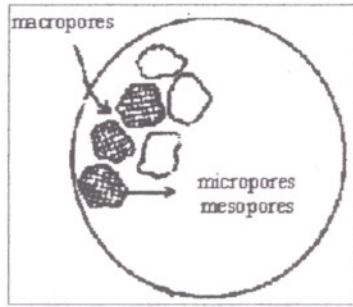
Figure 4.2. Schematic diagram for the biporous adsorbent particle [38]

The adsorption of molecules occurs in three steps: first the adsorbate molecules go from the gas phase to the adsorption sites within the adsorbent through the gas layer around the adsorbent pellets, then diffuse in macropores between the porous particles, and at the end diffuse in micropore and mesopores within the adsorbent crystals to adsorption sites. Therefore, a biporous adsorbent of the type sketched in Figure 4.2 offers distinct resistances to mass transfer as the diffusional resistance of the micropores of the zeolite crystals, and diffusional resistance of the meso and macropores. In addition, when adsorption occurs from binary or multicomponent fluid phase, there maybe an external resistance associated with diffusion through the laminar fluid film.

Since adsorption is in general an exothermic process the temperature of the adsorbent will remain constant only when the rate of heat dissipation by conduction, convection, and radiation is high relative to the adsorption rate. There are also three distinct resistances to heat transfer; conduction through micro and macro particles and convection/radiation from the external surface. The latter is generally the most important.

4.2.1. Diffusion in Micropores

Diffusion within a pore structure is composed of the inaccessible regions corresponding to the rigid framework, active sites, windows between cages and free volume within a cage. Diffusion in micropores is dominated by interactions between the diffusing molecule and the pore wall. Steric effects are important. Diffusion through micropores often occurs as an activated jumping process in which the adsorbate molecule jumps from one adsorption site to the next. This process is characterized by the micropore (configurational or intarcrystalline) diffusion coefficient [38].

The micropore diffusion coefficient for the diffusing molecule is related to the zeolite pore geometry and size; zeolite composition (Si/Al ratio), type, charge and distribution of exchangeable cations, shape, size and polarity of the sorbate molecules; concentration of sorbate molecules and temperature. It changes strongly with the molecular dimensions of the sorbate molecule and the free dimensions of the openings (6-, 8-, 10- and 12-rings) through which adsorbate molecules diffuse. If the sorbate molecules can occupy both window and cage sites, the probability of passage through that window will be prohibited or greatly reduced by the presence of a molecule within a window site. The diffusivity is reduced more strongly by molecules within the intersections, since blockage of an intersection prohibits passage through four different channel segments [13].

4.2.2. Diffusion in Mesopores

Within the mesopore range, the role of surface is relatively less important. Diffusion through these pores usually occurs by molecular diffusion or Knudsen diffusion, depending on the conditions and the relative size of pore to the mean free path length of the diffusing molecule. The bulk or molecular diffusion mechanism occurs since collisions between the diffusing molecules occur more frequently than collisions between a diffusing molecule and the pore wall. Knudsen diffusion is generally more important but there may also be significant contributions from surface diffusion and capillary effects. When the mean free path is comparable with the pore diameter, both of those collisions are significant and diffusion occurs by the combined effects of both molecular and Knudsen diffusion mechanisms [38].

4.2.3. External Film Resistance

Besides the internal diffusional resistances (micropore and mesopore diffusional resistances), there exists external resistance to mass transfer when there is more than one component in the fluid phase. This arises due to the fact that the surface of an adsorbent particle is always surrounded by a laminar boundary layer through which transport can occur only by molecular diffusion. Significance of the external film resistance depends on the hydrodynamic conditions. In general, for porous particles, this external resistance to mass transfer is smaller than the internal pore diffusional resistance but it may still be large enough to have a significant effect on mass transfer [38].

4.3. Relative Significance of Mass and Heat Transport Parameters

Relative importance of internal and external mass and heat transfer resistances can be determined by the Biot numbers for mass, $(Bi)_m$, and heat $(Bi)_h$, transfer representing the ratio of internal-to-external gradients and are defined by:

$$(Bi)_m = \frac{kR_p}{3\varepsilon_p D_p} \qquad (4.8)$$

$$(Bi)_h = \frac{hR_p}{3\lambda_s} \qquad (4.9)$$

or in terms of Sherwood ($Sh = \dfrac{2kR_p}{D_m}$) and Nusselt numbers ($Nu = \dfrac{2hR_p}{\lambda_g}$):

$$(Bi)_m = \frac{Sh}{6}\frac{D_m}{\varepsilon_p D_p} \qquad (4.10)$$

$$(Bi)_h = \frac{Nu}{6}\frac{\lambda_g}{\lambda_s} \qquad (4.11)$$

where λ_g is thermal conductivity of gas phase and λ_s is thermal conductivity of solid. Since $Sh \geq 2$ and $D_p \leq D_m/\tau$, the minimum value of $(Bi)_m$ is given by $\tau/3\varepsilon$ (~3.0). Thus, even under these extreme assumptions the internal concentration gradient is greater than the external gradient. Under most practically realisable conditions the intraparticle resistance is more important than film resistance in determining the mass transfer rate. Assuming that the temperature is uniform throughout an adsorbent particle, the major resistance to heat

transfer lies in the external fluid film rather than within the particle. For a gaseous system, $\lambda_s/\lambda_g \sim 10^2$-$10^3$ so at any reasonable Reynolds number $(Bi)_h \leq 1.0$, indicating that the external temperature gradient is much greater than the temperature gradient within the particle [39].

Internal mass transfer mechanisms depend on the channel geometry and the nature of diffusing molecules, their interactions with each other and with the surrounding. In any particular system, the nature of the controlling mechanism may generally be established by varying experimental conditions, for example, varying the sizes of crystals and the particles, micropore and mesopore diffusion resistances can be distinguished experimentally.

A single effective diffusion coefficient is not enough to characterize the mass transfer within an adsorbent particle with a bimodal pore size distribution, when the contributions from both pore systems, micropores and macropores, occur [40]. Depending on the particular system and the conditions, either macropore or micropore diffusion resistances or more than one resistance may control the transport behaviour or both resistances may be significant. The relative importance of micropore and macropore resistances depends on the ratio of the diffusional time constants, $(D_c/r_c^2)/(D_p/R_p^2)$, where D_p is macropore diffusivity; r_c and R_p are crystal and particle radii, respectively.

Therefore, the diffusion must be described in terms of effective diffusivity. In this case, the kinetic data is interpreted with a model including both "micropore" and "macropore" diffusional resistances.

4.4. Methods of Measuring Transport Diffusivities

Measurement of transport diffusivities includes determination of the resultant molecular fluxes of the system which is subjected to nonuniform concentration of sorbate. These measurements may be performed under steady-state conditions in which the concentration gradient is kept constant during the experiment or under transient conditions in which the concentration gradient and the resulting fluxes vary continuously during the measurement. The later measurement is called as direct measurement, since the diffusivity is calculated directly from the experimentally measured quantities. The most commonly used experimental techniques are given in Table 4.1 [38].

Table 4.1. Some Experimental Methods for Measuring Transport Diffusivities

I. Steady-State Measurement Techniques
    Wicke-Kallenbach Method
    Membrane Method

II. Transient Measurement Techniques
    NMR Technique
    Tracer Exchange Method
    Uptake Rate Methods
    Batch Methods (eg. Gravimetric, volumetric)
    Flow Methods (eg. Chromatography, ZLC)

The range of intracrystalline diffusivities can be determined experimentally and is bounded by both upper and lower limits due to practical considerations.

4.4.1. Steady-State Measurement Techniques

4.4.1.1. Wicke–Kallenbach Method

This is a steady-state method of measuring transport diffusion in microporous solids. A stream of carrier gas containing a small concentration of the test gas passes over one face of the pellet while pure carrier is passed over the other face. The pressures at both faces of the pellet are equalized by differential pressure cell to provide efficient mixing. The composition and flow rate of the gas streams leaving both sides of the cell are monitored, then the effective diffusivity, D_{eff} can be calculated from:

$$J = D_{eff} \frac{\Delta c}{t_p} \tag{4.12}$$

where Δc is the concentration difference between the two faces of the pellet and t_p is the pellet thickness. The apparatus is shown in Figure 4.3 [38].
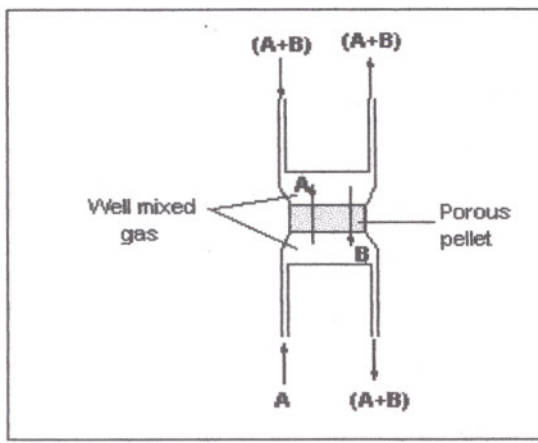
Figure 4.3. Schematic diagram showing the Wicke-Kallenbach apparatus

It is possible to measure the relative contribution of Knudsen and molecular diffusion by making measurements over a range of concentration. However, effective intraparticle diffusivity determined by the Wicke–Kallenbach Method is usually smaller than the values determined from transient uptake rate measurements, since blind pores contributing to the flux in a transient measurement make no contribution in this system. Moreover, the measurement of micropore diffusivity by this technique has some diffuculties such as mounting and sealing a single zeolite crystal.

4.4.1.2. Membrane Technique

In this method, a membrane made up of a large single zeolite crystal of a few hundred micron in size and of thickness L is mounted in a metal plate and sealed with epoxy resin. After activation of the zeolite by heating in vacuum, the inflow side of the membrane is exposed to diffusing gas at a constant pressure. Experimental set up for this method is given in Figure 4.4 [38].
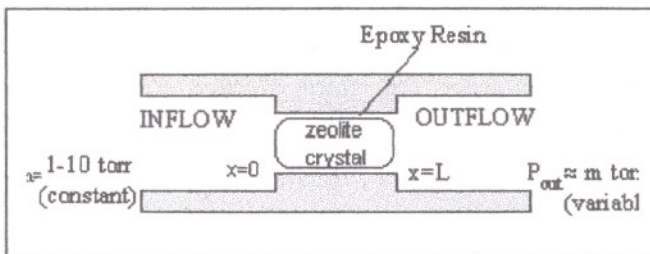
Figure 4.4. Schematic diagram of the membrane technique

The micropore diffusivity can be determined by monitoring the increase in pressure with time in the constant volume cell at the outflow side of the membrane. Since the molar fluxes through the membrane are extremely small, a steady-state approach is generally valid. The membrane technique is only suitable for zeolite types allowing the synthesis of very large single crystals. However, the perfectness of these crystals is questionable.

4.4.2. Transient Measurement Techniques

4.4.2.1. Nuclear Magnetic Resonance (NMR) Method

NMR technique provides more convenient method for the measurement of self-diffusivities as compared to the tracer exchange method. A pulsed magnetic gradient field is applied to a sample in which the nuclear spins are excited by a radio frequency magnetic pulse of suitable duration and intensity. The nuclear spins preceed with an angular velocity determined by the position of the molecule at time zero. After a known time interval the gradient pulse is reversed. If there were no diffusion, the second gradient pulse is exactly counteracting the effect of the first pulse. However, as a result of molecular migration the cancellation is incomplete and square the displacement during the known time interval between gradient pulses. Nuclear magnetic resonance relaxation times are related to the motion of molecules, i.e., molecular mobility, which is expressed in terms of the self-diffusivity. Therefore, the self-diffusivity value can be estimated from the known average jump length. Schematic diagram of the system is shown in Figure 4.5 [38].
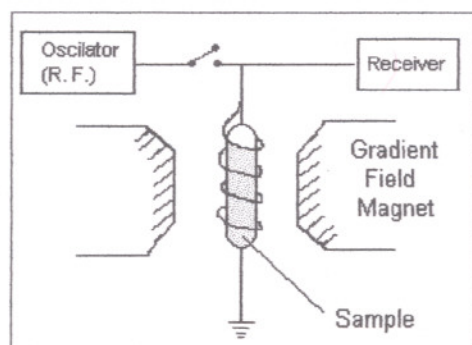
Figure 4.5. Schematic diagram showing the principal features of NMR method

The method has the disadvantage of being restricted to the measurements only for species such as hydrocarbons which contain a sufficiently high concentration of unpaired nuclear spins. In addition, the method is limited to the measurement of self-diffusivities for relatively rapidly diffusing systems ($D > \sim 10^{-8}$ cm^2/ s). In the modified type of the NMR techniques, the self-diffusivity is measured directly and the jump length is not needed.

4.4.2.2. Tracer Exchange

By this method, using isotopicaly labelled species, it is possible to measure the self-diffusivities. The adsorbent particle is exposed to a change in the concentration of an isotopically labelled tracer at constant total sorbent concentration. This method is particularly convenient when one of the isotopes is radioactive. Nonradioactive isotopes may also be used if the progress of the exchange is followed by mass spectrometer analyzing the surrounding vapour [38].

4.4.2.3. Uptake Rate Measurements

The uptake rate measurement methods for determination of intraparticle or intracrystalline diffusivities involve measurement of the sorption rate when a sample of adsorbent is subjected to a step change in the surface concentration or pressure of an adsorbable species. Then the diffusivity may be determined by matching the experimental uptake curve to the appropriate transient solution of the Fick's second law equation (Equation 4.8) for the relevant boundary conditions.

In applying this method to the measurement of intracrystalline diffusivities in zeolites, the adsorbent sample should be as small as possible in order to minimize external mass transfer resistances. The contribution of external mass transfer resistance should be checked by changing the adsorbent amount. Also, it is required to test the importance of intracrystalline diffusion by varying the crystal size. The system linearity should be verified varying the concentration step size and measuring both adsorption/desorption curves, since for a linear system, the uptake curve should remain the same.

Uptake rate methods provide a straightforward way for the estimation of intraparticle or macropore diffusivities, since the intrusion of heat transfer effects may be eliminated by the use of sufficiently large adsorbent particles and the effect of nonlinearities may be eliminated by making the experimental measurements over a small

42

differential concentration change. On the other hand, the interpretation of the experimental data is less straightforward.

4.4.2.4. Gravimetric Method

In this method, an adsorbent sample outgassed at high temperature in vacuum prior to the adsorption run, is subjected to a step change in sorbate pressure at time zero, and the change in the weight of the adsorbent is recorded as a function of time using a microbalance system. The pressure of the sorbate is kept constant during the experiment. Simplified set-up for gravimetric measurements is given in Figure 4.6.
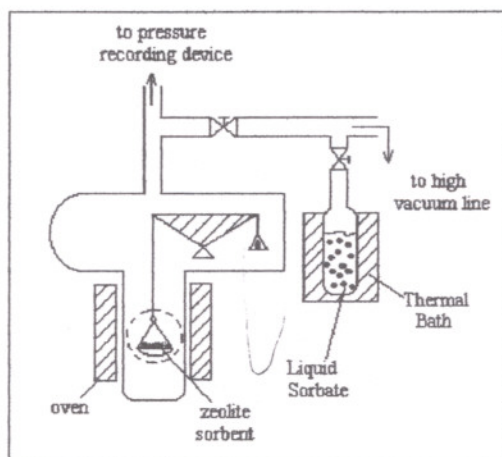
Figure 4.6. Set-up for gravimetric measurements

In order to reduce the effects of bed diffusion and heat transfer, amount of adsorbent sample size should be kept as low as possible. It is required to vary the adsorbent weight, particle size and crystal size in order to separate the contributions of the various diffusion resistances. However, the interpretation of the transient curve obtained by the gravimetric method may be too complicated.

4.4.2.5. Volumetric (Uptake) Method

As in the gravimetric method, the volumetric method involves subjecting a zeolite sample to a step change at zero time. The pressure of the sorbate is varied during the experiment and the reliable measurements of this change in pressure is recorded as a function of time . A simplified set-up for volumetric experiments is shown in Figure 4.7.
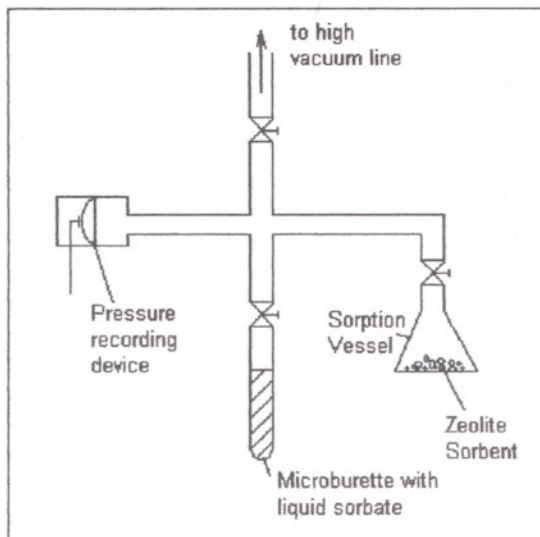
Figure 4.7. Set up for volumetric measurements

The variation of sorbate pressure during the uptake experiments makes the analytical solution of the diffusion equation complex. No simple, straightforward analytical solutions are available.

4.4.2.6. Zero Length Column (ZLC) Method

The ZLC measurements are carried out under limiting conditions of high flow rate to maintain a very low sorbate concentration at the external surface of the particles such that the column behave as a differential bed. The initial sorbate concentration is kept low within the Henry's Law region, so the desorption rate curves can be interpreted simply. Set up for ZLC method is shown in Figure 4.8 [38].
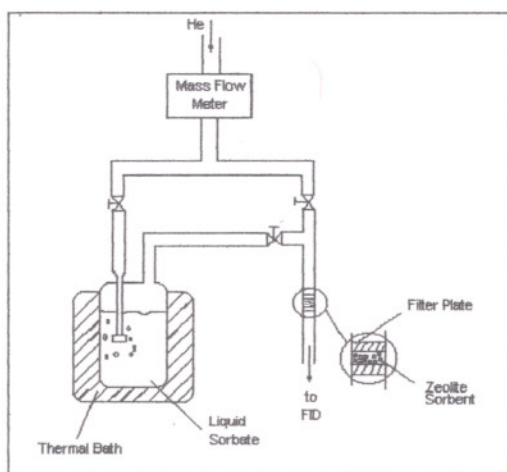
Figure 4.8. Set up for ZLC measurements

The ZLC method not only has the advantage of good heat transfer and external mass transfer of the chromatographic method but also eliminates the problem that arises from axial dispersion. The absence of significant extracrystalline resistance can be tested using two different carrier gases with different molecular diffusivities and by varying the purge flow rate.

The applicability of the ZLC method is limited to zeolite samples having crystals larger than a few micrometers in size, since the high purge flow rates is required in order to maintain isothermal conditions.

4.4.2.7. *Chromatography*

In the chromatographic method, the mass transfer resistance is determined measuring the dynamic response of a column to a pulse of a sorbate at the column inlet. During the measurements a flow of an inert carrier is passed through a small column packed with the adsorbent under study. At time zero a small pulse of sorbate is injected at the column inlet and the effluent concentration is monitored continuously. Schematic diagram for chromatograph is given in Figure 4.9.
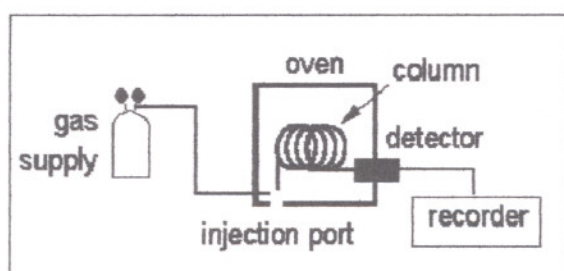
Figure 4.9. Schematic diagram of a gas chromatograph

The mean retention time is a measure of the adsorption equilibrium (Henry's Law constant) while the dispersion of the response peak is determined by the combined effects of mass transfer resistance and axial mixing in the column. By conducting measurements over a range of conditions it is possible to separate the contributions to the peak broadening from mass transfer resistance and axial mixing.

Performing the experiments at low concentrations within the Henry's Law region of the isotherm simplifies the interpretation of the data. In this region of the isotherm, the retention time becomes independent of the size of the sorbate pulse, so changing the pulse size the validity of linearity assumption can be checked.

Chromatographic method offers simplicity and rapidity in producing data, suitability for higher temperature and pressure, applicability in a wider range of diffusivity values and in low sorbate concentration measurements than the more conventional static (gravimetric, volumetric) methods. Furthermore, external mass and heat transfer effects are minimized, since the carrier gas continuously passes through the packed bed. The method can be applied over the entire concentration range. Moreover the equilibrium is not affected since the pulse size is small. However, the method is limited to the low concentration region, if the moment method will be used for analysis of the chromatographic data. Also, as the chromatographic method measures only the total mass transfer resistance, the measurements should be carried out under different experimental conditions to separate the contributions from film, macropore and micropore resistances.

In this study, the chromatographic method was found suitable for determination of micropore diffusivity of carbon monoxide in clinoptiolite due to its advantages.

4.5. Mathematical Model for a Chromatographic Column

Transport properties can be obtained using chromatography by comparing the experimental peaks with mathematical models to obtain equilibrium and transport parameters by chromatographic method. Gas flow through a packed column is generally represented by the axially dispersed plug flow model. A carrier gas containing adsorbate concentration of c (z,t) flows through this column. The differential mass balance equations for an element and for an adsorbent particle within this element are derived from a mass balance on the element of the column that is shown in Figure 4.10 [38], as ;

$$-D_L \varepsilon \frac{\partial^2 c}{\partial z^2} + \varepsilon \frac{\partial}{\partial z}(vc) + \varepsilon \frac{\partial c}{\partial t} + (1-\varepsilon)\frac{\partial \overline{q}}{\partial t} = 0 \qquad (4.13)$$
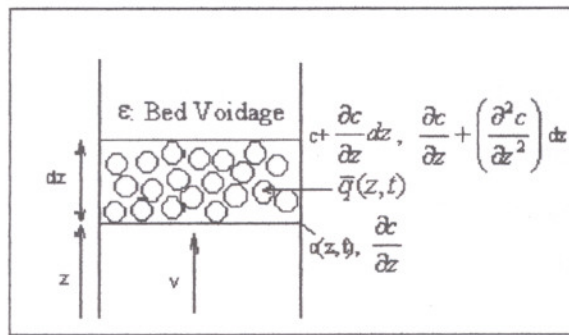
Figure 4.10. Mass balance on a differential element of the chromatographic column

If the system is isothermal, the pressure drop is negligible and the concentration of the adsorbate is small, the gas velocity can be assumed constant through the column and Equation (4.13) reduces to:

$$-D_L \varepsilon \frac{\partial^2 c}{\partial z^2} + \varepsilon v \frac{\partial}{\partial z} c + \varepsilon \frac{\partial c}{\partial t} + (1-\varepsilon) \frac{\partial \overline{q}}{\partial t} = 0 \qquad (4.14)$$

The $\partial q / \partial t$ term represents the local mass transfer rate averaged over an adsorbent particle. To obtain the dynamic response of the system, $c=c(z,t)$, Equation (4.14) must be solved simultaneously with the mass transfer rate expression:

$$\frac{\partial \overline{q}}{\partial t} = f(c,q) \qquad (4.15)$$

where $\overline{q}$ is adsorbed phase concentration averaged over an adsorbent particle. The relevant boundary conditions for pulse perturbation to initially sorbate-free column are as follows:

$$c(z,0) = q(z,0) = 0, \qquad c(0,t) = c_o \delta(t) \qquad (4.16)$$

where c_o is the initial sorbate concentration in the bulk phase. In chromatographic measurements of intraparticle diffusivities, since the sorbate concentration perturbation (size of the pulse) is small, linear systems are concerned so that the equilibrium relationship can be expressed in the form of;

47

$$q^* = Kc \tag{4.17}$$

where q* is the adsorbed sorbate concentration at equilibrium and K is the dimensionless Henry's law constant. Transport properties can be obtained by comparing the experimental response peaks with a mathematical model to obtain equilibrium and transport parameters by chromatographic method either by moment method or by time domain analysis.

4.6. Perturbation Chromatography

In perturbation chromatography, a sorbate-free column is initially brought to equilibrium with a flowing pure or multicomponent carrier gas. Then the system is perturbated by either a pulse of the pure adsorbate or a pulse of the radioactive isotope of one or more components. The former is referred to as the concentration pulse method, the latter as the tracer pulse method.

The concentration pulse chromatography technique involves injection of a small amount of single or multi-component gas mixture carried by pure or multicomponent carrier gas to the column and monitoring the detector output as a function of time (Figure 4.12). The perturbation can be performed as either a step change (step input) or as a small pulse of sorbate at the column inlet (pulse input). The response to a step input is commonly called the breakthrough curve while the pulse response is often referred to as the chromatographic response. As long as the perturbation is small, the technique can be used for high concentrations. Exactly the same information may be derived from the response to either input and the choice is therefore determined by practical convenience rather than by more fundamental theory.

The chromatographic response peaks obtained (illustrated in Figure 4.13) are processed and integrated numerically to determine the first and second moments. Information on adsorption equilibrium and kinetics can be obtained through mathematical analysis. The analysis can be accurate only under the conditions of low sorbate concentration, isothermal operation, axially dispersed plug flow regime in the column, instantaneous equilibrium between the sorbate containing carrier gas and adsorbent phases for both concentration and temperature and negligible pressure drop across the packed column.
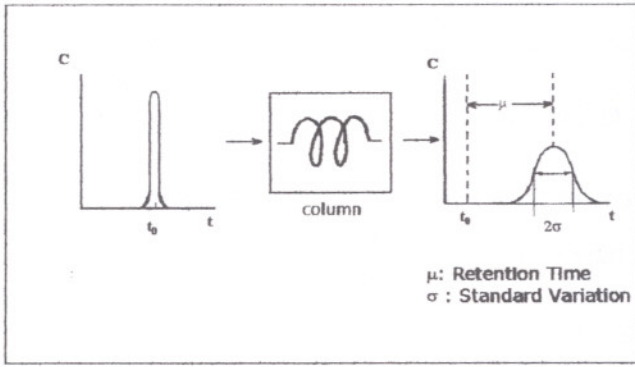
Figure 4.11. Pulse injection and response peak
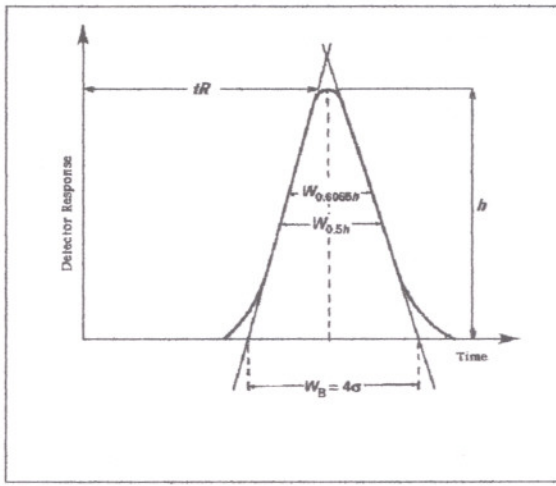
Figure 4.12. Chromatographic response peak.

However, Hyun and Danner [41] have shown that even under idealized conditions the mathematical analysis of the data can not be accurately achieved for mixtures containing three or more components. The results obtained by using this method have been shown to be close to those by the dynamic and static methods.

If the time of passage through the column is shorter than the time constant for micropore diffusion ($\frac{r_c^2}{15KD_c}$), the adsorbate molecules penetrate only the macropores. Therefore, a Gaussian response peak is obtained with a mean retention time equal to the hold-up in the macropores and the intraparticle void space, $t \approx \frac{L}{\varepsilon v}[\varepsilon + (1-\varepsilon)\varepsilon_p]$. The symbol of r_c represent the crystal radius, ε and ε_p represent bed and particle porosity, respectively, and v is interstitial velocity of the carrier gas.

49

If the time of passage through the column is longer than the time constant for macropore diffusion ($\frac{R_p^2}{15\varepsilon_p D_p}$), where R_p is particle radius and D_p is pore diffusivity, the adsorbate molecules will completely penetrate into the micropores. Thus, a nearly Gaussian response peak is observed which is centered on the mean retention time, as given by $\mu = \frac{L}{v}\left[1 + \left(\frac{1-\varepsilon}{\varepsilon}\right)K\right]$. If the time of passage is comparable to the micropore time constant, then the strongly tailed response peak is obtained with the maximum located between t and $\tilde{t} = \frac{L}{\varepsilon v}\left[1 + (\frac{1-\varepsilon}{\varepsilon})K\right]$. These three cases were reported by Sarma and Haynes [42] for diffusion of Argon in 3A, 4A, and 5A zeolites as shown in Figure 4.13.
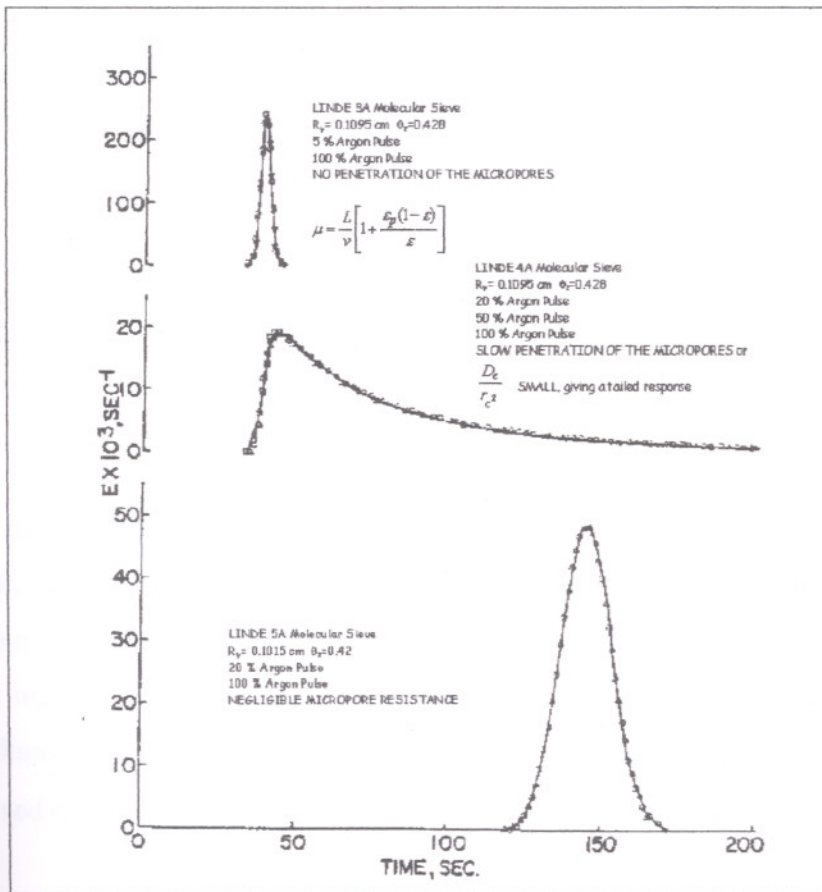
Figure 4.13. Experimental response curves for Ar in a He carrier, measured under similar conditions in columns packed with 3A zeolite pellets (no penetration of the micropores), 4A zeolite pellets (slow penetration of the micropores, a tailed response), and 5A zeolite pellets (negligible micropore resistance) [42].

50

4.7. The Moment Method

The moment method is the simplest and straightforward way of analyzing the chromatographic data. The first statistical moment of the chromatographic response peak is a measure of how strongly the gas is adsorbed and can be calculated from the experimental concentration versus time curve. At infinite dilution, the mean retention time which is directly related to the equilibrium constant is called as Henry's Law Constant. Furthermore, the broadening of the response peak is the result of combined effects of axial dispersion and mass transfer resistances. As mass transfer resistance increases, broader peak is obtained. The first and second moments of the response peak can be directly calculated from numerical peak data by integrating the following expressions:

$$t_{R,packed} = \frac{\int_0^\infty t c(t) dt}{\int_0^\infty c(t) dt} \qquad (4.18)$$

$$\sigma^2_{packed} = \frac{\int_0^\infty (t - \mu)^2 c(t) dt}{\int_0^\infty c(t) dt} \qquad (4.19)$$

where $c(t)$ is the gas phase concentration measured by the detector, $t_{R,\ packed}$ and σ^2_{packed} are experimentally determined first and second moments of the response peak, respectively.

These moments contain also contributions due to non-column effects, i. e., gas flow between the injector and the column inlet, between the outlet of the column and the detector. These dead volume terms are represented by t_{empty} and σ^2_{empty}, and the net moments (μ and σ^2) are calculated from the following expressions [43]:

$$\mu = t_{R,packed} - t_{R,empty} \qquad (4.20)$$

$$\sigma^2 = \sigma^2_{packed} - \sigma^2_{empty} \qquad (4.21)$$

Haynes and Sarma [40] have developed moment expressions for concentration pulse chromatography at infinite dilution region. These equations are valid for a bidisperse system of spherical particles:

$$\mu = \frac{L}{v}\left[1+\left(\frac{1-\varepsilon}{\varepsilon}\right)K\right] \qquad (4.22)$$

where L is the column length, v is the interstitial velocity and K is the dimensionless equilibrium constant expressed in terms of pore volume (moles adsorbed per unit pore volume/moles per unit volume in gas phase) or Henry's Law constant. Equation (4.22) reveals that the retention time of a pulse is approximately proportional to both the equilibrium constant and the residence time of a carrier gas (L/v). Temperature dependence of the Henry's Law constant obtained at various temperatures is given by the van't Hoff equation as:

$$K = K_{o}\,\exp\!\left(\frac{-\Delta U_{o}}{RT}\right) \qquad (4.23)$$

where K_o is pre-exponential factor and ΔU_o is the internal energy change of adsorption at low concentration within the Henry's law region. K_o and ΔU_o are derived from the intercept and the slope of the van't Hoff plot (semi-log K versus 1/T), respectively. Then ΔH_o, limiting heat of adsorption (isosteric heat of adsorption, heat of adsorption at zero coverage) can be calculated as;

$$-\Delta H_{o} = -\Delta U_{o} + RT \qquad (4.24)$$

where T is taken as the mean of the experimental temperature range. From Equation (4.19), the general form of the second moment for a biporous adsorbent can be expressed as;

$$\frac{\sigma^{2}}{2\mu^{2}} = \frac{D_{L}}{vL} + \frac{\varepsilon v}{L(\varepsilon-1)}\left(\frac{R_{p}}{3k} + \frac{R_{p}^{2}}{15\varepsilon_{p}D_{p}} + \frac{r_{c}^{2}(K-\varepsilon_{p})}{15D_{c}K^{2}}\right)\left(1+\frac{\varepsilon}{(1-\varepsilon)K}\right)^{-2} \qquad (4.25)$$

For gaseous systems, since K is often large, $\varepsilon/(1-\varepsilon)$ K is small and $(K-\varepsilon_p)/K^2 \approx 1/K$, thus Equation (4.25) is simplified to;

$$\frac{\sigma^2 L}{2\mu^2 v} = \frac{D_L}{v^2} + \frac{\varepsilon}{\varepsilon - 1}\left(\frac{R_p}{3k} + \frac{R_p^2}{15\varepsilon_p D_p} + \frac{r_c^2}{15 D_c K}\right) \tag{4.26}$$

In order to determine the micropore diffusivity, other mass transfer contributions must be estimated. Experimental conditions should be chosen such that micropore diffusion is the dominant mechanism for mass transport.

The first term on the right-hand side of the Equation (4.26) stands for the contribution from axial dispersion. Axial dispersion of a gas through a packed column can be represented by;

$$D_L = \tau_L D_m + \beta v 2 R_p \tag{4.27}$$

where v is the interstitial velocity, D_m is molecular diffusivity, τ_L and β are constants, typically $\tau_L = 0.7$ and $\beta = 0.5$. Since at low Reynolds where axial dispersion occurs primarily by molecular diffusion, D_L is approximately independent of velocity.

Relative importance of molecular or Knudsen diffusivity in macropores is largely determined by the average diameter of the macropores. The macropore diffusion resistance arises from collisions between diffusing molecules. Molecular diffusion is the dominant mechanism if the mean free path of the gas molecule is smaller than the pore diameter. The mean free path (λ) is defined as the average distance travelled between molecular collisions and can be estimated from the expression by Cunningham and Williams [44]:

$$\lambda = \frac{k_B T}{\sqrt{2}\pi\sigma_{ii}^2 p} \tag{4.28}$$

where k_B is Boltzman constant, σ_{ii} is the collision diameter of the diffusing molecules. In small pores and at low pressure, the mean free path becomes greater than the pore diameter.

Under these conditions diffusing molecules collide with the pore walls more frequently than they collide with each other. In this case Knudsen diffusion predominates in the macropore and Knudsen diffusivity can be calculated as:

$$D_K = 9700\bar{r}\sqrt{\frac{T}{M}} \qquad (4.29)$$

where D_K is the Knudsen diffusivity, $\bar{r}$ is the mean macropore radius and M is the molecular weight of the diffusing molecule [38]:

The macropore diffusivity (D_p) can be estimated as:

$$D_p = D_K 9700\bar{r}\sqrt{\frac{T}{M}} \qquad (4.30)$$

On the other hand, molecular diffusion becomes significant in larger macropores. If transport within the macropores occurs only by molecular diffusion, the pore diffusivity is given by:

$$D_p = \frac{D_m}{\tau} \qquad (4.31)$$

where τ is the tortuosity factor in which effects of pore orientation, size variation and connectivity on diffusion are lumped. Experimental macropore tortuosity factors reported generally lie in the range of 1.7 to 6 [39]. Tortuosity factor is typically 3 for straight cylindrical pores.

In the transition region, where both mechanisms are significant in macropore diffusion, the pore diffusivity can be calculated according to the equation;

$$\frac{1}{D_p} = \tau\left(\frac{1}{D_m} + \frac{1}{D_K}\right) \qquad (4.32)$$

D_m can be estimated by the use of Chapman-Enskog theory [45]:

$$D_m = \frac{0.001867 T^{3/2} \sqrt{\frac{1}{M_1} + \frac{1}{M_2}}}{P \sigma_{12}{}^2 \Omega} \tag{4.33}$$

where M_1 and M_2 are molecular weights of the diffusing gases and P is the total pressure in atm $\sigma_{12} = \frac{1}{2}(\sigma_1 + \sigma_2)$ is the collision diameter from the Lennard-Jones potential, $\Omega = f(\frac{\varepsilon'}{k_B T})$ where $\varepsilon' = \sqrt{\varepsilon_1 \varepsilon_2}$ is the Lennard-Jones force constant. These constants are given in Table 4.2 [96].

Table 4.2. Lennard-Jones constants for the carrier gas (He) and for adsorbate (CO)

Substance	σ_1 (Å)	ε'/k (K)
He	2.551	10.22
CO	3.690	91.7

Besides the internal diffusional resistances (micropore and macropore diffusional resistances), there exists external resistance to mass transfer whenever there is more than one component in the fluid phase. This arises due to the fact that the surface of an adsorbent particle is always surrounded by a laminar boundary layer through which transport can occur only by molecular diffusion.

Significance of the external film resistance depends on the hydrodynamic conditions. In general, for porous particles, this external resistance to mass transfer is smaller than the internal pore diffusional resistance but it may still be large enough to have a significant effect on mass transfer. The capacity of the fluid film is smaller than that of the adsorbent particle, thus there is very little accumulation of sorbate within the film. This implies a constant flux and a linear concentration gradient through the film. The external film resistance is generally correlated in terms of dimensionless numbers of the type [39]:

$$Sh \equiv \frac{k(2R_p)}{D_m} = f(\text{Re}, Sc) \tag{4.34}$$

For an isolated spherical adsorbent particle in a stagnant fluid, Sherwood number is equal to 2. At low Reynolds numbers, the external film mass transfer coefficient may be estimated as:

$$Sh \equiv \frac{2kR_p}{D_m} \quad \text{or} \quad \frac{kR_p}{D_m} \approx 1 \tag{4.35}$$

where R_p is the particle diameter.

Ranz and Marshall [46] suggested the following expression for the determination of the Sherwood number for packed columns:

$$Sh = \frac{2R_p k}{D_m} = 2 + 0.6Sc^{0.33}\,\text{Re}^{0.5} \tag{4.36}$$

where Sc is Schmidt number $Sc = \dfrac{\mu}{\rho D_m}$ and Re is Reynolds number $\text{Re} = \dfrac{2\rho v_i \varepsilon R_p}{\mu}$.

The contributions from mass transfer resistance and axial dispersion can be separated by measurements over a range of fluid velocities. Consequently, the micropore diffusion coefficient is calculated by subtracting the contributions of axial dispersion, external mass transfer and macropore diffusional resistance from the overall dispersion. Reliable values for the micropore diffusivity can only be obtained when it is the dominant mass transfer mechanism.

CHAPTER 5

PREVIOUS STUDIES

This chapter is dedicated to review the previous studies on adsorption kinetics and equilibrium performed by gas chromatography. The first section deals with the development and application of chromatographic models for determination of equilibrium and kinetic parameters in gas-solid systems. Then, the experimental studies carried out to study the effects of regeneration conditions and structural properties of zeolites will be reviewed.

5.1. Adsorption Equilibrium and Kinetic Models

A mathematical model is required to analyze and interpret the data from a chromatographic experiment. The adsorption kinetic and equilibrium parameters can then be derived by matching the experimentally determined response peaks to the model parameters. Chromatographic processes can be described theoretically by the plate and rate theories. The plate theory assumes that equilibration is infinitely fast. The rate theory is more realistic description of the processes inside a column and considers the time taken for the solute to equilibrate between the adsorbent and carrier gas.

The first scientist to recognize chromatography, as an efficient method of separation was the Russian botanist Tswett, who employed a primitive form of liquid solid chromatography to separate and isolate various plant pigments in the late 1890s. Martin and Synge [53] were first to use chromatography for physicochemical measurements. They developed a theory for solute migration through a chromatographic column. The plate theory, in which the column is represented as a series of hypothetical well-mixed stages, was introduced in their study. In 1952, Lapidus and Amundson [102] first applied rate

theory to chromatographic systems. They solved the column mass balance equation analytically including an axial dispersion term.

Van Deemter et al. [47] compared the results of the plate and rate theories and developed simple model. This model assumed a linear isotherm. It is based on single pore diffusivity and correlates the sources of band broadening to the theoretical plate height (H.E.T.P.) and carrier gas velocity as:

$$H.E.T.P. = A + B/v + Cv \qquad (5.1)$$

where v is interstitial carrier gas velocity. The constants A, B and C can be related to the sources of band broadening; eddy diffusion, molecular diffusion and resistance to mass transfer, respectively. They analyzed their experimental data by plotting H.E.T.P. versus the carrier gas velocity. C was determined from the limiting slope at high carrier gas velocities and related to the molecular diffusion coefficient, D_m and the effective diffusion coefficient in the porous adsorbent, D_{eff}.

Ma and Mancel [51] applied the equation developed by van Deemter et al. (Equation 5.1) to obtain effective diffusion coefficients of CO_2, NO, NO_2 and SO_2 on 5A, 13X and mordenites in the temperature range of 133 to 325°C. The adsorbents were regenerated at 400°C for 15 hours under helium atmosphere prior to the experimental runs. They discussed the effective diffusivity resulted from contributions of micropore and macropore diffusion terms, but in which manner these two diffusion terms combined was not known, since the theory of van Deemter was applicable only to an adsorbent with unimodal pore size distribution. The diffusion coefficients and isosteric heats of adsorption for these systems were measured by gas chromatographic methods. The variation of diffusion coefficients, heats of adsorption, and activation energies were discussed in terms of the interaction between the surface and gas molecules, and also in terms of the relative openings of the pores with respect to the size of the diffusing molecules. The effective diffusion coefficient of NO in 13X sieves was found larger than in 5A due to the large openings of the 13X and due to reaction of NO with the 5A sieve. They couldn't observe response peak for SO_2 in the temperature range of 133-261°C due to very strong adsorption of SO_2 on 13X. It was concluded that relative size of the pores of zeolites to the size of diffusing molecules was important in diffusion. Additionally, it was reported that if the

pore size of molecular sieve zeolite was comparable to that of the diffusing molecules, the interaction occurred between the cations in the zeolite framework and the gas molecules. These interactions play an important role in diffusion and adsorption. They have also reported that the low diffusion coefficient was associated with the high activation energy and high isosteric heat of adsorption.

The theoretical description of chromatographic processes through the use of rate theory continued through the 1960's and 1970's. The more exact theory of chromatography taking various mass transfer resistances in the packed column into account was introduced by a single pore model of Kucera [48] and Kubin [49]. In this model, the moments of the chromatographic peak were related to the mass transfer parameters. They accounted for axial dispersion flow through the column, external film resistance at the particle surface, intraparticle diffusion and finite rate of adsorption to the pore surface. Carleton et al. [101] modified the Kubin-Kucera first moment equation by subtracting a pressure-dependent concentration, velocity, and axial dispersion coefficient into the original mass balance equation. Cerro and Smith [50] used this model for nonadsorbable and slightly adsorbable tracers to evaluate mass transfer parameters in packed beds and reported that this technique could be used to obtain accurate intraparticle and external mass transfer rate parameters for adsorbable or slightly adsorbable gases. However, the obtained macropore diffusivity was much greater than the macropore diffusivity and much less than the micropore diffusivity from the single pore diffusivity model. Therefore, the correct values of the diffusivities could not be obtained.

Van der Vlist and van der Meijden [52] developed a method of predicting binary gas mixture isotherms from concentration pulse retention volume data. They determined the adsorption isotherms of the O_2-N_2 components of binary gas mixtures on Linde molecular sieve 5A at temperatures from 10 to 50°C by gas chromatography. The adsorbent was activated at 400°C for 24 hours in a stream of helium. The retention volume (V_r) of a concentration pulse was measured as function of the partial pressure of component 1 (p_1) at constant total pressure (p) and temperature. They used the chromatographic equation of Martin and Synge [53], Haydel and Kobayashi [54]:

$$V_r = V_g + \frac{m}{c}(c_2 \frac{dw_1}{dc_1} + c_1 \frac{dw_2}{dc_2})$$

(5.2)

where V_r is retention volume, V_g is the free gas volume, m is the mass of adsorbent in the column, $c = c_1 + c_2$ is the total gas phase concentration, c_1 and c_2 are the gas phase concentrations of components 1 and 2, w_1 and w_2 are specific amounts of components 1 and 2 adsorbed, and dw_1/dc_1 and dw_2/dc_2 are the slopes of the individual isotherms at the composition c_1 and c_2. The Equation (5.2) related the retention volume of a concentration perturbation in a binary gas mixture at fixed composition to the slopes of the individual isotherms of the components. It was reported that the model was valid under the conditions of constant temperature and pressure, homogenously packed column and negligible gas phase diffusion and axial effects.

Ruthven and Kumar [62] followed the procedure suggested by van der Vlist and van der Meijden [52]. They determined single-component and binary adsorption isotherms for Ar, O_2, N_2, CH_4, and CO in 4A molecular sieve and for Ar, O_2, N_2, CH_4, CF4, C_2H_6, C_2H_4, and C_3H_8 in 5A molecular sieve by step input chromatographic method. Regeneration of the adsorbents was carried out overnight at 375°C under a purge of helium. Carrier gas (He) was supplied at different adsorbate concentrations through the column and small step change in composition (typically 1-2%) was introduced. Since the changes in concentration were small that the equilibrium relationship were considered linear. The mean retention time determined from the response curve and Henry's Law constant, K, was obtained directly from the following expression:

$$\frac{t_R v}{L} = 1 + \left(\frac{1-\varepsilon}{\varepsilon}\right) K \tag{5.3}$$

where t_R is the mean retention time. The equilibrium isotherms were obtained directly by integration of the slopes (Henry's law constants) determined for different carrier gas compositions using the following expression:

$$K = (1 - X)\frac{dq_1}{dc_1} + X\frac{dq_2}{dc_2} \tag{5.4}$$

where X is the mole fraction of adsorbable component and dq_1/dc_1 is the slope of the isotherm. The molecular volume values (β) were obtained by fitting the experimental

isotherms to the simplified model [60]. The obtained Henry's law constants and molecular volumes are given in Table 5.1.

Table 5.1. Henry law constants and molecular volumes calculated from single-component isotherms of CO on 4A sieve (cavity volume, $\upsilon = 776$ Å^3)

Temperature (°C)	β (Å^3/molecule)	K (molecule/cavity.torr)
32	86	53
35	97	49
93	97	12

The CO adsorption capacity of 4A molecular sieve (molecules/cage) determined by chromatographic method was compared with the results obtained from volumetric method by Harper et al. [63] as given in Table 5.2.

Table 5.2. Comparison of the results for CO adsorption capacity of 4A molecular sieve using chromatographic and volumetric methods

Temperature (°C)	q* (molecules/cage)	Method	Reference
32	1.9	Chromatographic	Ruthven, Kumar [62]
93	0.7		
150	1.4	Volumetric	Harper et al. [63]

They concluded that the concentration pulse technique provided a simple alternative to conventional gravimetric or volumetric methods of determining equilibrium isotherms for both single-component and binary systems. The simple statistical model applied in this study [60] was adequate to represent both the single-component and binary isotherms. It was also concluded that this model provided useful method for determination of binary equilibrium isotherms from the single-component isotherms.

Hyun and Danner [41] determined the pure component adsorption isotherms of C_2H_4 and C_2H_6 on 13X molecular sieve by concentration and tracer pulse techniques at several temperatures. Prior to the chromatographic experiments, the column containing the adsorbent was regenerated at 257°C for at least 48 hours and before each run the column was brought to the same temperature for 10-12 hours. The Henry's Law constants were

determined for different carrier gas compositions. The pure and binary adsorption isotherms were obtained using the data reduction method of van der Vlist and van der Meijden (Equation 5.2) [52]. The concentration-pulse retention volumes determined from the static mixture isotherms were fitted well with a third-order polynomial. These data was in good agreement with the static data. This study showed that combined concentration pulse and tracer pulse techniques could be used for determination of binary adsorption isotherms for nonideal isobutane-ethylene mixture where the concentration pulse method could not be used.

Another model was developed by Ruthven [60] who investigated single and binary adsorption behaviour of CO, CH_4, O_2 and N_2 on 5A zeolite. A statistical thermodynamic model was constructed in which sorbate-sorbent interactions was accounted for in terms of the Henry's Law constant, and sorbate-sorbate interactions was accounted for in terms of the effective molecular volumes of the sorbates. The model isotherm was based on the interaction between an adsorbed molecule and the adsorbent which was characterised by the Henry's law constant. The model assumed that the adsorbed molecules were confined with in particular cavities of the zeolite lattice but not adsorbed at specific sites within a cavity. It was reported that the sorbate-sorbate interaction caused reduction in the free volume due to the finite size of the molecules. Henry's constants and molecular volumes of CO, CH_4, O_2 and N_2 were given for the temperature range of -128 to 25°C. The interaction between an adsorbed molecule and the sieve was characterized by the Henry's law constant by c=Kp. The pure component isotherm equation gave the sorbate concentration, q (molecules per cavity) as a function of Kp and the parameter υ/β (the ratio of cavity to molecular volume of the sorbate). υ was defined as the volume of cavity of 5A sieve, 776$Å^3$, and β as the effective molecular volume of sorbate in $Å^3$/molecule. The Henry's constants were obtained experimentally from the slope of the single-component isotherm at low sorbate concentration and the curve matching procedure was used to determine the molecular volume. It was concluded that this model could represent both the single-component and binary mixture isotherms. However, since molecular volumes were estimated from the van der Waals covolumes, the use of the model was limited to concentrations less than about half of saturation. In order to apply the model at high sorbate concentrations, accurate values of the molecular covolumes were required which are difficult to estimate.

Although Ma and Mancel [51] discussed the effective diffusivity including contribution from both the micropores and macropores, but it was not possible to differentiate the contribution of microprores from that of macropores. Haynes and Sarma [40] and Sarma and Haynes [42] developed a model to describe transient diffusion in a gas chromatographic column and applicable to bidispersed structured catalyst particles. They reported that a single effective diffusion coefficient was not sufficient to characterize the mass transfer within a bidisperse-structured catalyst. Therefore, they included two diffusion coefficients (effective macropore and effective micropore diffusivity) to describe the diffusion. This model was applicable when the micropore diffusivity was considerably smaller than the macropore diffusivity. This method is given in details in Section 4.7. Pelletized particles and some molecular sieves can be described realistically by this type of model. Thus, the bidispersed pore model has been applied in most of the recent chromatographic studies on estimation of intraparticle diffusivities in molecular sieves [55, 56, 57, 58].

Farooq [85] determined the Henry's law constants and intracrystalline diffusivities of O_2 and N_2 in molecular sieve RS-10 by the pulse chromatographic method. The adsorbent column was regenerated overnight at $350°C$ under a helium purge. The experimental response curves were analyzed by both moment and time domain-fitting methods. In the application of the moment method the model of Haynes and Sarma (Equations 4.22 and 4.26) [40] was used. Heats of adsorption and activation energies were estimated from the equilibrium and kinetic measurements performed at different temperatures. It was concluded that the equilibrium data from both analysis methods were in good agreement. Breakthrough curve (BTC) method was also applied to obtain the equilibrium and kinetic parameters. The diffusivity values from BTC were found to be higher than those obtained by moment and time domain analysis for both O_2 and N_2.

Shah and Ruthven [55] applied the concentration pulse technique to study the adsorption and diffusion of CH_4, C_2H_6, C_3H_8 and cyclo-C_3H_6 in 5A molecular sieve. They used the model developed by Haynes and Sarma (Equations 4.22 and 4.26) [40] to describe the chromatographic response of the column packed with the biporous adsorbent. They defined the first moment of the chromatographic peak as the slope of the equilibrium isotherm. The Henry 's law constants were directly obtained from the data obtained with a pure helium carrier. Then, the complete isotherm was determined by integrating the slopes

obtained with different carrier gas compositions. The equilibrium constants obtained were in good agreement with those obtained by volumetric and gravimetric method. The second moments of the response peaks were used for estimation of the micropore diffusion time constants. The diffusional time constants determined by gas chromatography were found in good agreement with the previously obtained results by the gravimetric technique. Therefore, it was concluded that both experimental techniques could be applied in adsorption and diffusion studies.

However, previously reported chromatographic data by Sarma and Haynes [42] for argon in 4A and by Hashimoto and Smith [61] for n-butane in 5A were different from those by gravimetric method due to differences in the definition of the micropore diffusivity. In chromatographic method, the diffusivity was assumed to be independent of concentration which was valid for most systems at low adsorbate concentrations. They claimed that the measurement of intracrystalline diffusional time constants (D_c/r_c^2) by chromatographic method was restricted with upper and lower limits. The upper limit occurred due to rapid intracrystalline diffusion. In this case axial dispersion and the other resistances controlled the mass transfer as in the case of rapid diffusion of CH_4 in 5A. The other mass transfer resistances were eliminated in order to obtain reliable intracrystalline diffusivities by chromatographic method. The lower limit occurred because of slow intracrystalline diffusion. In this case, the peak would not equilibrate during passage through the column, and the retention time would correspond only to the small macropore capacity of the adsorbent.

Ruthven and Haq [64] measured Henry's law constants and intracrystalline diffusivities for O_2, N_2, CH_4 and CO_2 in 4A zeolite and effect of moisture on the Henry's Law constants and intracrystalline diffusivities by the chromatographic method. They analyzed the chromatographic data by matching the first and second moments of the response peaks to the theoretical expressions derived from the dynamic model of Haynes and Sarma (Equations 4.22 and 4.26) [40]. They verified the dominance of intracrystalline resistance to mass transfer by changing the particle size and obtained the same intercept from the $\sigma^2 L/2\mu^2 v$ versus $1/v^2$ plots for two different particle sizes. Then, Henry's law constants, heats of adsorption and diffusion coefficients were determined. This data was in good agreement with previously reported gravimetric data. Therefore, the validity and usefulness of the chromatographic method for studying the kinetics and equilibrium of

sorption in 4A zeolite was confirmed. The 4A sieve was found to be suitable to allow a reasonably efficient pressure swing adsorption (PSA) separation of N_2 and CH_4, but not applicable for separation of O_2 and N_2 due to low separation coefficient for this system with respect to that for N_2/CH_4 system.

Furthermore, Ruthven and Haq [65] studied adsorption and diffusion of O_2, N_2, CH_4, CO_2, cyclo-C_3H_6 and cis-C_4H_8 in commercial 5A zeolite using the same technique. They have achieved the values of equilibrium constants and heats of sorption which were in good agreement with previously obtained gravimetric method. For diffusion of O_2, N_2, CH_4 and CO_2 in 5A molecular sieve, the intracrystalline resistance was not found to be dominant in mass transfer. Thus, they concluded that diffusion of these smaller molecules was too rapid that their intracrystalline diffusivities could not be measured reliably by chromatographic method.

Tezel and Apolonatos [69] studied the adsorption characteristics of H-mordenite, chabazite, 4A and 5A molecular sieve zeolites, and clinoptilolite from western Anatolia for N_2, CO and CH_4. The chromatographic response peaks were obtained by pulse chromatography method. Equilibrium and kinetic parameters were then derived by matching the first and second moments of the response peaks to the model of Haynes and Sarma (Equations 4.22 and 4.26) [40]. The adsorption column was regenerated by heating to $350^{\circ}C$ for 24 hours under helium purge before the experiments to remove impurities and moisture adsorbed from the air. Helium was passed continuously through the system also between the experimental runs. The Henry Law constants for N_2, CO and CH_4 were found higher for the 5A zeolite and H-mordenite systems which was attributed to their larger surface areas and larger pore sizes. The Henry law constant determined for 5A zeolite was higher than those for 4A zeolite. The only difference between the 4A and 5A zeolites was reported to be cation content in their frameworks. It was reported that 5A zeolite had high Ca^{2+} cation content leading to the lower framework density and larger channel size. They explained the higher N_2, CO and CH_4 adsorption capacity of 5A by these larger channels. Micropore diffusion was found dominant mass transfer mechanism only for N_2/H-mordenite, 4A zeolite and chabazite systems. They expected higher micropore diffusion resistance for H-mordenite, due to its one-dimensional channel network. However, it was recognized that the diffusion resistance was higher for N_2/4A zeolite system, although 4A

had three-dimensional channel network which was more accessible to the N_2 molecule. This was explained by the smaller pore size of 4A than that of H-mordenite.

Triebe and Tezel [70] investigated the adsorption of N_2, CO, CO_2 and NO on 5A, 4A, H-mordenite, activated carbon, and on a natural Turkish clinoptilolite. They used concentration pulse method and the model derived by Haynes and Sarma (Equations 4.22 and 4.26) [40] to determine the Henry's Law constants and diffusion coefficients for each system over various temperature ranges. The adsorbents were regenerated under helium purge first at $100°C$ for 2 hours to remove moisture and then at $350°C$ for 24 hours to remove any further impurities. They couldn't observe an interpretable response peak for adsorption of CO_2 on the clinoptilolite which was attributed to its strong adsorption. It was observed that NO was most strongly adsorbed in the natural clinoptilolite and least strongly on the carbon. This was explained by the strong dipole-cation interaction of NO as compared to the weak quadropole-cation interaction of N_2. Adsorption equilibrium parameters (K_o, ΔU_o and ΔH_o) for CO adsorption on 4A, 5A zeolites, H-mordenite and clinoptilolite determined using Equations (4.23) and (4.24) are given in Table 5.3.

Table 5.3. Parameters K_o, ΔU_o and ΔH_o for CO adsorption on 4A, 5A zeolites, H-mordenite and clinoptilolite

Adsorbent/Adsorbate	Temperature Range($°C$)	K_o (dimensionless)	$-\Delta U_o$ (kcal/mol)	$-\Delta H_o$ (kcal/mol)
CO/Clinoptilolite	50 - 200	7.3×10^{-5}	10.8	11.6
CO/5A zeolite	-10 - 90	6.2×10^{-4}	7.2	7.8
CO/ 4A zeolite	-30 - 90	2.2×10^{-3}	6.0	6.6
CO/H-mordenite	30 - 100	5.0×10^{-3}	5.0	5.6

The stronger adsorption of CO in 5A with respect to that in 4A was explained by the presence of stronger adsorption sites (bivalent Ca^{++} cations in 5A as opposed to Na^+ cations of 4A) which are available to interact with the strong CO dipole. The heats of adsorption of CO on H-mordenite, 4A zeolite and 5A zeolite obtained were in good agreement with the values in the literature. The larger K values measured for clinoptilolite was attributed to the structure and the cation content of the clinoptilolite framework. The cation content of the clinoptilolite was reported as in decreasing order of $Ca^{2+}>K^+>Mg^{2+}>$

Na$^+$. Thus, they explained the stronger adsorption of CO by complexing of CO also with Mg^{2+} [72].

The contributions of different mass transfer resistances to total dispersion for CO in clinoptilolite were determined by relating the second moments of the response peaks to kinetic parameters and the results are given in Table 5.4.

Table 5.4. Contributions of different mass transfer resistances to total dispersion of CO in clinoptilolite

Temperature ($^{\circ}$C)	D_I/v^2 (s)	$R_p^2/3D_m$ (s)	$R_p^2/15\varepsilon_p D_p$ (s)	$\sigma^2 L(1-\varepsilon)/2\mu^2 v\varepsilon$ (s)
75	1.36	11.8 x10^{-4}	5.05 x10^{-3}	0.14
100	1.02	10.5 x10^{-4}	4.60 x10^{-3}	0.15
125	1.27	9.42 x10^{-4}	4.22 x10^{-3}	0.10
150	1.26	8.51 x10^{-4}	3.89 x10^{-3}	0.13

The micropore diffusivity was found as the dominant mechanism for CO/clinoptilolite system. The temperature dependence of the micropore diffusivity was determined by an Arrhenius type equation $\dfrac{D_c}{r_c^2} = \dfrac{D_o}{r_c^2}\exp\left(\dfrac{-E_a}{RT}\right)$ where Ea is the diffusional activation energy. The results are given in Table 5.5.

Table 5.5. Parameters D_o/r_c^2 and E_a for CO adsorption in clinoptilolite

Adsorbent/Adsorbate	Temperature Range ($^{\circ}$C)	D_o/r_c^2 (s^{-1})	E_a (kcal/mol)
Clinoptilolite/CO	75-150	4.60 x 10^3	10.0

Triebe and Tezel [71] also examined N$_2$ and CO adsorption capacity of a Turkish clinoptilolite at near ambient conditions. Pure and binary adsorption isotherms up to 101.3 kPa were determined at 30°C by concentration pulse chromatography method. The clinoptiloltie particles were regenerated under the same conditions in the study of Triebe and Tezel [70]. The adsorption isotherm shape for N$_2$/clinoptilolite system at 30°C was found similar to those measured by Ackley and Yang [73] for various ion exchanged-clinoptilolite. N$_2$ adsorption capacity of clinoptilolite at 91.19 kPa was determined as 9 mL

(STP)/g of clinoptilolite and fell within the range of 0.2–0.6 mmol/g for ion exchanged forms determined by Ackley and Yang [73]. CO/clinoptilolite gave similar rectangular shaped isotherms as those obtained by Sirkecioğlu et al. [74] at 20°C by volumetric method and NO on 5A, 4A, H-mordenite, activated carbon, Turkish natural clinoptilolite. The CO adsorption capacity of the clinoptilolite at 30°C was determined as 20 mL (STP)/g which was 30% less than that at 20°C, as expected. Sirkecioğlu et al. [74] reported the capacity as 31 ml (STP)/g at 20°C. They also studied the binary adsorption isotherms of CO and N_2 on Turkish clinoptilolite in the same study. CO was adsorbed 5 to 10 times faster than N_2 which was obtained from the ratio of Henry's Law constants.

Triebe et al. [75] also examined a natural clinoptilolite from Turkey in air purification and separation applications. Henry's Law constants for adsorption of CO_2, CO, NO, and N_2 were measured on clinoptilolite, 4A and 5A zeolites, and H-mordenite over temperature range of –30 to 200°C by gas chromatographic method. Pure component adsorption isotherms were determined for N_2 and CO_2 on clinoptilolite at 30°C and up to 1atm and they were found to be rectangular. Henry's Law constants and heats of adsorption for CO, N_2, and NO on clinoptilolite between 50 and 200°C have been reported to be higher than those on other sorbents tested. Furthermore, clinoptilolite exhibited the highest separation factors for NO/N_2 and CO/N_2 systems over the temperature range.

Sheikh et al. [100] also determined the equilibrium and kinetic parameters for CH_4 and N_2 on an activated carbon using both volumetric and concentration pulse chromatographic methods. They determined the pure component adsorption isotherms and the effective transfer coefficients. The Henry's constants were determined using the virial adsorption isotherm while using volumetric method. The chromatographic data was analyzed by moment method provided by Haynes and Sarma (Equations 4.22 and 4.26) [40] and by van Deemter plots. The values of Henry's constants predicted by the chromatographic method agreed with 7% to the corresponding values determined from the volumetric method for each sorbate. The mass transfer coefficients reflected very low resistances for both CH_4 and N_2. They determined the Henry's constants as 20.19 and 6.69 for CH_4 and N_2, respectively by chromatographic method.

In summary, the adsorption equilibrium and diffusion parameters obtained by concentration-pulse technique and by the application of the model of Haynes and Sarma

[40] were found in good agreement with the results obtained by conventional volumetric and gravimetric techniques.

5.2. Adsorption Properties of Adsorbents

There is considerable amount of study on the natural zeolite formations in Middle-Western Anatolia [17, 19, 20, 43, 67, 86, 103-105]. Ülkü et al. [86] examined the local clinoptilolite from Bigadiç for air drying in packed column. Adsorption equilibrium relationships and heat and mass transfer rates were used to explain the dynamic behaviour of the adsorbent bed. Adsorption equilibrium experiments were performed by static weight gain method. The mass and heat balance relationships were coupled through the temperature dependence of equilibrium relationship to describe the process. Analytic solutions for breakthrough curves were found by applying the available models for isothermal columns and linear adsorption isotherms. The effective diffusion coefficient of water in natural zeolite was determined as 5×10^{-10} cm^2/sec from isothermal uptake rate measurements. It was indicated that no significant effect of air velocity on breakthrough curves was observed since intraparticle mass transfer controlled the overall mass transfer process. They concluded that local clinoptilolite has promising future for drying air in industrial applications as a cheap alternative to expensive synthetic adsorbents.

Sirkecioğlu et al. [18] investigated the mineralogical and chemical properties of Bigadiç clinoptilolite and studied the change in ammonium ion exchange capacity with zeolite content. They observed that the zeolite rich tuffs of Bigadiç were mainly in the form of coarse-grained, glassy, ash tuffs at the bottom and fine-grained, glassy, dust tuffs on top. Esenli and Kumbasar [66] investigated thermal behaviour of heulandites and clinoptilolites from Bigadiç, Gördes and Mustafakemalpaşa using differential thermal analysis (DTA) and thermogravimetric analysis (TGA). The zeolite contents were found to vary mainly between 55 and 100%, while most of the representative samples contained more than 80% clinoptilolite.

Altav et al. [68] investigated the cation content, ion-exchange and adsorption properties of the clinoptilolite from Bigadiç. The clinoptilolite content of the tuffs was reported as 95%. H$_2$S and SO$_2$ adsorption isotherms for raw, Na, H, K and Ca-exchanged clinoptilolites were determined using constant volumetric method upto 100kPa. The

69

adsorption isotherms for H_2S and SO_2 on Na, K and H-exchanged clinoptilolite showed Type I shape. H_2S adsorption capacity decreased in the order of H>K>Raw>Na>Ca-exchanged forms and SO_2 adsorption capacity decreased in the order of H>Na>Raw>K>Ca-exchanged forms. Adsorption capacity for H_2S was found in the range of 0.28-2.98 mmol/g and for SO_2 in the range of 2.99-3.67 mmol/g. H-exchanged forms exhibited the highest capacity both for H_2S and SO_2 due to their interactions with the H^+ atoms in the channels. Ca-exchanged clinoptilolite did not adsorb SO_2. The lowest capacity of Ca-exchanged clinoptilolite for H_2S was explained by blockage of the eight-member ring channels by Ca^{2+} cations. Na-exchanged form exhibited lower capacity with respect to H-exchanged form due to lower electronegativity of Na^+ cations. Adsorption isotherms were modelled by Freundlich, Langmuir and Dubinin-Astakhov (D-A) models. D-A model was found to be the most suitable model and micropore volumes were calculated in the range of 0.086-0.157 cm^3/g and characteristic adsorption energy in the range of 2.62-16.06 kJ/mol.

Numerous studies on the regeneration of the adsorbents and effects of structural characteristics of zeolites on their adsorption properties are available in the literature. Tsitsishvili et al. [82,83] reported that the presence of highly hydrated cations (Ca^{2+} and Mg^{2+}) in clinoptilolite blocks the channels and prevents the free movement of the guest molecules. They noted that thermal activation of the raw material below 300°C does not completely remove the water molecules arranged near Ca^{2+} and Mg^{2+} cations. For this reason, and in order to define the best conditions of activation, the clinoptilolite samples were heated at different temperatures in the range of 280-600 °C, for different time periods. The water contents of these samples were determined and their molecular sieve capacities were evaluated for the O_2/N_2 separation from air. They concluded that the best separation efficiencies were achieved with the samples heated in the range 400-500°C. Özkan and Ülkü [67] regenerated the clinoptilolite particles from Bigadiç at 160°C in a vacuum oven for 9 hours, at 400°C and 600°C in an oven for 3 hours prior to the breakthrough experiments for water vapor adsorption by the clinoptilolite using a packed column. As the regeneration temperatures increased from 160°C to 400°C, the sharper and later concentration breakthrough occurred, i.e. the water vapor adsorption capacity of the column increased approximately 26%. However increasing to 600°C resulted in decrease of the adsorption capacity of the clinoptilolite.

Barrer and Coughlan [25] studied the adsorption of a non-polar molecule (Kr), a molecule with a quadrupole moment (CO_2) and one with a dipole moment (H_2O). These gases have different polarizabilities, electric multiple moments and molecular sizes, however comparable to the effective dimension of the channels reported for the different cationic forms of clinoptilolite [24]. The gas chromatographic retention volumes and the adsorption entalphies of CO, O_2, N_2 and CH_4 on the different samples were experimentally determined and are discussed in terms of polarizability of the gases, polarizing power of the cations and their location in the zeolite framework. Consequently, higher polarizing power of cation resulted in lower diffusivity. Tsitsishvili et al. [23] reported that the adsorption capacity of zeolites in chromatographic processes is governed by both the strength of the sorbate-adsorbent interactions and the molecular diffusion rate through the pores.

Emesh and Gay [72] carried out experiments with Zn^{2+}, Cd^{2+}, Na^+ and Ca^{2+}-exchanged A zeolites and found that CO forms a specific complex with divalent ions in the framework of type A zeolite. It was also reported that the adsorption capacity of A zeolite increased as divalent ion content increased. However, the capacity decreased if excess amount of divalent ions were exchanged, due to inaccessibility of some of the divalent ions.

Other studies on structural effects on adsorption properties of zeolites were performed by Ackley and Yang [73] and Ackley et al. [24]. They published a review of the general structural and adsorptive characteristics of clinoptilolite based on the experimental results obtained by gravimetric method. The ion-exchanged clinoptilolite and 4A zeolite were compared according to their properties of separation of CH_4 from N_2. The 2-D channel structure of clinoptilolite was changed by ion - exchange to study the effects of cation size, location, and distribution on the diffusion of N_2 (weakly polar) and CH_4 (nonpolar) molecules in terms of channel blockage. The diffusion time constants (D/L^2) were determined from the gravimetric uptake measurements for fully exchanged K^+, Na^+ and H^+ clinoptilolite, and highly-exchanged Ca^{+2} and Mg^{+2} clinoptilolite. A constant pressure, constant flow and constant concentration of a single adsorbate in helium were introduced to the zeolite sample on the electrobalance and maintained until equilibrium was achieved. It was shown that the intracrystalline diffusion was dominant mechanism for diffusion of N_2 and CH_4 molecules in clinoptilolite. Diffusion time constants were

determined comparing either the plane sheet or parallel channel diffusion model with the uptake data obtained at 27 and 50°C.

In the application of the plane sheet model, each layer of clinoptilolite channels was assumed as an independent plane sheet diffusion layer. This model was found suitable for diffusion in K^+-clinoptilolite, since all c channels were blocked by K^+ cations and diffusion occurred along A and B channels. The Fick's law for concentration-independent diffusion coefficient was applied and one dimensional diffusion equation (Equation 4.7) was derived for a plane sheet.

A parallel channel diffusion model was derived using Equation (4.7) to represent the rapid and slow components of diffusion evident from the uptake rate data. This allowed the determination of the concentration-dependent diffusion time constants for both the eight- and ten-member ring channels of the clinoptilolite structure. In this study, for some of the exchanged clinoptilolites, two distinct uptake regions (rapid and slow) were observed for CH_4 diffusion which were explained by the different diffusion mechanisms due to differences in channel geometry and blockage. Different diffusion control processes were involved in the bidisperse model proposed by Ruckenstein et al. [76] for transient diffusion in porous adsorbent containing both micropores and macropores. For each in micropores and macropores, two different diffusion coefficients were defined due to different diffusion mechanisms. Ca^{2+} and Na^+ cations blocked eight-member ring channels, while Mg^{2+} blocked the ten-member ring channel. Therefore, it was concluded that the cation location was important to channel blocking than the size or number.

Ackley and Yang [30] also investigated the adsorption characteristics of fully exchanged-K^+, Na^+ and H^+ clinoptilolite, and highly-exchanged Ca^{+2} and Mg^{+2} clinoptilolite. They applied Dubinin-Astakhov volume filling model to adsorption isotherm to determine the pore volume using N_2 and CH_4 at their normal boiling points. Adsorption capacity and heat of adsorption were related to structural properties of the clinoptilolite such as cation type and location. It was resulted that the pore structure of the clinoptiolite could be modified by cations for desired gas separations.

The interaction of CO with the cationic Lewis sites of transition metal (Fe^{2+}, Co^{2+}, Ni^{2+}) and Cu-exchanged Y and X zeolites was studied by Rakic et al.[77] using Fourier transform infrared spectroscopy (FTIR). During adsorption of CO, IR absorption bands in the 2200-2000 cm^{-1} spectral region, characteristic for symmetric stretching of CO adsorbed

on zeolites, indicating molecular adsorption of CO on Cu-exchanged samples. In the case of all other samples investigated, disproportion of CO was noticed during its adsorption and temperature-programmed desorption. It was reported that the C-O stretch bands of CO molecules adsorbed on a zeolite surface occur between 2000 and 2230 cm^{-1}, i.e., in the same region where the CO gas-phase frequency (2143 cm^{-1}) appears. Three overlapping bands in the C-O stretch region were obtained for the iron-, nickel- and cobalt-exchanged zeolites: one band near 2200 cm^{-1} and two bands at 2170 and 2120 cm^{-1} for all the zeolites studied. Weak overlapping bands near 1600 cm^{-1} were also found during CO adsorption on these samples. The appearance of a band near 2349 cm^{-1} has already been reported in the case of CO adsorption on monovalent and bivalent-cation-exchanged forms of FAU-type zeolites [78]. They explained the appearance of the bands near 2350 cm^{-1} by formation of CO_2 during the adsorption of CO on transition-metal cation-exchanged zeolites. The simultaneous appearance of the C-O stretch bands and the band at 2350 cm^{-1}, observed during the adsorption of CO on Fe, Co and Ni-exchanged zeolites, confirms that disproportionation of CO and the formation of weakly bound CO_2 occurs during CO adsorption.

CHAPTER 6

EXPERIMENTAL STUDY

In this chapter experimental procedures for characterization of clinoptilolite and chromatographic experimental set-up and procedure for investigation of CO adsorption equilibrium and kinetics on the clinoptilolite is given. The clinoptilolite sample is characterized in order to determine its physical, chemical and thermal properties and effects of these properties on adsorptive characteristics of the clinoptilolite. The results are given in the Chapter 7.

6.1. Preparation of Clinoptilolite Particles

The clinoptilolite excavated from Gördes, in western Anatolia, was supplied as particles smaller than 0.7 mm and in the size range of 0.7-1.8 mm. Particles from these two size ranges were mixed and sieved to a desired particle size range of 500-850 μm (35-20 mesh). Then, the particles were put into deionized water and the mixture was heated on a hot plate until it was boiled in order to remove soluble impurities. After that, the particles were filtered. This washing and filtering process was repeated three times. A glass rode was used to mix the mixture during heating. After washing and filtering, the particles were rinsed with deionized water and put into the oven at 100°C for 6 hours.

Those dried particles were sieved again for narrow particle size distribution, since they might be broken during washing. After sieving process, the particles were divided into two groups, one group was placed into saturated NH_4Cl environment (wet desiccator) to bring it to constant relative humidity, and the other group was placed into the $CaCl_2$ desiccator (dry desiccator) in order to prevent the particles adsorbing water vapour from the atmosphere, at least for two weeks. These prepared particles were named as "washed clinoptilolite", while those used as received were named as "unwashed clinoptilolite".

74

6.2. Characterization of Clinoptilolite

6.2.1. Determination of Clinoptilolite Density

In order to determine the wet and dry densities, clinoptilolite specimen of rectangular prism in shape was cut. The volume of the specimen was calculated as 4.714 cm^3. Then it was placed in an oven at 400°C for 24hrs and cooled in dry desiccator and weighted (m_{dry}). After that it was immerged in deionized water and vacuumed at -500 mmHg at room temperature until the exit of air bubbles stopped. The specimen was taken out of the water and dried with a tissue and weighted again (m_{wet}). Knowing the volume of the specimen, the dry (ρ_{dry}) and wet (ρ_{wet}) densities of the clinoptilolite were calculated as 1.240 and 1.502 g/cm^3, respectively. Then, the bed voidage was calculated as 32.57%. The dry clinoptilolite density was used in this calculation regarding regeneration of the particles before adsorption experiments. The calculation details are given in Appendix C.

6.2.2. Particle Size Distribution Measurements

Laser diffraction based-particle size analyzer (Malvern MastersizerS Ver.2.14) was utilized for determination of the particle size distribution of clinoptilolite particles packed into the column. This instrument allows measurement of particle size distributions in the range of 0.05-3500μm, with a precision of better than 0.5%. Particles were suspended in water in a magnetically stirred cell during analysis. When a particle passes through a laser beam it causes light to be scattered at an angle that is inversely proportional to its size [106].

6.2.3. Elemental Analysis by Inductively Coupled Plasma (ICP)

Varian Model LibertyII ICP-AES was used to determine the quantities of framework elements and charge-balancing cations. The method is based on the principle that the energy of emission is specific for each element.

The analysis was performed as follows. Clinoptilolite sample weighing 0.1003 g was taken from the wet desiccator and put into a platin crucible. Then 6.4 mL of HF was added in order to dissolve the sample. The crucible was heated on a hot plate until all HF was evaporated. To check complete dissolution of silica, 2 mL more HF was added and the crucible was heated again until white precipitate was observed. After keeping the sample in an oven at 400°C for 2 hours, it was placed in the dry desiccator for 5 minutes.

The weight of the crucible containing the white precipitate was recorded. The precipitate was taken out of the crucible and 100 mL deionized water was added in order to prepare solution of 306 ppm. This solution was diluted to 76.5 ppm and 1 mL cesium was added. Then this liquid sample was fed to the ICP where it was atomized. The sample was then carried by argon gas into the plasma where the elements are thermally excited.

The weight difference between the initial and final weight of the sample was equated to the evaporated mass of SiO_2 and H_2O (0.0697g). The amount of water evaporated was taken as the average weight loss observed from thermal analysis, as 10.57 g. Then the evaporated water weight corresponded to 0.0107 mg. Therefore, evaporated SiO_2 weight was found as 59.09 mg. The data was utilized in the determination of chemical composition of the clinoptilolite.

The reliability of this analysis was verified by stating the mass balance between the evaporated H_2O (0.0106 mg) and evaporated SiO_2 (58.917 mg), and the final sample mass (97.475 mg). Therefore, 2.525 mg sample was lost during solution preparation or analysis.

6.2.4. Fourier Transform Infrared Spectroscopy (FTIR)

The infrared spectra of samples were taken by Shimadzu FTIR-8601 Fourier Transform Infrared Spectrophotometer using KBr pellet technique [79]. Typical pellet containing 2 % weight sample in KBr pellet was prepared by mixing 4 mg sample with 200 mg of KBr. The amount of sample in KBr pellet was chosen so to provide linear dependence of optical density of characteristic IR bands versus sample content. Pure KBr powder was used as the blank and the reference spectrum of dry KBr was recorded. Then infrared spectra were observed in the wavelength mid-infrared region range of 400 – 4000 cm^{-1}, since this range of the spectrum contains the fundamental vibrations of the framework Al, Si-O_4 or (TO_4) tetrahedra.

The IR spectra of washed, regenerated and CO adsorbed clinoptilolites were determined and compared considering typical bands for clinoptilolite.

6.2.5. Thermal Analysis

The thermal properties of Gördes II clinoptilolite were analyzed by thermogravimetric and differential thermal analysis methods. These analyses involve the investigation of the evolution of water, decrease in unit cell volume and structural breakdown or modification i. e., conversion to another amorphous or crystalline phase. The

details of thermal behaviour of natural zeolites give useful information about their structural and physicochemical properties such as adsorption capacity and differential heat of adsorption which are required for their practical applications including as water adsorbents. The 10 mg clinoptilolite samples from the wet desiccator was utilized in thermal analysis.

6.2.5.1. Thermogravimetric Analysis (TGA)

Shimadzu TGA-51 thermobalance was used to perform thermogravimetric analysis for washed and unwashed clinoptilolite particles upto the maximum temperature of 800 °C under different analysis conditions. Nitrogen at different flow rates (5, 10 and 20 mL/min) and three different heating rates (2, 5 and 10°C per minute) were employed for the analysis. The percent weight losses as they were heated were determined from TGA curves.

6.2.5.2. Differential Thermal Analysis (DTA)

Differential thermal analysis for both washed and unwashed clinoptilolite samples were carried out by Shimadzu DTA -50. Differential Thermal Analysis (DTA) measures the difference in temperature between a sample and a thermally inert reference as the temperature increases. Maximum temperature for this analysis was 1000°C. Heating rate of 5°C/min was applied. DTA provides information on the temperatures at which exothermic and endothermic reactions taking place within the sample, since the sample undergoes a transformation, it either absorbs (endothermic) or releases (exothermic) heat. Temperatures for phase transitions and structural destruction can be determined by DTA.

6.2.6. Pore Volume and Surface Area Analysis

Accelerated Surface Area and Porosimeter (ASAP 2010, Micromeritics) was applied to determine the pore and surface characteristics of the clinoptilolite sample. A clinoptilolite sample weighing 0,2371g was taken from the dry desiccator. It was outgassed by applying heat, vacuum and flowing gas to remove adsorbed contaminants acquired from atmospheric exposure and organic impurities. The outgassing was performed under 10 µmHg vacuum and argon purge. The temperature of the sample was kept at 50°C for 1 hour. Then, the temperature was increased by 50°C/hour until it reaches to 350°C. The sample was left at this temperature for 24 hours. Then the sample was allowed to cool

77

under vacuum to analysis temperature of 87.40 K. Argon was admitted as an adsorptive to the adsorbent in controlled increments. After each of dose of adsorptive, the pressure was allowed to equilibrate and the quantity of gas adsorbed was determined.

The gas volume adsorbed at each pressure (at constant temperature) defines adsorption isotherm. ASAP 2010 instrument measures the molar quantity of gas n (standard volume V_a, or general quantity q) taken up (adsorbed) or released (desorbed) at a constant temperature by an initially clean solid surface as a function of gas pressure [80]. The thickness of the adsorbed film increases as adsorption process continues to the point of bulk condensation of the adsorptive. Then, desorption process begins, pressure is systematically reduced and the adsorbed molecules are released. Analysis of the isotherms yields information about the surface characteristics of the material.

6.3. Experimental Set-Up for Adsorption Equilibrium and Kinetic Studies

An experimental-set up was constructed for this study. The diagram of the experimental set-up is given in Figure 6.1.

A Shimadzu GC-17A, Ver.3 gas chromatograph equipped with thermal conductivity detector (TCD) was used for all measurements. The stainless steel column with 0.46 cm inlet diameter and 10 cm length packed with the washed clinoptilolite particles was used. The packed column was placed in the GC oven for accurate temperature control.

Ultra high purity He carrier gas (99.999 %) was used to transport the 0.25 mL CO gas sample through the column in order to reduce baseline fluctuations and excessive detector noise. Gases were supplied to the instrument from gas cylinders. Two-stage pressure regulators were employed with gas cylinders to reduce the pressure to a desired pressure, since constant delivery pressure is required for a gas chromatograph. Digital mass flow controller capable of delivering 0-500 mL/min of gas was used for adjustment and control of the He gas flow rates. Check valve was used after the mass flow controller to provide gas flow in only one direction. A soap-bubble meter was connected to the TCD outlet to verify the flow rates measured by mass flow controllers.
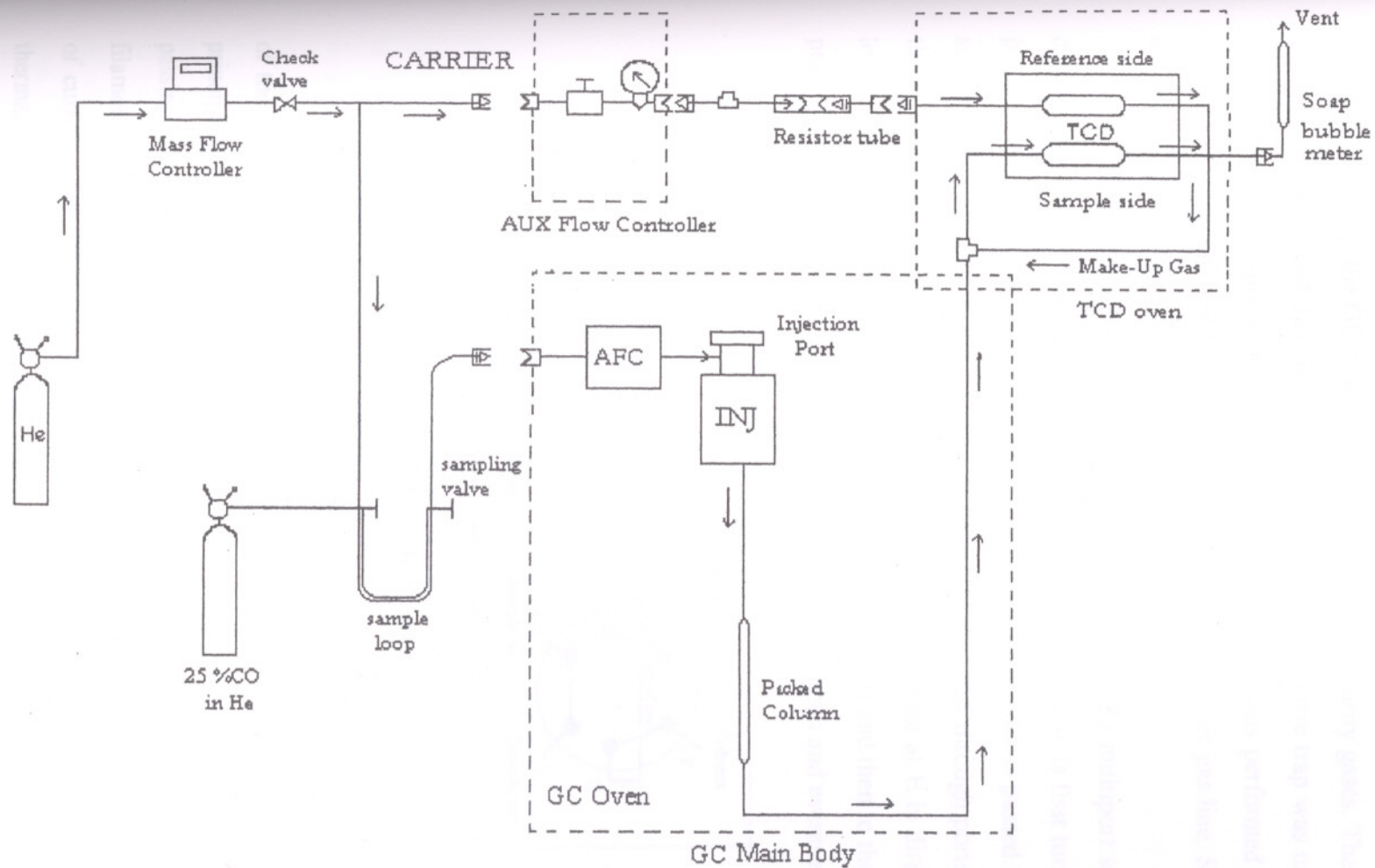
Figure 6.1. Experimental Set-up

Clean chromatographic grade 1/8" tubing was used to plumb gases to the GC. The tubing was cut with a hand-held device guiding a cutting wheel along the outside surface of the tubing. Compression fittings were used to provide gas-tight, leak-free connections. The oxygen trap adsorbing oxygen at room temperature was employed to prevent impurities entering the GC system with even ultra high purity gases. These impurities can cause ghost peaks and detector signal noise. Molecular sieve trap was used for removing trace levels of moisture from carrier gas. Leak checking was performed including all the fittings inside the GC and the external fittings along the carrier gas line. Soap solution was used for leak detection.

The CO pulse of 0.25 mL was injected by means of a multiport sampling valve. A diagram of a multiport valve is shown in Figure 6.2. The valve is first turned to the charge position and 1 mL gas from the 25% CO–He mixture cylinder is passed into port A. The sample flows through B into the loop and the excess is lost through ports C and D. When the valve is turned to the discharge position the He entering at E is directed through the loop causing the sample to be swept onto the injection port and then to the column through port F [81]. The pulse then passed through the packed column and eventually the TCD.
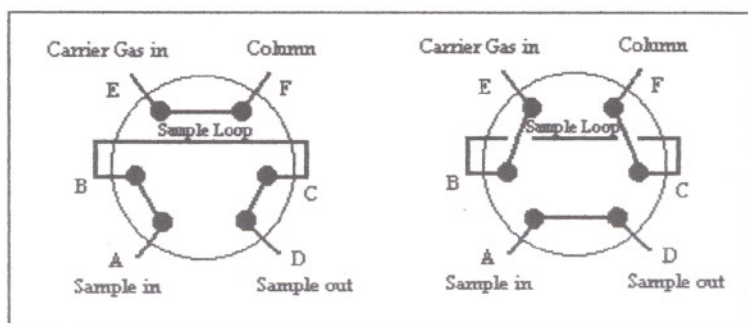
Figure 6.2. The multiport sampling valve

Thermal conductivity detector (TCD) response is proportional to the concentration of the sorbate in the carrier gas. The detector cell includes two separate filaments. The principle of operation is based on the relative change in the thermal conductivity of the gas passing across the detector filament as sorbate elutes from the column. Heat is lost by the filament through the carrier gas to the cell wall of the detector. By measuring the amount of current required to maintain as constant filament temperature as gases of different thermal conductivities cross the filament, a concentration-dependent chromatographic

signal is produced. Thermal conductivity of the carrier gas used in this study is 34.31 x10^{-5} cal/s.cm.°C and for CO it is 5.43x10^{-5} cal/s.cm°C.

6.3.1. Packing and Regeneration of the Adsorbent Column

The column was packed with 1.389 g of washed clinoptilolite particles of size in the range of 500-850 μm. The procedure for packing a column was simple; the particles were packed into the stainless steel column by an attachable aluminium funnel. For homogenous packing, a vibrator was utilized. Attention was paid to not to break the particles during packing in order to prevent inhomogeneous packing since uniform, near spherical particles with narrow size distribution is required for homogenous packing of the column. Small amount of glass wool was placed at column ends to trap the adsorbent in the column and to prevent the particles reaching the detector. Details of the adsorption column are given in Table 6.1.

Table 6.1. Adsorption column characteristics.

Mass of packing, $m_{packing}$	1.389 g
Particle size range	20-35 mesh (500-850 μm)
Column I. D.	0.46 cm
Column Length	10 cm
Column length-to-column diameter ratio	21.74

The aim of regeneration is to remove volatile impurities and water from the packed clinoptilolite. If the adsorbent is not properly regenerated, these impurities will slowly elute off the column during the analysis leading to baseline disturbances and a high background signal. In order to decide the appropriate regeneration conditions, previous studies carried out with similar adsorbents and under similar experimental conditions were rewieved in Chapter 5. In this study, regeneration conditions were decided after a series of chromatographic runs: CO pulse of 0.25 mL was injected to the packed column after it was regenerated at various temperatures (300 and 350°C) and for different time periods (6, 12, 24 and 48 hours). The chromatograms were obtained under same analysis conditions (50 mL/min He flow rate, 60°C column temperature) for each injection and compared. These peaks were compared and it was seen that the characteristics of peaks (retention time, peak

area and height) which were obtained after regeneration for 6 and 12 hours. Similar peak characteristics were observed after regeneration at 350°C for 24 hours. These regeneration conditions were found appropriate. In our study, the column regeneration process was carried out within the GC oven first at 100°C for 2 hours in order to remove the moisture, then at 350°C for 24 hours to remove further impurities under 50 mL/min helium purge. The GC oven temperature increased by 10°C/min upto 350°C. During regeneration process, the column was disconnected from the TCD. The regenerated column was not taken out of the GC after regeneration in order to prevent adsorption of impurities or moisture from the air, and it was allowed to cool to the analysis temperatures and then connected to the TCD. A carrier gas flow of helium was also flowed continuously through the system for purging between experimental runs.

6.3.2. Experimental Conditions

Adsorption equilibrium and kinetic experiments were performed under different column temperatures and carrier gas flow rates. Carrier gas flow rates were changed as 30, 40, 50 and 60 mL/min at each column temperature of 60, 80, 100 and 120°C. Since the He flow rates were measured at room temperature, the interstitial He velocities were corrected to the column temperature. These experimental parameters are given in Table 6.2.

Table 6.2. Experimental parameters applied in the gas chromatography experiments.

Column Temperature (°C)	Volumetric flow rate of the carrier gas (mL/min)	Superficial velocity v_s (cm/sec)	Intersitial velocity $v = v_s/\varepsilon$ (cm/sec)	Corrected velocity (cm/sec)
60	30	3.01	9.23	10,31
	40	4.01	12.31	13,75
	50	5.02	15.39	17,19
	60	6.02	18.47	20,63
80	30	3.01	9.23	10,94
	40	4.01	12.31	14,59
	50	5.02	15.39	18,24
	60	6.02	18.47	21,88
100	30	3.01	9.23	11,56
	40	4.01	12.31	15,41
	50	5.02	15.39	19,27
	60	6.02	18.47	23,15
120	30	3.01	9.23	12,18
	40	4.01	12.31	16,24
	50	5.02	15.39	20,30
	60	6.02	18.47	24,36

6.3.3. Gas Chromatography Experiments

The chromatographic peaks were obtained by injection of 0.25 mL CO pulse to the column after the column was brought to equilibrium.

At the beginning, 1 mL pure CO pulse was injected into the column and several peaks were observed in the chromatograms. This was attributed to the large pulse size. The sampling loop volume smaller than 1 mL was not available for the sampling valve. Therefore, the pulse was introduced to the system from the 25% CO–He mixture cylinder corresponding to the CO pulse size of 0.25 mL.

Prior to the chromatographic experiments, the linearity of the thermal conductivity detector (TCD) response with the inlet CO concentration was tested. 0.25 mL CO pulses of different concentrations (2.5-100 %) were introduced to the empty column and the response peaks were obtained at 60°C column temperature for He flow rates of 30, 40, 50 and 60 mL/min. The retention time, peak area and peak height of these peaks were anlyzed.

Before the packed column experiments, 0.25 mL CO pulse was injected to the empty column under the analysis conditions given in Table 6.2. Then, the obtained response peaks were utilized for determination of the dead retention times and the first and second moments for empty column.

The packed column experiments were carried out in the same manner, 0.25 mL CO pulse was introduced after equilibrium was reached in the column. The aim of using different column temperatures was to estimate the heats of adsorption and dependence of total dispersion on temperature. He flow rates were changed in order to separate the axial dispersion from other mass transfer resistances, while the column temperature was kept constant at 60, 80, 100 and 120°C.

CHAPTER 7

RESULTS AND DISCUSSION

7.1. Density Measurements

The dry and wet densities of the clinoptilolite were determined as 1.240 and 1.502 g/cm^3 (see Appendix C), respectively and the bed voidage was calculated as 32.61 % knowing the volume of the clinoptilolite packed into the column. The bed density was calculated as 0.837 g/cm^3. Then the pressure drop across the packed column was calculated as 0.034-0.731 kPa using the Equation A.1 given in Appendix A and accepted as negligible.

7.2. Particle Size Distribution Measurement

Particle size distribution measured is presented as differential percent volume versus the corresponding particle size in Figure 7.1.
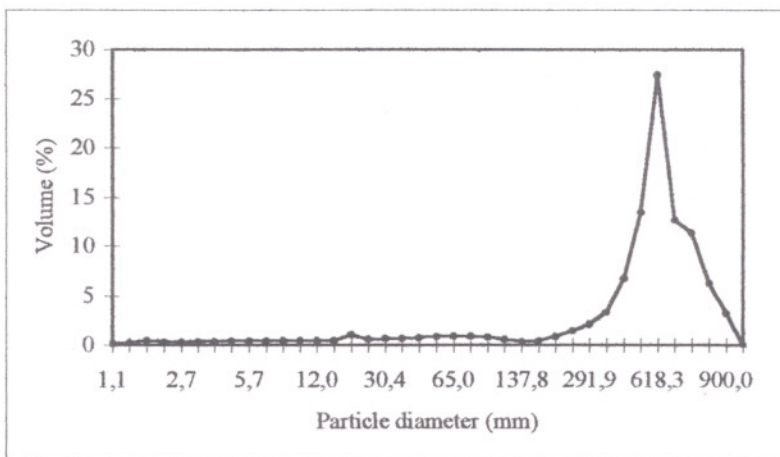

Figure 7.1. Clinoptilolite particle size distribution

Figure 7.1 suggests that the particles have narrow size distribution that is required for homogenous packing of the column. The mean diameter was calculated from the size distribution as 603.791 μm. However, the particles out of the sieved range (500-850 μm). were also detected. Presence of larger particles could be due to agglomeration of zeolite particles. Detection of particles smaller than 500 μm may be explained by breaking of zeolite particles during dispersing them by magnetic stirrer.

7.3. Elemental Analysis by Inductively Coupled Plasma

The chemical composition of the clinoptilolite sample as percent weight sample is given in Table 7.1.

Table 7.1. Chemical compositions of the clinoptilolite

Element	Element % weight
Ag_2O	0.012
Al_2O_3	12.355
B_2O_3	0.144
BaO	0.066
CaO	4.906
Co_3O_4	0.003
Cr_2O_3	0.005
Cu_2O	0.092
Fe_2O_3	1.561
K_2O	3.276
MgO	1.255
MnO	0.016
Na_2O	1.176
NiO	0.177
PbO	0.023
SiO_2	72.101
ZnO	0.303

Si/Al for the clinoptilolite sample of interest was found as 5.84. Thermal stability of clinoptilolite depends on the Si/Al ratio. Thermal behaviour of zeolites increases as Si/Al ratio increases. This ratio was reported in the 4.25–5.25 range by Breck [13] and in the 4.5–5.5 range by Tsitsishvili et al. [22].

In this study Ca^{2+}/K^{+} ratio was calculated as 1.498. The amount, type and location of these cations affect intracrystalline diffusivity and molecular sieve properties as previously explained in Chapter 3. Tsitsishvili et al. [82] examined that the presence of Ca^{2+} in clinoptilolite blocks the channels reducing diffusivity of the gases especially of small molecules such as water vapour. They also studied the effects of cations on thermal stability and reported that zeolites containing Ca^{2+} retained their water to higher temperatures with respect to those containing K^{+} ions [82]. Consequently, thermal activation below 300°C was found impossible to completely remove the water molecules arranged near these cations.

Role of exchangeable cations on the molecular sieve properties of a clinoptilolite was also well stated by Arcoya et al. [87]. Capability of the natural clinoptilolite exchanged with amonium, alkaline and alkaline-earth cations was examined for the separation of CH_4, O_2, N_2 and CO in terms of polarizing power and locations of the cations in the zeolite framework. It was also reported that the volume and location of the cations affected the retention volumes in chromatographic studies of gases in clinoptilolite. With regard to CO molecule, the highest retention volume values were obtained due to permanent dipole moment of CO molecule. On the other hand, retention volumes for CO on variously exchanged clinoptilolites increased in the order: Cs-CLI<H-CLI<K-CLI<Na-CLI<Ca-CLI<Mg-CLI<Ba-CLI. Except for the Ba-exchanged clinoptilolite, this sequence was observed to increase with the increasing polarizing power of the cations (3.08 for Mg, 2.02 for Ca, 1.48 for Ba, 1.05 for Na, 0.7 for K, 0.59 for Cs) [87].

Other studies on the effects of cations on adsorption properties of zeolites were reviewed in Chapter 5.

7.4. Fourier Transform Infrared Spectroscopy Analysis

Infrared spectroscopy was used to characterize the nature of OH groups in the structure, vibrations of the framework elements and adsorbed CO molecules on the clinoptilolite. Vibrations of the frameworks of zeolites give rise to typical bands in the mid-infrared region. The original assignments of the main IR bands are given in Table 7.2.

Table 7.2. Zeolite IR Assignments (cm^{-1})[13]

Internal Tehrahedra	
Asymmetrical strech	1250-950
Symmetrical strech	720-650
T-O bend	500-420
External Linkages	
Double ring	650-500
Pore opening	420-300
Symmetrical strech	750-820
Asymmetrical strech	1150-1050

Unwashed, washed, regenerated and CO adsorbed clinoptilolite samples showed the similar absorption bands as shown in Figure 7.2–7.4. The strongest band was observed around 1050 cm^{-1} and was assigned to internal T-O stretching mode. The second strongest band in the spectra was found around 450 cm^{-1} which was assigned to internal T-O bending mode. This vibration is not sensitive to the Si/Al ratio of the framework. The band at 600 cm^{-1} in the spectrums was related to the presence of the double rings in the framework structures. The peaks in 750-820 cm^{-1} region were assigned to the stretching modes involving mainly the tetrahedral atoms and are sensitive to the Si-Al composition of the framework [13]. Flanigen et al. [88] reported relationships between the frequency of internal asymmetrical stretch (1250-950 cm^{-1}) and symmetrical stretch (720-650 cm^{-1}) of X- or Y- type zeolites and the Si/Al ratio of the framework. Another common bands were observed at about 3400 and 1645 cm^{-1} for washed, unwashed, regenerated and CO adsorbed clinoptilolite samples. The broad band in the stretching region at about 3400 cm^{-1} is characteristic of the isolated H_2O molecules (hydrogen-bonded OH), and the band at 1645 cm^{-1} represents the usual bending vibration of water [13]. The isolated OH streching is attributed to interaction of the water hydroxyl with the cation. The other band is attributed to the hydrogen bonding of the water molecule to a surface oxygen and to the bending mode of the water [89].

The influence of washing on clinoptilolite content of zeolite was examined by considering typical bands for clinoptilolite, 609 cm^{-1} and 450 cm^{-1} bands. After washing, no significant changes were recorded in absorbance values of these peaks as shown in Figure 6.2. The slight increase in both band intensities may be explained by removal of the soluble impurities on the external surface due to washing.
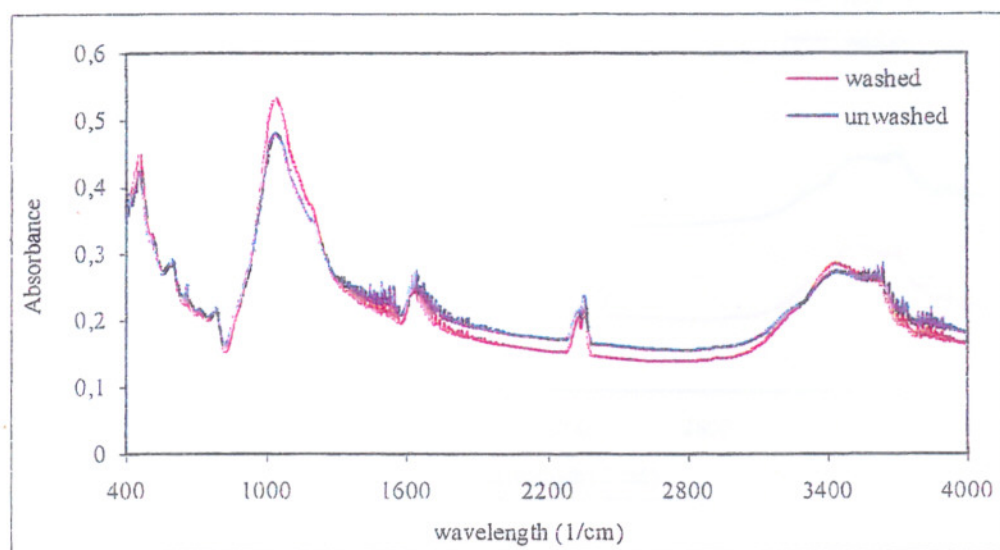
Figure 7.2. FTIR spectra for unwashed and washed clinoptilolite samples

The influence of regeneration at 350°C for 24 hours on the spectrum of clinoptilolite can be clearly seen in Figure 7.3. The intensities of the bands at 450 cm^{-1} (internal bending vibration of tetrahedra) and 1050 cm^{-1} (asymmetric stretching of internal T-O) were increased significantly after regeneration. This increase might indicate the removal of impurities from the surface of the zeolite sample. The slight increase in the band at 450 cm^{-1} was detected in the spectrum of regenerated sample. This may be attributed to the lattice vibrations caused by the movements due to dehydration as claimed by Flanigen et al. [88]. Rodriguez-Fuentes et al. [90] studied the influence of regeneration in natural zeolites considering the bands at 455, 1205 and 1645 cm^{-1}. Similar frequency shift was observed for the 1205 and 455 cm^{-1} band for thermally treated zeolite samples. Regeneration process also resulted the band intensities around 1650 and 3600 cm^{-1} to increase, since adsorbed H_2O gives rise to a typical deformation band around 1640 cm^{-1}. The IR spectra showed several adsorption bands around 1600 cm^{-1} caused by deformation of water molecules and in the stretching region (3400–3700 cm^{-1}), the spectra contain adsorption bands due to the isolated H_2O molecules [22].
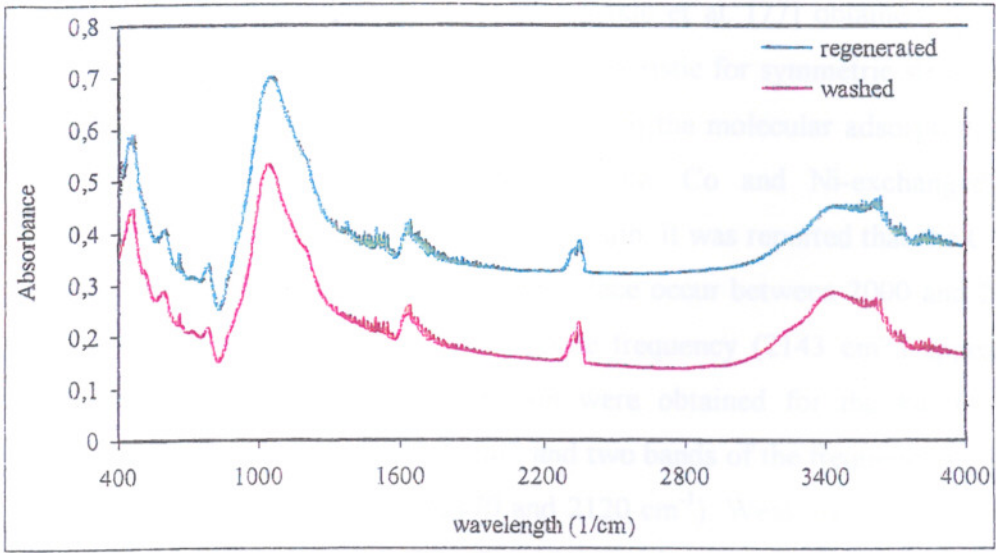
88

Figure 7.3. FTIR spectra for washed and regenerated clinoptilolite

The FTIR spectrum for CO adsorbed clinoptilolite and its comparison with the regenerated clinoptilolite is given in Figure 7.4.
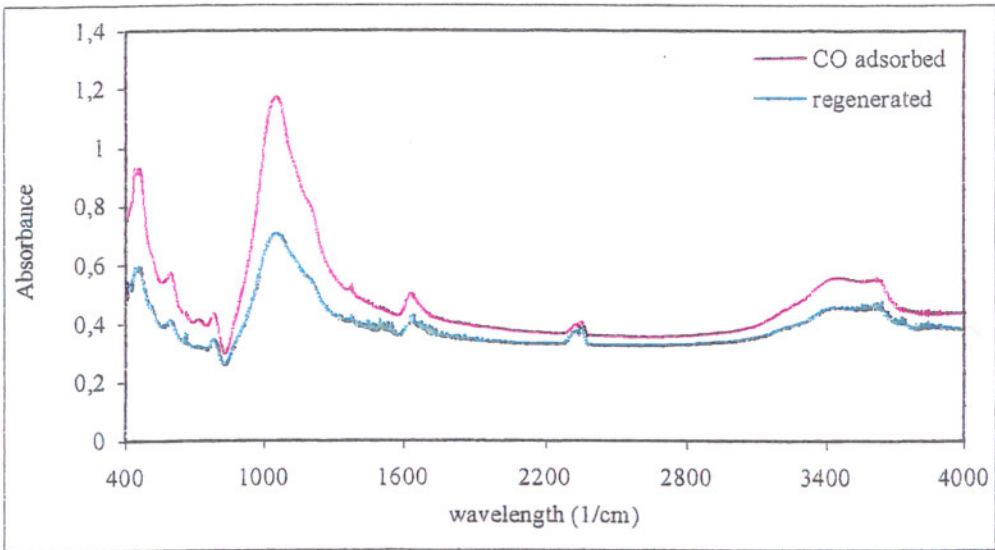

Figure 7.4. FTIR spectra for regenerated and CO adsorbed clinoptilolite

89

No significant difference was observed between the IR spectrum of regenerated and CO adsorbed clinoptilolite except the increases in all band intensities. However, during adsorption of CO from the gas stream (insitu) Rakic et al. [77] obtained IR absorption bands in the 2200-2000 cm^{-1} spectral region, characteristic for symmetric stretching of CO adsorbed on zeolites. These bands were attributed to the molecular adsorption of CO on Cu-exchanged Y and X zeolite samples. For Fe, Co and Ni-exchanged zeolites, disproportion of CO was noticed during its adsorption. It was reported that the C-O stretch bands of CO molecules adsorbed on a zeolite surface occur between 2000 and 2230 cm^{-1}, i.e., in the same region where the CO gas-phase frequency (2143 cm^{-1}) appears. Three overlapping bands in the C-O stretch region were obtained for the Fe, Co and Ni-exchanged zeolites: one band near 2200 cm^{-1} and two bands of the frequencies which were the same for all the zeolites studied (2170 and 2120 cm^{-1}). Weak overlapping bands near 1600 cm^{-1} were also found during CO adsorption on these samples. The appearance of a band near 2349 cm^{-1} has already been reported in the case of CO adsorption on monovalent and bivalent-cation-exchanged forms of FAU-type zeolites [78]. They explained the appearance of the bands near 2350 cm^{-1} by formation of CO_2 during the adsorption of CO on transition-metal cation-exchanged zeolites. The simultaneous appearance of the C-O stretch bands and the band at 2350 cm^{-1}, observed during the adsorption of CO on Fe^{2+}, Co^{2+} and Ni^{2+}-exchanged zeolites, confirms that disproportionation of CO and the formation of weakly bound CO_2 occurs during CO adsorption.

These reported characteristics bands for CO adsorption on zeolites were not observed on clinoptilolite zeolite, although the clinoptiloltie was rich in divalent cations. The possible reason may be that the FTIR spectra were not collected insitu during CO adsorption in this study or low adsorbed concentration of CO that could not be detected by FTIR detector.

7.5. Thermal Analysis

The weight percent losses both for washed and unwashed clinoptilolite samples for different N_2 flow rates and heating rates were obtained from TGA curves. The results are presented in Table 7. 3.

Table 7.3. Percent weight loss for unwashed and washed clinoptilolite samples obtained from thermogravimetric analysis

Heating Rate (°C/min)	N$_2$ Flow Rate (mL/min)	% weight loss	
		Unwashed	Washed
2	20	11.446	11.800
5	20	10.563	8.555
10	20	9.934	9.822
10	10	9.249	12.056
10	5	11.485	12.157

The average percent weight losses upto 800°C were calculated as 10.535 % for unwashed and as 10.878 % for washed clinoptilolite samples. The percent weight loss for washed sample was found to be smaller than that reported by Bish [91] who reported the weight loss of 14.50 %. The percent weight losses for washed samples were found generally greater than those were for unwashed samples, although there were exceptions. These differences in percent weight loss could be resulted from the differences in water contents which depends on the amount and type of the extra-framework cations [22, 13].

TGA curves of unwashed and washed clinoptilolite samples under analysis conditions of 10 mL/min N$_2$ flow rate and 10°C/min heating rate are given in Figure 7.5 and 7.6. There was no relationship between the percent weight loss and N$_2$ flow rate for both unwashed and washed samples. However, percent weight loss for the washed clinoptlolite sample increased with decreasing N$_2$ flow rate. There was no such linear relationship for the unwashed sample. Both samples showed continuous dehydration curves as a function of temperature. This indicated that the deydration process was reversible [13].

The water in clinoptilolite was classified in three groups as externally adsorbed water, loosely bound water and tightly bound water [92]. Thus, the dehydration occurs in stepwise manner, mainly at three steps, due to the different binding energies among water molecules and cations [91].

In order to distinguish these steps, tangents lines were drawn to the linear portions of TGA curves and vertical lines were dropped from their intersection points, so the boundaries between the linear portions were determined. The low temperature inflection point was observed at approximately 80°C. This could be explained by desorption of

externally adsorbed water. Other inflection point was detected at about 180°C and assigned to desorption of loosely bound water. These temperatures were in good agreement with those reported by Knowlton et al. [92] as 80°C and 170°C. They reported the high temperature inflection portion at about 260°C where slow desorption of tightly bound water from clinoptilolite started. For the clinoptilolite of interest in this study, the weight losses were recorded as 4.21 % up to about 80°C, 3.61 % from 80 to 180°C, 1.41 % from 180 to 260°C and 3.43 % from 260 to 800°C.

D-TG curves were obtained by differentiating the TGA curves with respect to time. A peak was observed at 47.46°C for unwashed and at 44.78°C for washed clinoptilolite samples. The weight loss rates were determined directly from the peak heights and were found approximately –0.00165 mg/min both for unwashed and washed samples.
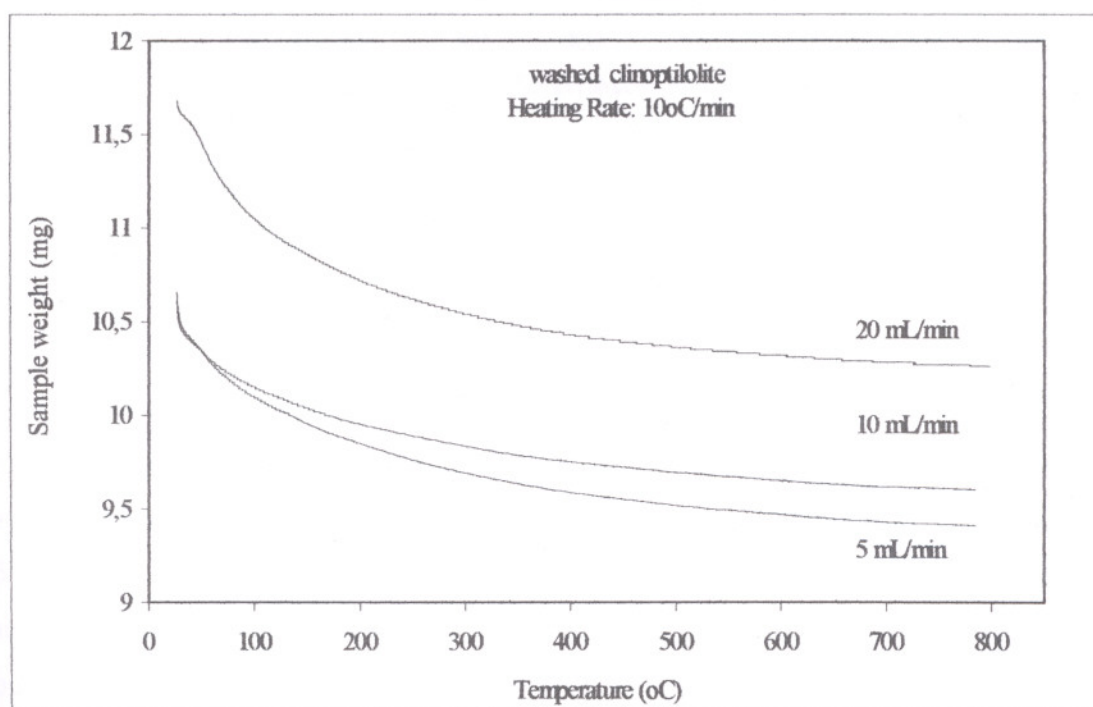

Figure 7.5. TGA curves for washed clinoptilolite samples showing the effect of N_2 flow rate on percent weight loss
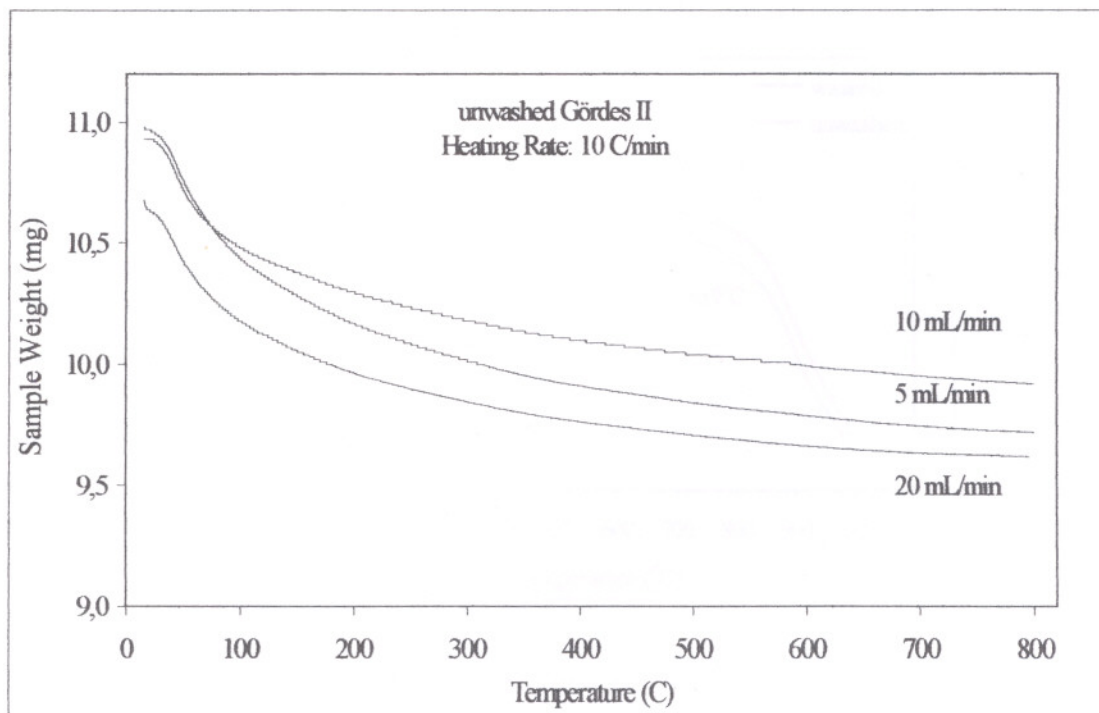
Figure 7.6. TGA curves for unwashed clinoptilolite samples showing the effect of
N_2 flow rate on percent weight loss

DTA curves obtained for both washed and unwashed clinoptilolite samples were
plotted in Figure 7.7. An endothermic and an exothermic peak were seen in DTA curves
for both unwashed and washed clinoptilolite samples. Endothermic peak was observed at
$45^\circ C$ which could be associated with the release of loosely bound water. The detection of
this peak at lower temperature as compared those reported in the literature ($125\text{-}160^\circ C$)
could be explained by the type of exchangeable cations [93, 94, 22, 92, 66]. According to
Tsitshivili et al. [22], this peak was expected at higher temperatures since our sample was
rich in Ca^{2+}. It was reported that the presence of such high-hydration-energy cations such
as Ca^{2+} causes the zeolite to retain their water to higher temperatures. Esenli and Kumbasar
[66] experienced also other endotherm at about $230^\circ C$. The presence of this peak was
explained by Na+K/Ca+Mg ratio between 0.58-1.27. Although this ratio is 0.723 for our
sample, such an endothermic peak were not observed during thermal analysis.
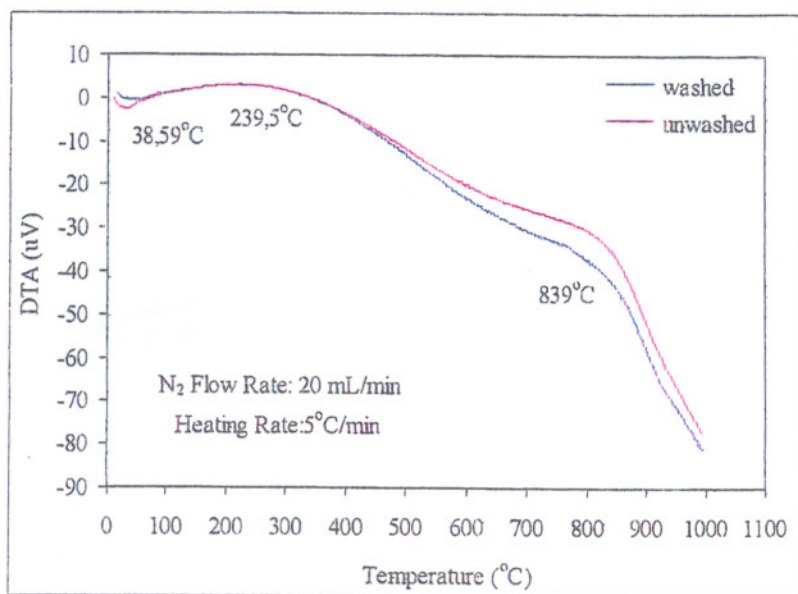
Figure 7.7. Comparison of DTA curves for unwashed and washed clinoptilolite samples
(N$_2$ Flow Rate: 20 mL/min, Heating Rate: 5°C/min)

The clinoptilolite samples exhibited no major structural change on dehydration up to 840°C. At this temperature the clinoptilolite might be converted to another amorphous or crystalline phase. The destruction temperature was reported as more than 1000°C by Meier [93], Barrer and White [94] and Milton [95], 750-800°C for clinoptilolite, as 550-600°C for its Ca- exchanged form by Tsitshivili et al.[22], as 750°C for clinoptilolites and 700°C for Ca- and Mg-rich clinoptilolites by Esenli and Kumbasar [66]. The high destruction temperature was attributed to the high Si/Al ratio of the clinoptilolite of 5.836. This was supported by Esenli and Kumbasar [66] who reported the destruction temperature of 700-750°C for Western Anatolian clinoptilolite with Si/Al ratio of 4.58-5.10.

7.6. Pore Volume and Surface Area Measurements

Argon adsorption and desorption isotherms obtained by volumetric adsorption method are plotted in Figure 7.8. Characteristic Type IV isotherm with characteristic hysteresis loop was obtained for argon on washed and unwashed clinoptilolite at 87.40 K
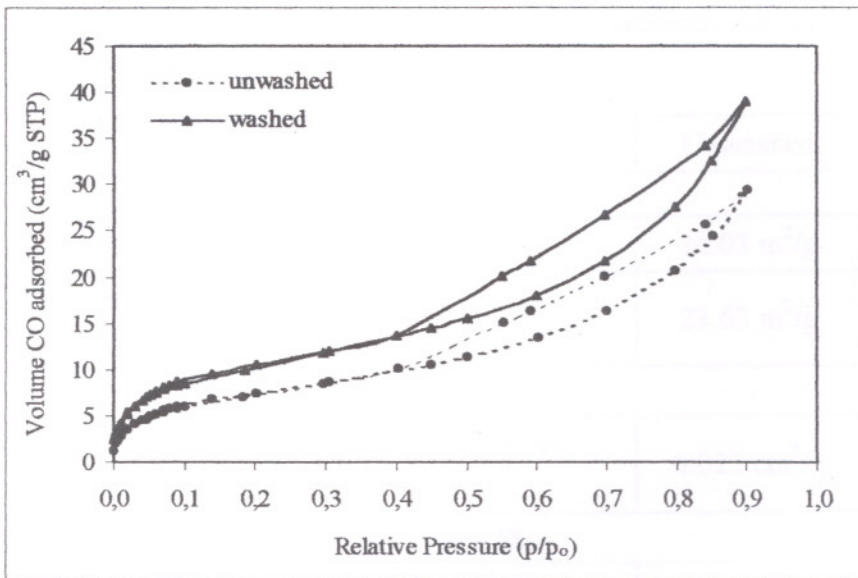
Figure 7.8. Adsorption and desorption isotherms
for Argon/Clinoptilolite system at 87.40 K

The initial rise in the adsorption isotherm is due to adsorbing molecules interacting first with the most energetic regions of the adsorbent surface. In this part of the isotherm, adsorption is restricted to monolayer on the pore walls. Then, the isotherm deviated upwards at a certain relative pressure. At this relative pressure, multilayer adsorption has started. Then at the interception of the hysteresis loop (p/p_o=0.4016) capillary condensation starts in mesopores. Hysteresis loop may exhibit various shapes depending on the specific pore structures. For the clinoptilolite characterized in this study, no any limiting adsorption was observed at high relative pressures. The same shape of hysteresis loop was observed with aggregates of plate-like particles giving rise to slit-shaped pores [97]. As the pressure was increased, wider pores were filled until the saturation pressure at p/p_o=0,9002.

Surface area was calculated by the Brunauer-Emmett-Teller (B.E.T) adsorption model using the equations (B.2 and B.3) given in Appendix B. Pore size distribution and surface area information in the micropore region was obtained by the application of Dubinin-Astakhov (D-A) and Horvath-Kawazoe micropore models applying the equations given in Appendix B. Pore size distribution for the micropore range for the clinoptilolite could not be determined, since Argon molecules are large to enter the clinoptilolite micropores. Pore size distribution for mesopore range was determined applying the Kelvin equation to the desorption branch of the isotherm and by BJH method as shown in Figure 7.9. The results of physisorption analysis for unwashed and washed clinoptilolite are given in Table 7. 4.

95

Table 7.4. Summary of adsorption and desorption measurements for unwashed and washed clinoptilolite (Argon at 87.4K)

| Parameter	Unwashed	Washed
Area		
BET Surface Area	24.03 m²/g	33.11 m²/g
BJH Desorption Cumulative Surface Area of Pores between 17 and 3000 Å diameter	23.63 m²/g	33.55 m²/g
Volume		
BJH Desorption Cumulative Pore Volume of Pores between 17 and 3000 Å diameter	0.022 cm³/g	0.039 cm³/g
Pore Size		
Average Pore Diameter (4V/A by BET)	62.54 Å	60.34 Å
BJH Desorption Average Pore Diameter (4V/A)	36.47 Å	46.28 Å
H – K Method		
Maximum Pore Volume at Relative Pressure 0.09024	0.008 cm³/g	0.010 cm³/g
Median Pore Diameter	8.91 Å	8.49 Å
D-A Method		
Micropore Surface Area (Astakhov)	37.607 m²/g	50.887 m²/g
Limiting Micropore Volume	0.023 cm³/g	0.031 cm³/g
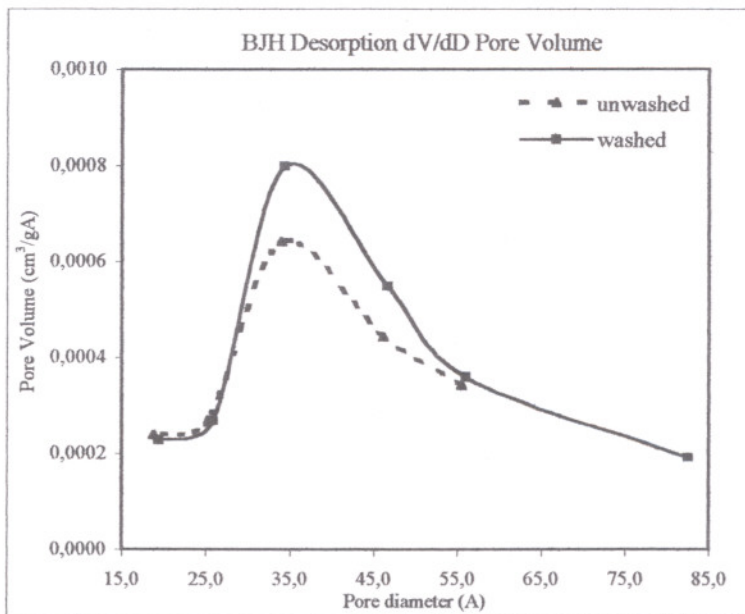
Figure 7.9. Mesopore size distribution for unwashed and washed clinoptilolite samples

7.7. Gas Chromatography Experiments

All chromatographic studies were carried out by the concentration pulse chromatography technique. Prior to the packed column experiments, different concentrations of CO pulses (2.5-100 %) were injected through the empty column in order to test the linearity of the thermal conductivity detector (TCD) response. The response peaks were analyzed at the column outlet and results are presented in Figure 7.10. This figure showed that there was a linear relationship between the inlet CO concentration and detector response for each flow rate studied.

The time passes between injection of CO pulse to the packed column and peak maximum obtained by GC is termed as retention time and that obtained using empty column is referred as dead retention time. Dead retention time values were obtained by the injection of 0.25 mL CO through the empty column. Net retention times were determined by subtracting the dead retention times from those for the packed column. The response peak characteristics are given in Table 7.5 and shown in Figures 7.11 – 7.14.
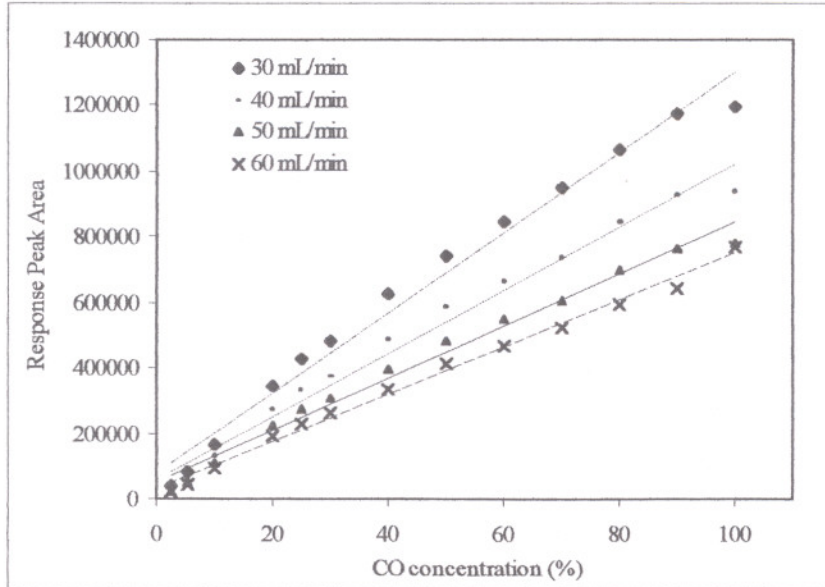

Figure 7.10. Diagrams showing change of TCD response with the
inlet CO concentration for different He flow rates (Column temperature: 60°C)

Table 7.5. Characteristics of response peaks for empty and packed columns

| T (°C) | He Flow Rate (mL/min) | PACKED COLUMN | | | EMPTY COLUMN | | | NET |
		Retention Time (min)	Peak Area	Peak Height (µV)	Retention Time (min)	Peak Area	Peak Height (µV)	Retention Time (min)
60	30	16.662	389156	333	0.610	290233	17261	16.052
	40	13.096	305904	327	0.419	232483	20360	12.677
	50	10.470	241815	321	0.375	194629	20937	10.095
	60	9.128	205907	322	0.369	187916	19529	8.759
80	30	6.358	400665	1068	0.623	297386	17111	5.735
	40	4.942	327255	1051	0.426	231724	20443	4.516
	50	3.911	249524	1027	0.401	188254	17552	3.510
	60	3.450	229769	1054	0.367	186367	20389	3.083
100	30	3.175	439209	2953	0.603	293856	17355	2.572
	40	2.186	329959	3073	0.410	231568	20804	1.776
	50	1.519	264463	3239	0.378	190118	18986	1.141
	60	1.486	259101	3294	0.351	186503	20136	1.135
120	30	2.078	406546	5574	0.578	289561	17507	1.500
	40	1.671	306787	5364	0.413	231020	20690	1.258
	50	1.358	251597	5378	0.366	190472	19056	0.992
	60	1.343	261451	5634	0.366	186450	19126	0.977

Although the peaks were symmetric for empty column data, tailed peaks were obtained from the packed column experiments. These tailed peaks designated the existence of significant intraparticle resistances, but due to the high carrier gas velocity, micropore resistance could not be determined [38]. Tailed response peaks also indicated the slow penetration of micropores, i.e. time of passage through the column by the He carrier gas containing CO pulse was comparable to the micropore time constant ($r_c^2/15KD_c$) [38].

This chromatographic data was also analyzed in terms of adsorbed and desorbed CO amounts at different He flow rates and column temperatures. Since the response peak area gives information about the adsorbed amount of CO, multiplication of the response peak area with the He flow rate is related to the desorbed amount of CO. The change of desorbed amount of CO with the column temperature and He flow rate is given in Table 7.6 and in Figure 7. 11. The desorbed amount of CO did not change significantly with He flow rates and column temperatures indicating negligible effect of external mass transfer resistance contributing to CO diffusion and adsorption in clinoptilolite except at high He flow rates.

Table 7.6. Change of adsorbed amount of CO with the column temperature and He gas flow rate

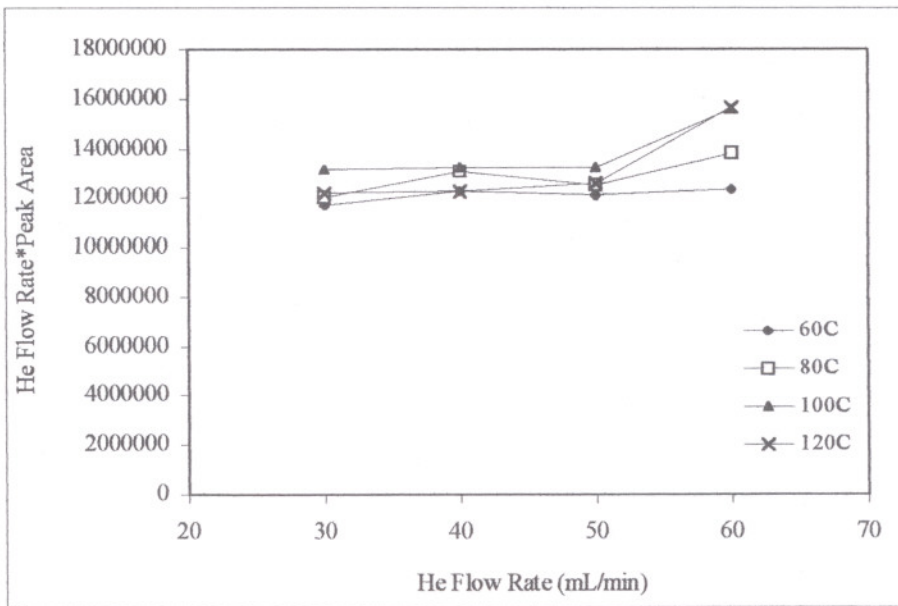| T (°C)	He Flow Rate (mL/min)	He Flow Rate * Peak Area
60	30	11674680
	40	12236160
	50	12090750
	60	12354420
80	30	12019950
	40	13090200
	50	12476200
	60	13786140
100	30	13176270
	40	13198360
	50	13223150
	60	15546060
120	30	12196380
	40	12271480
	50	12579850
	60	15687060

Figure 7.11. Change of adsorbed amount of CO with column temperature and He flow rates
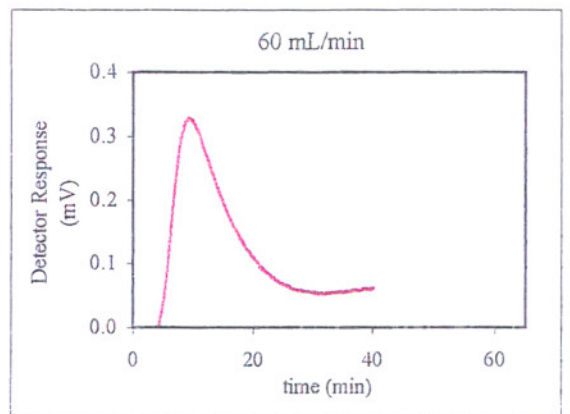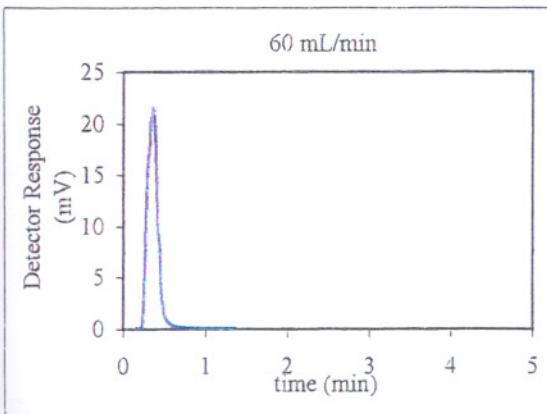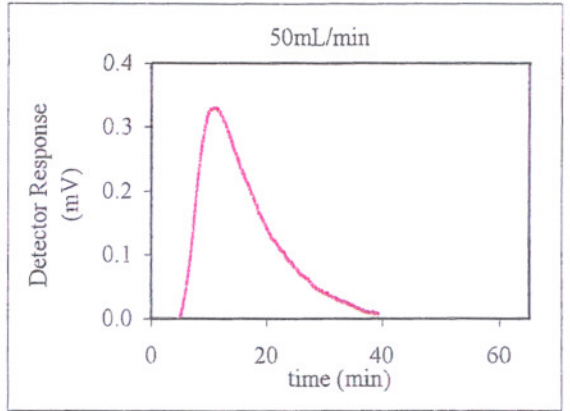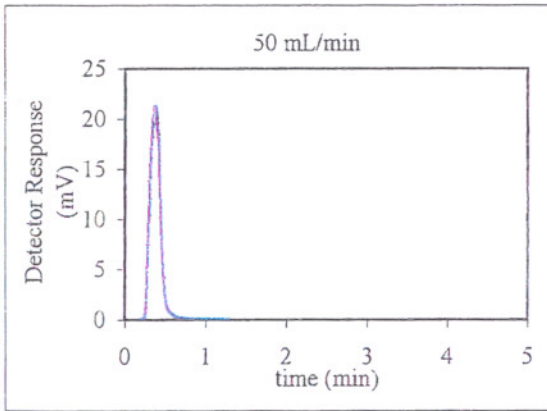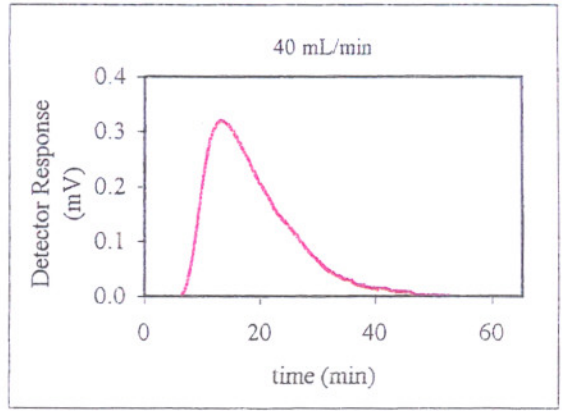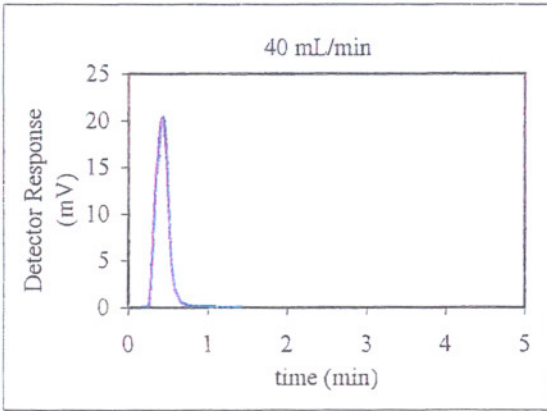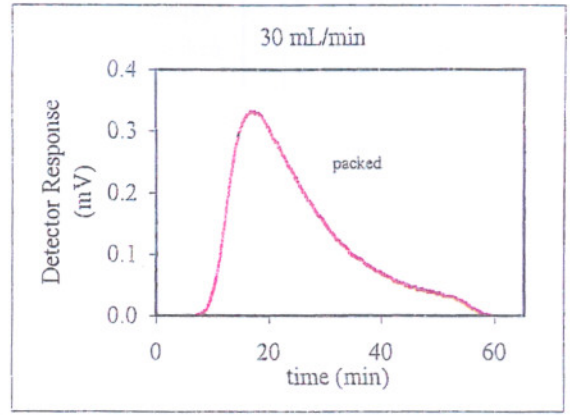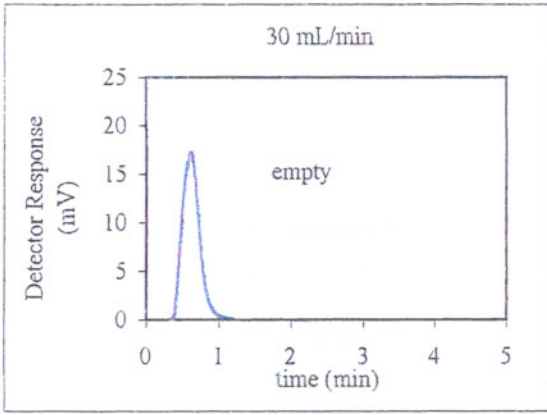
Figure 7.12. Chromatographic response peaks for empty and packed columns (60°C)

Figure 7.13. Chromatographic response peaks for empty and packed columns (80°C)

Figure 7.14. Chromatographic response peaks for empty and packed columns (100°C)

Figure 7.15. Chromatographic response peaks for empty and packed columns (120°C)

These response peaks were then processed and integrated numerically. The first and second moments of the chromatographic peaks were calculated by trapezoidal integration method using Equations (4.18) and (4.19) for both empty and packed columns. The net first and second moments were calculated by subtracting the empty column fir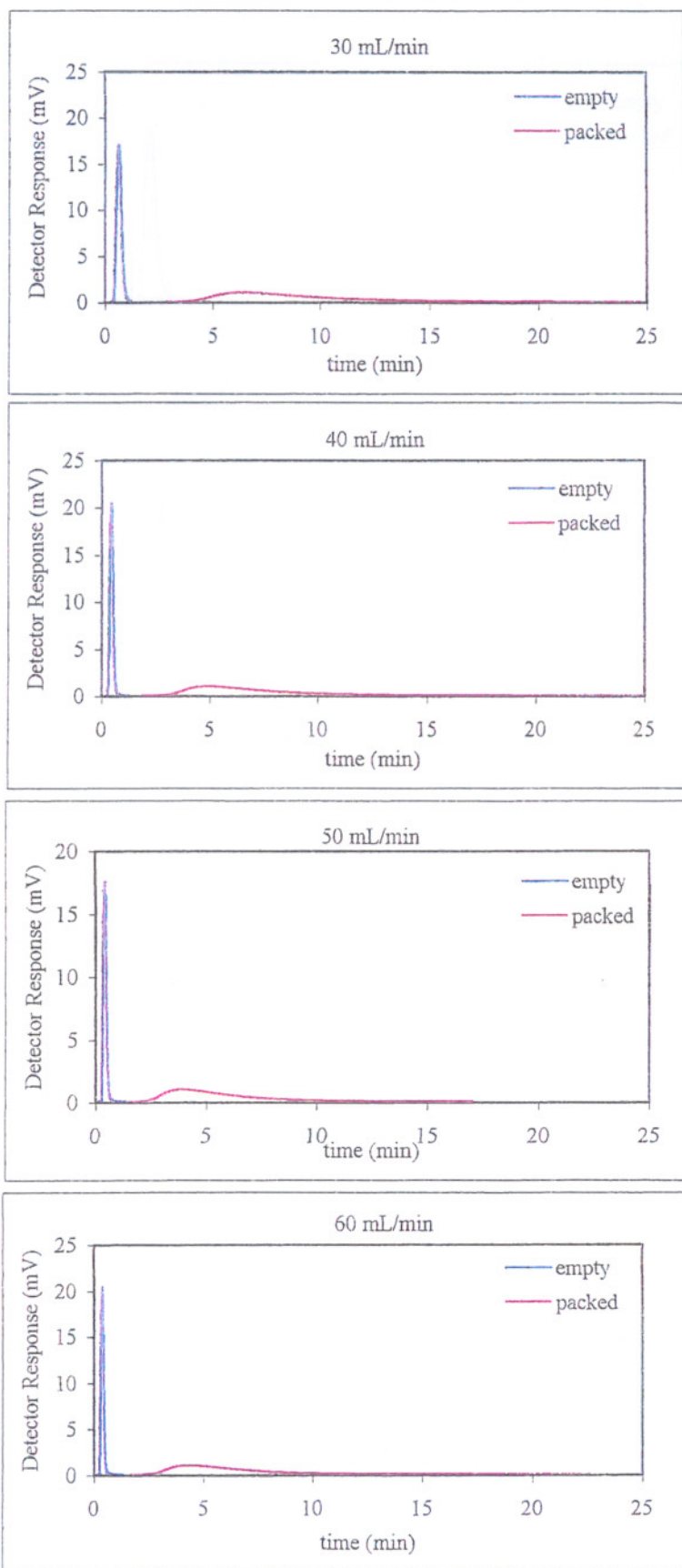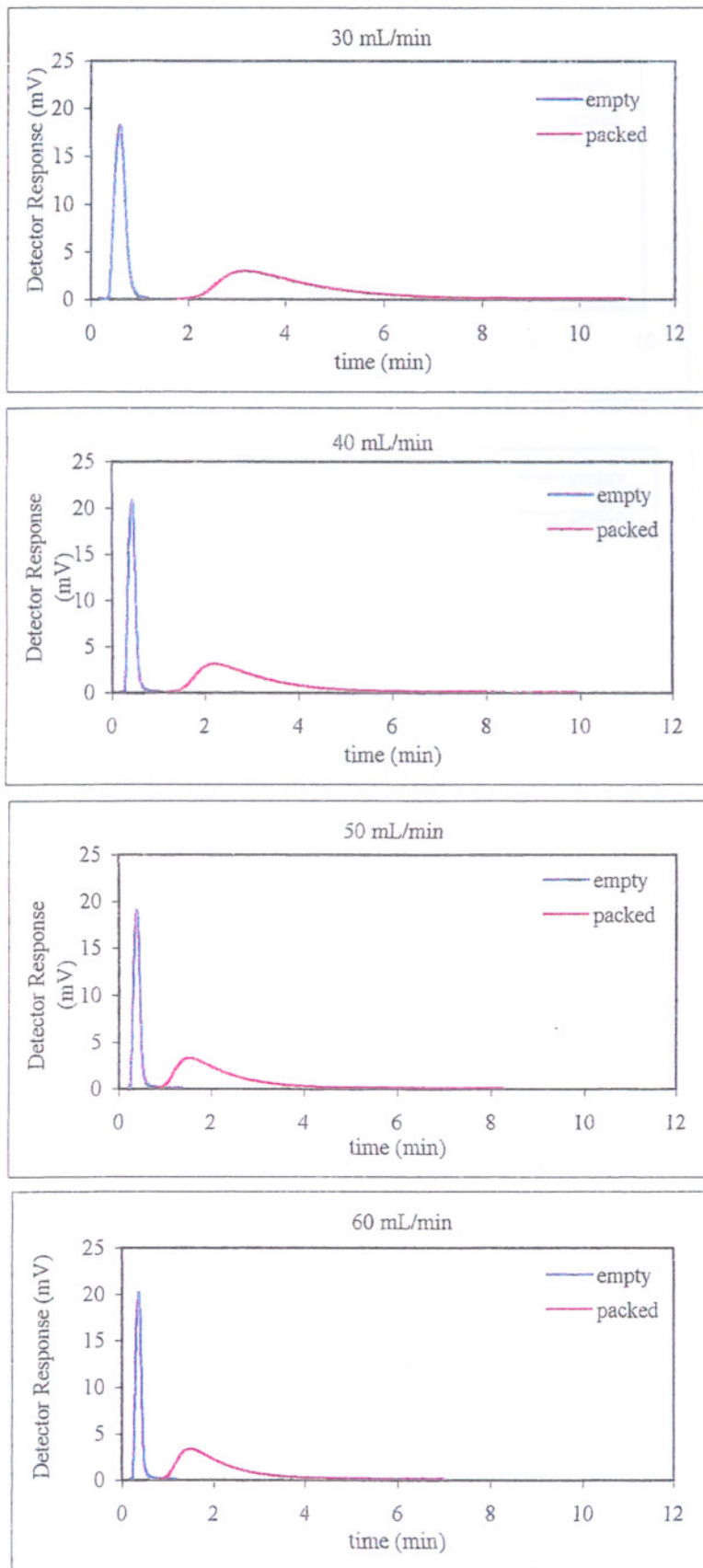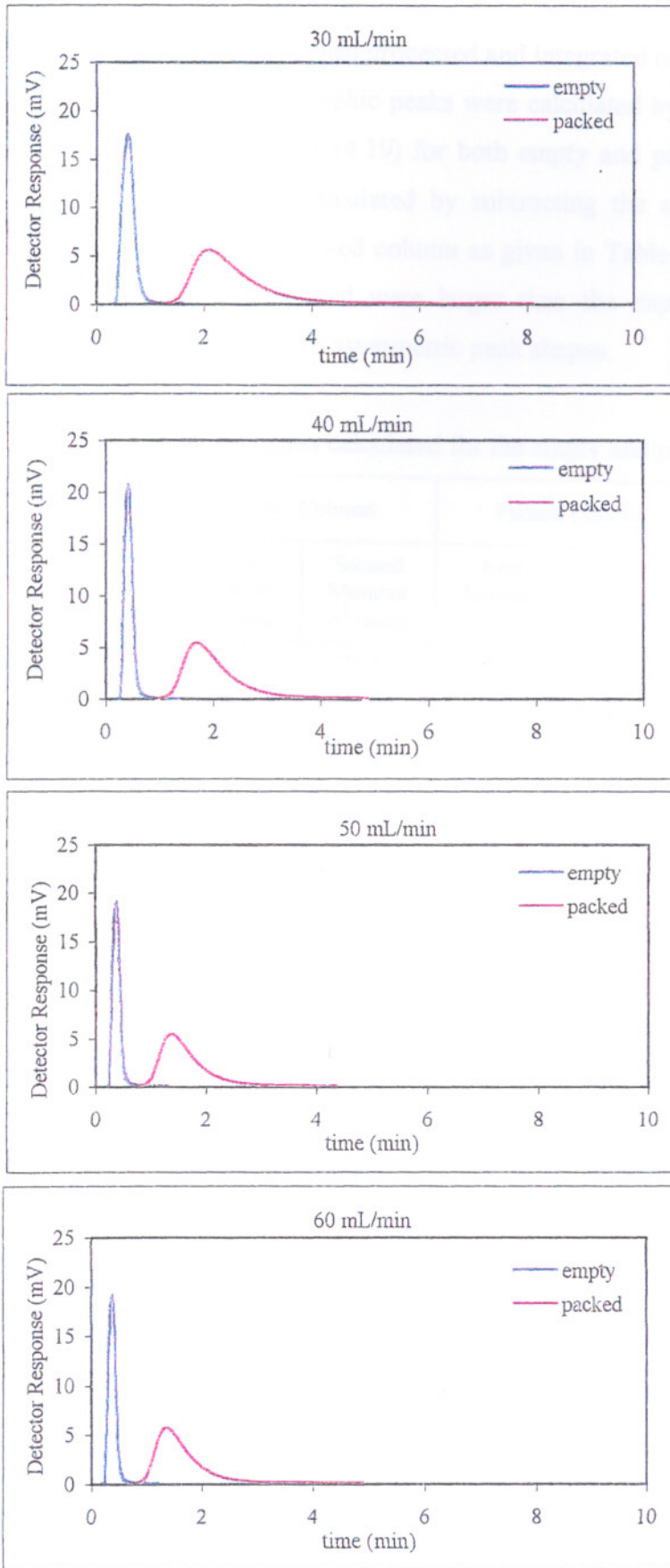st and second moments from those for packed column as given in Table 7.7. The first moments for chromatographic peaks calculated were larger than the experimentally determined retention time. This was attributed to asymmetric peak shapes.

Table 7.7. First and second moments calculated for the empty and packed columns

Column Temperature (°C)	He Flow Rate (mL/min)	Empty Column		Packed Column		Net	
		First Moment μ (min)	Second Moment σ^2 (min)	First Moment μ (min)	Second Moment σ^2 (min)	First Moment (min)	Second Moment (min)
60	30	0.627	0.014	24.883	105.124	24.256	105.110
	40	0.433	0.086	18.308	42.523	17.875	42.437
	50	0.379	0.079	15.734	45.134	15.355	45.055
	60	0.364	0.104	16.747	81.981	16.383	81.877
80	30	0.640	0.014	9.048	13.252	8.408	13.238
	40	0.441	0.050	7.567	15.051	7.127	15.001
	50	0.415	0.090	5.990	8.203	5.575	8.113
	60	0.378	0.087	6.827	13.423	6.449	13.336
100	30	0.600	0.019	4.177	2.091	3.557	2.073
	40	0.422	0.092	2.989	1.426	2.567	1.334
	50	0.390	0.101	2.127	0.782	1.737	0.681
	60	0.361	0.082	2.038	0.606	1.677	0.524
120	30	0.604	0.073	2.551	0.608	0.608	0.535
	40	0.425	0.077	1.974	0.308	0.308	0.231
	50	0.376	0.081	1.613	0.200	0.200	0.119
	60	0.376	0.064	1.607	0.220	0.220	0.156

It was observed that the CO pulse retained in the column shorter time as the flow rate increases. Small differences were recorded in the peak area values as the column temperature increased. However, the peak area changed linearly with the increasing carrier gas flow rate. It was also noticed that the peak height increased as temperature increases.

Analysis of the moments obtained under different experimental conditions was performed in two groups. The first part involves determination of the adsorption equilibrium constants and heats of adsorption for CO adsorption on clinoptilolite. The first moments of the chromatographic peaks obtained under constant carrier flow rates and changing column temperatures were analyzed for these purposes. In order to check whether the equilibrium was reached in the column or not, the net first moments versus $1/v_i$ were plotted for temperature range as in Figure 7.16. Linear relationship between the net first moment values and reciprocal of the interstitial velocity was obtained at low He gas velocities which verified that the equilibrium was reached in the column. Significant deviation from linearity was observed indicating that nonequilibrium effects existed at higher He flow rates.
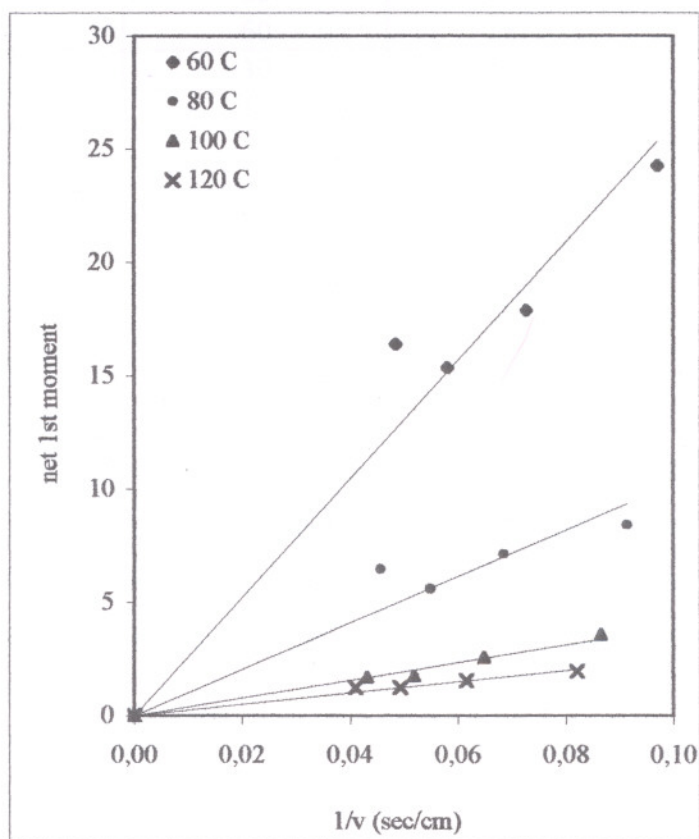
Figure 7.16. Dependence of the first moment on carrier gas flow rate

The dimensionless Henry's Law constants were calculated at 60, 80, 100 and 120°C column temperatures from the first moment Equation (4.22) and the results are given in Table 7.8.

Table 7. 8. Dimensionless Henry's Law constants (K) for CO/clinoptilolite system

T (°C)	He Flow Rate (mL/min)	K (dimensionless)
60	30	696,72
	40	684.24
	50	737.00
	60	951.83
80	30	237.92
	40	272.73
	50	266.09
	60	380.45
100	30	90.99
	40	85.76
	50	68.10
	60	83.66
120	30	39.80
	40	44.02
	50	43.82
	60	58.05

The Henry's constants were found to decrease with increasing temperature and change slightly with He flow rate. The temperature dependence of the Henry's Law constants is described by Arrhenius type equation (4.23). The Henry's Law constants versus reciprocal of temperature for CO adsorption on the clinoptilolite (van't Hoff plots) is shown in Figure 7.17.

Then, K_o, dimensionless equilibrium constant of adsorption, was determined from the y-axis intercept and internal energy change of sorption, $-\Delta U_o$ from the slope of the straight lines. The heat of adsorption at zero coverage, $-\Delta H_o$ for CO on clinoptilolite was calculated using the Equation (4.24) and their comparison with literature are given in Table 7.9.

Figure 7.17. Dependence of Henry Law constants on temperature
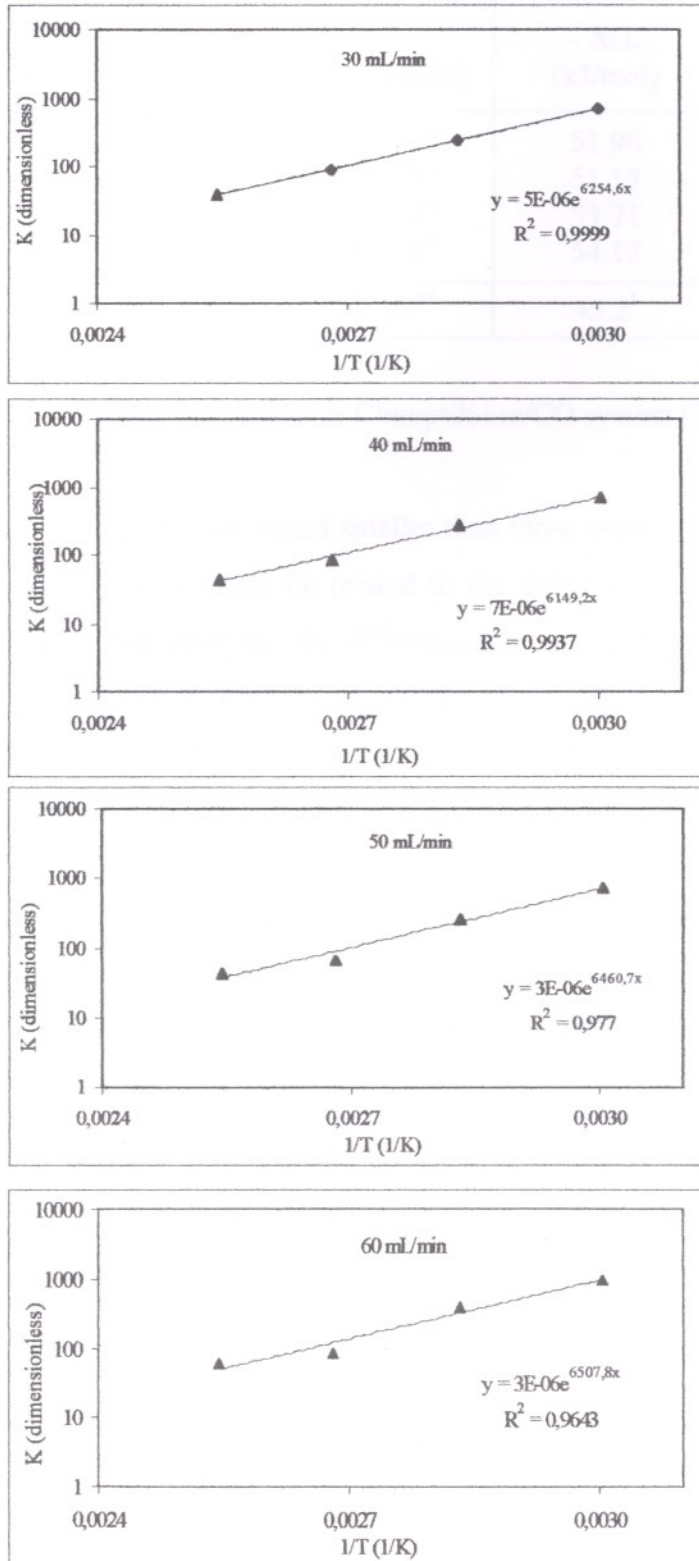for CO/clinoptilolite system (van't Hoff plots).

Table 7.9. Parameters K_o, $-\Delta U_o$ and $-\Delta H_o$ for CO on clinoptilolite

Temperature Range (°C)	He Flow Rate (mL/min)	K_o (dimensionless)	$-\Delta U_o$ (kJ/mol)	$-\Delta H_o$ (kJ/mol)
60 – 120	30	4.82×10^{-6}	51.96	54.98
	40	6.71×10^{-6}	51.13	54.15
	50	2.71×10^{-6}	53.71	56.73
	60	3.13×10^{-6}	54.12	57.14
50 – 200[*]	7-15[*]	7.3×10^{-5}[*]	45.2[*]	48.5[*]

[*] Results obtained by Triebe and Tezel for Clinoptilolite/CO system [70].

The measured K_o values were found smaller than those were given by Triebe and Tezel [70] in the literature. This might be related to the different carrier gas flow rates studied. It could be also explained by the differences in the nature of the adsorbent-adsorbate and adsorbate-adsorbate interactions which depends on the structure and cation type and content of the clinoptilolite sample. Although the adsorbent/adsorbate pair was the same, the inconsistency of the natural zeolite sample might have led into such difference.

The second group of chromatographic data analysis was performed to estimate the transport properties. For this purpose, the second moments of the chromatographic peaks were compared to the theoretical values. First of all, contribution from micropore diffusional resistance to total mass transfer resistance was checked by examining the dependence of the total dispersion ($\frac{\sigma^2 L}{2\mu^2 v}$) on the column temperature under constant He flow rates. Total dispersion values obtained using the net second moment data are presented in Table 7.10. The results are also given as total dispersion versus column temperature plots in Figure 7.18.

Table 7.10. Dependence of dispersion on temperature for CO/ Clinoptilolite system

Temperature (°C)	Carrier gas Flow rate (mL/min)	Total dispersion ($\sigma^2 L/2\mu^2 v$) (sec)
60	30	0.087
	40	0.086
	50	0.070
	60	0.058
80	30	0.048
	40	0.101
	50	0.066
	60	0.030
100	30	0.056
	40	0.072
	50	0.059
	60	0.019
120	30	0.074
	40	0.073
	50	0.040
	60	0.021
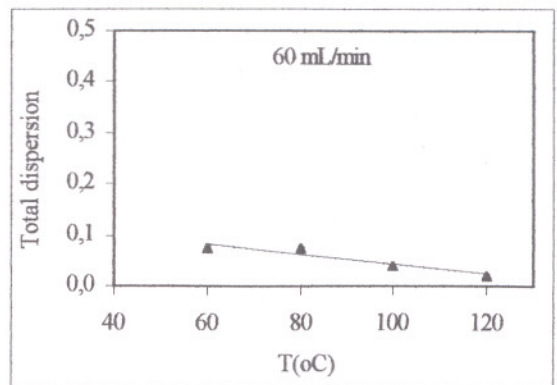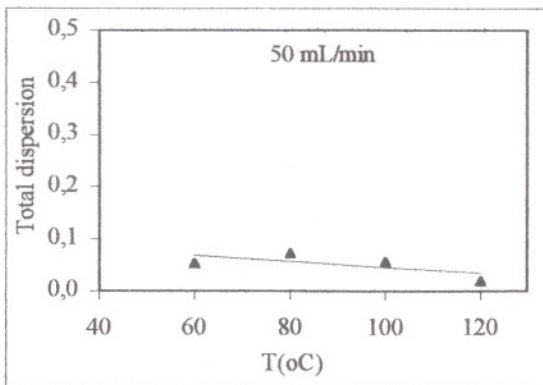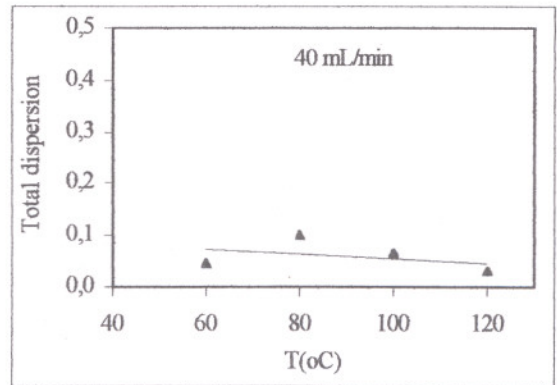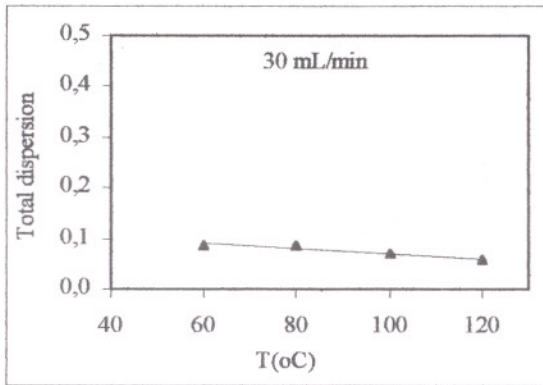
Figure 7.18. Total dispersion versus temperature for different He flow rates

Figure 7.18 suggested that the total dispersion changed slightly as a function of column temperature for the He flow rates examined. It might be concluded that the micropore diffusion was not a significant resistance under the experimental conditions of interest, since the only strongly temperature dependent resistance on the right hand side of the second moment equation (4.26) is micropore diffusion. Therefore, micropore diffusion coefficient for CO in clinoptilolite could not be measured under the experimental conditions studied.

Furthermore, in order to separate the contributions from axial dispersion and other mass transfer resistances, the plots of $\sigma^2 L/2\mu^2 v$ versus $1/v^2$ were plotted for different temperatures, shown in Figure 7.19.
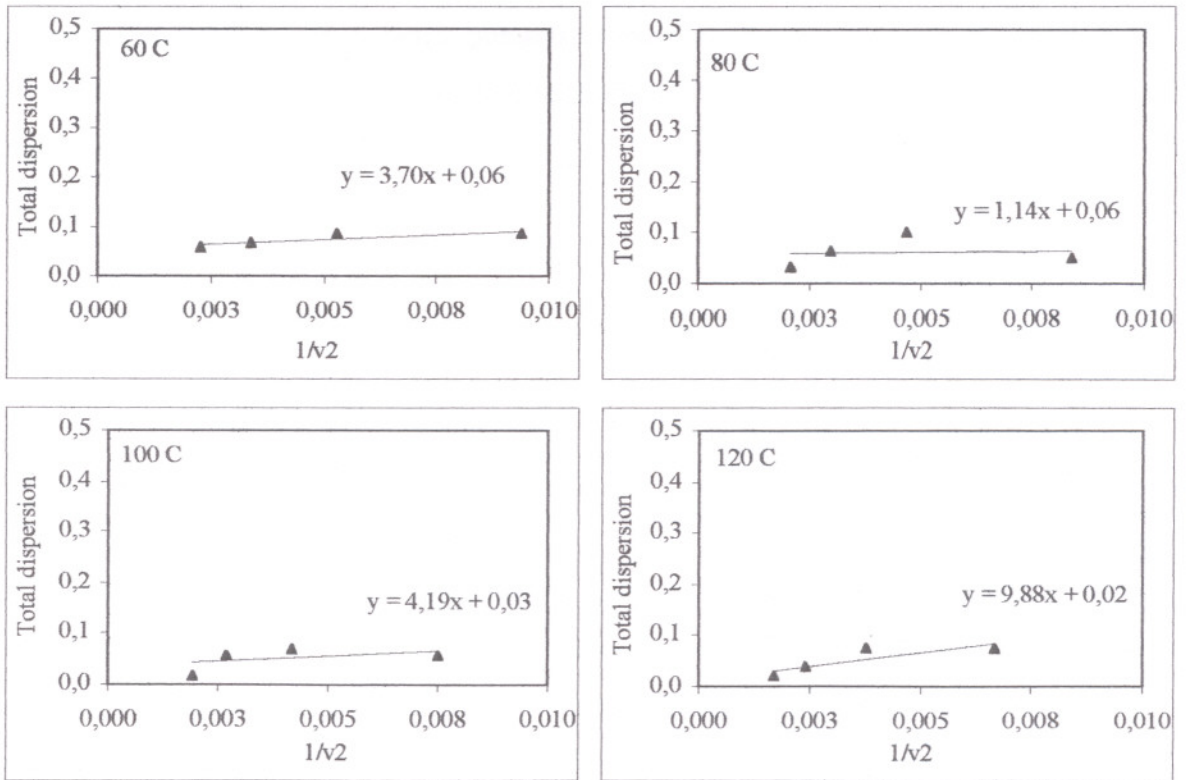
Figure 7.19. Dependence of total dispersion on carrier gas velocity at different temperatures

$\sigma^2 L/2\mu^2 v$ increased very gradually as $1/v^2$ increased. This gradual increase was caused by the contribution from longitudinal dispersion. The total dispersion versus $1/v^2$ plots exhibited poor linearity, except that at 60°C. This poor linearity could be explained by the dependency of the axial dispersion on the carrier gas velocities studied in the experiments.

The slope of the total dispersion versus $1/v^2$ plot represents the axial dispersion, D_L, and the intercept represents the other combined mass transfer resistances. These values were calculated in the range of 1.14 - 9.88 cm²/sec and 0.02 - 0.06 s, respectively.

In order to determine the micropore (zeolitic) diffusivity, other mass transfer contributions were estimated. The macropore diffusional coefficient and external film resistances were calculated by using empirical correlations previously given in Chapter 4.

The molecular diffusion coefficient of CO in He gas was estimated using collision diameter from the Lennard–Jones potential theory as 3.121 Å using the data from Hirschfelder et al. [96] and the equation developed by Chapman and Enskog (4.33). The results obtained are given in Table 7.11.

Table 7.11. Molecular diffusion coefficients for CO in He

Temperature (°C)	D_m (cm²/sec)
60	0.843
80	0.920
100	0.999
120	1.081

Relative importance of molecular or Knudsen diffusivity in macropore diffusion depends on the ratio of average macropore diameter and mean free path length. The mean free path was calculated from Equation (4.28) in the range of 1049.30 at 60°C and 1238.36 Å at 120°C. Mean free path was found to be higher than the average mesopore diameter of 46.28 Å determined from volumetric adsorption analysis implying that the collisions of CO molecules with the pore walls occurred more frequently than collisions between diffusing CO molecules. Thus, under these conditions, Knudsen diffusion was more significant and it was calculated from Equation (4.29) in the range of 0.0155 - 0.0168 cm²/sec. Then, macropore diffusion coefficient, D_p, was calculated in the range of $2.54\times10^{-3} - 2.76\times10^{-3}$ cm²/sec taking both Knudsen and molecular diffusion into account according to Equation

(4.32). In this calculation tortuosity factor (τ) was chosen as 6 for the calculation, estimating the maximum contribution of the macropore diffusion resistance.

The external film resistance was correlated as in Equation (4.34). The Schmidt numbers were calculated in the range of $1.14 - 1.46$ and Reynolds numbers in the range of $0.18 - 0.29$. Sherwood number was estimated in the range of $2.24 - 2.37$ from Equation (4.36). Thus, the clinoptilolite particles were considered as isolated spherical particles in a stagnant fluid. Then, the external mass transfer coefficient, k was calculated in $31.29 - 42.44$ cm/sec range.

The Biot number for mass transfer which is the measure of the ratio of internal-to-external concentration gradients was calculated in the 487-546 range. Under these conditions, the internal mass transfer resistance was greater than the external, as expected.

Therefore the micropore diffusional resistance were then calculated by subtracting the contributions of axial dispersion, external mass transfer and macropore diffusional resistances from the overall dispersion. The contributions of mass transfer resistances to total dispersion for the CO/Clinoptilolite system were calculated and are given in the following Table 7.12. However, since the mesopore diffusion resistance was found to be dominant, it was equated to the total mass transfer resistance and D_p was calculated as 2.98×10^{-3} cm^2/sec. This value was in good agreement with the theoretically determined D_p value of $2.54 \times 10^{-3} - 2.76 \times 10^{-3}$ cm^2/sec.

Table 7.12. Contributions from different mass transfer resistances and axial dispersion and comparison with the values in the literature for CO/Clinoptilolite system

T (°C)	$\dfrac{D_L}{v^2}$ (s)	$\dfrac{R_p^2}{3D_m}$ (s)	$\dfrac{R_p^2}{15\varepsilon_p D_p}$ (s)	$\dfrac{r_c^2}{15D_c K}$ (s)
60	0.0087 - 0.035	$2.81 \times 10^{-4} - 3.61 \times 10^{-4}$	$0.065 - 0.070$	negligible
70*	1.36	11.8×10^{-4}	5.05×10^{-3}	0.14
100*	1.02	10.5×10^{-4}	4.60×10^{-3}	0.15
120*	1.27	9.42×10^{-4}	4.22×10^{-3}	0.10
150*	1.26	8.51×10^{-4}	3.89×10^{-3}	0.13

* Results reported by Triebe, Tezel [70].

CHAPTER 8

CONCLUSIONS

A number of conclusions can be made considering the results of this study:

Elemental analysis (ICP) indicated that the cation content of the clinoptilolite decreased in the order of Ca(4.91) > K(3.28) > Fe(1.56) > Mg(1.26) > Na(1.18) > Ni(0.18) > B(0.14). The major cations for the clinoptilolite were Ca^{2+} and K^+, followed by Fe^{2+} and Mg^{2+} and a small amount of Na^+. Si/Al ratio of clinoptilolite was determined as 5,836. The type, amount and location of the cations were shown to be determinant for the adsorption and diffusion properties of the adsorbent and heats of adsorption.

No interpretable band was observed in FTIR spectra for the CO-adsorbed clinoptilolite. Thus, the FTIR analysis should be performed insitu. Thermal analysis showed that the average percent weight loss up to $800^{\circ}C$ was 10.535 for unwashed and 10.878 for washed clinoptilolite samples. The destruction temperature for the clinoptilolite was determined as about $840^{\circ}C$ from DTA. This high temperature was attributed to the high Si/Al ratio.

Argon adsorption and desorption isotherm of Type IV with a hysteresis loop was obtained by volumetric adsorption method at 87.4 K. The adsorption isotherms of the washed and unwashed clinoptilolite samples were compared based on their adsorption capacity. The higher argon adsorption capacity of the washed clinoptilolite was explained by the removal of impurities from clinoptilolite structure by washing. The specific surface area of the washed clinoptilolite was determined as 33.11 m^2/g by BET model. Cumulative surface area, pore volume and average mesopore diameter were obtained by BJH method as 33.55 m^2/g, 0.0388 cm^3/g, and 46.28 Å, respectively. Maximum pore volume and median micropore diameter were calculated as 0.0103 cm^3/g and 8.49 Å, respectively by Horvath–Kawazoe model. Dubinin-Astakhov model was applied to determine the micropore surface area and found as 50.887 m^2/g.

Asymmetric or tailed chromatographic response peaks were obtained with packed column. These tailed peaks were associated with the dominance of micropore and mesopore diffusion resistances to mass transfers. Broader peaks were obtained with decreasing carrier gas flow rate due to increased micro and mesopore mass transfer resistances and increased residence time of CO in the column. Therefore, CO interacted with the aluminosilicate framework and cations more strongly leading to the longer diffusion times. The peak areas changed slightly as the column temperature increased while they decreased with increasing carrier gas flow rate. Moment analysis showed that equilibrium was reached in the column.

The Henry's law constants (K) were found to decrease with increasing temperature in the range of 40 - 952. The heats of adsorption almost remained constant with carrier gas flow rate, around 55.75 kJ/mol. The difference between the calculated heats of adsorption and those in the literature was attributed to the pore size, cation content and accessibility of cations in the clinoptilolite framework (affecting the nature of the adsorbent-adsorbate and adsorbate-adsorbate interactions).

Total dispersion including the contributions from micropore, mesopore and external mass transfer resistances changed slightly with temperature. It was concluded that the micropore diffusional resistance was not controlling mechanism in diffusion of CO in clinoptilolite under the experimental conditions studied and the mesopore diffusion resistance was dominant mechanism. This was not to say that micropore diffusion did not take place, but since the value of r_c^2/D_c was too small, i.e. the micropore diffusional time constant (D_c/r_c^2) was large and the diffusion of CO in micropores is slow, the chromatographic technique was too rapid to measure this slow diffusion in the micropores.

The total resistance from external mass transfer, micropore and mesopore diffusion was determined in the range of 0.02 - 0.06 cm^2/sec. Since the mesopore diffusion resistance was found to be dominant, it was equated to the total mass transfer resistance and the mesopore diffusion coefficient, D_p was calculated as 2.98×10^{-3} cm^2/sec. This value was in good agreement with the theoretically determined D_p value.

The diffusion of CO in clinoptilolite was controlled by the mesopore diffusion mechanism under the experimental conditions, so it was not possible to determine the micropore diffusivity. The dispersion of the response peak must be dominated by micropore resistance in order to measure the micropore diffusivity by gas chromatographic method.

APPENDIX A

Pressure Drop Calculation

Pressure drop across the packed column was calculated using the Ergun's correlation for dimensionless friction factor, f as [39]:

$$f = \left(\frac{1-\varepsilon}{\varepsilon^3}\right)\left[\frac{150(1-\varepsilon)}{Re} + 1.75\right]$$ (A.1)

For the interstitial velocities covered in this study, f was found in the 6723.8 - 13413.63 range and it was related to the pressure drop by:

$$f = \left(\frac{2R_p}{L}\right)\frac{\Delta p}{\rho_f (\varepsilon v)^2}$$ (A.2)

where Δp is the pressure drop (N/m^2) across a length L of packed column, εv is superficial fluid velocity.

The pressure at the column inlet was 100 kPa. Then the pressure drop was calculated as 0.034 - 0.731 kPa which was accepted as negligible.

APPENDIX B

Pore Size and Surface Area Measurements

Surface area is yielded from the lower region of the adsorption isotherm. The Langmuir and Brunauer-Emmett-Teller (B.E.T) adsorption models have been widely used to determine the surface areas of the adsorbents. These theories consider the number of molecules required for the completition of a monolayer [98]. Then, the surface area is determined from the product of the number of molecules in a completed monolayer and the specific surface area of the adsorbent is calculated from surface area occupied by a single adsorbed gas molecule (14.2 Å^2 for Argon). BET is the generalized form of the Langmuir theory and involves the multilayer adsorption.

BET Model assumes that all adsorption sites on a surface are identically energetic, and same forces are effective both in condensation and multilayer formation. The interactions between the adsorbed molecules on the surface are neglected. The BET model equation is given as;

$$\frac{p}{V_a(p_o - p)} = \frac{1}{V_m C} + \frac{C-1}{V_m C}\left(\frac{p}{p_o}\right) \tag{B.1}$$

where V_a is the amount adsorbed at the relative pressure p/p_o, V_m is the monolayer capacity and C is a constant which is related exponentially to the heat of adsorption for the first layer. C is usually between 50 and 300 when nitrogen is used as an adsorptive at 77 K. Negative and high C values (>300) indicates the presence of micropores and BET Model is questionable for surface area determination [80]. The range of linear relationship between $p/V_a(p_o-p)$ and p/p_o is required for the BET model and the linearity is restricted in the p/p_o range of 0.05 – 0.35. Then knowing the area occupied by a single Argon molecule (a_a=14.2 Å), the surface area of the adsorbent (A_s) was calculated as:

$$A_s = V_m N_A a_a \tag{B.2}$$

where N_A is the Avogadro's number. The mesopore size distribution was treated with using the Kelvin equation:

$$\ln\left(\frac{p^*}{p_o}\right) = -\left(\frac{2\gamma\varpi\cos\theta}{RTr_m}\right)$$ (B.3)

where p^* is the critical condensation pressure, θ is the contact angle between the adsorbent and condensed adsorptive, r_m is the mean radius of curvature of the liquid meniscus, and γ and ϖ are the surface tension and molar volume of the liquid condensate, respectively.

The Kelvin equation assumes that the adsorptive condensed in the pores is emptied in a stepwise manner, i.e. the film thickness on the pore walls (t) decreases as desorption occurs. It also assumed that the pores are rigid and of uniform shape, the pore size is restricted to the mesopore range, there is no pore blocking effects and the meniscus shape is controlled by the pore size and shape [99]. In straight, open-ended pores, r_m is related to the two primary radii r_1 and r_2 by;

$$\frac{1}{r_m} = \frac{1}{2}\left(\frac{1}{r_1} + \frac{1}{r_2}\right)$$ (B.4)

When the pores are emptying $r_m = r_1 = r_2$ and there is also a film of thickness, t on the pore walls which is expressed by Halsey's equation as;

$$t = 2.98\left[\frac{-5.00}{\ln\left(\frac{p}{p_o}\right)}\right]^{1/3}$$ (B.5)

where 2.98 is the thickness of one adsorbed layer of argon at 87.5 K and 5.00 is an empirical constant. Then substituting r_m with $(r-t)$ in Eqn. (B.3);

$$\ln\left(\frac{p^*}{p_o}\right) = -\left(\frac{2\gamma\varpi\cos\theta}{RT(r-t)}\right)$$ (B.6)

for the desorption branch. Desorption branch is preferred for calculation of pore size distribution if pore blocking effects are absent [99]. Then the volume desorbed from the adsorbent at decreasing relative pressures is converted to equivalent liquid volumes, since it was assumed that desorption occurs from the pores filled with liquid rather than gas. Then the BJH Model was used to calculate the incremental pore volume versus pore size intervals.

Pore size distribution information in the micropore region is obtained by the application of Dubinin-Astakhov (D-A) and Horvath-Kawazoe micropore models. D-A Model is expressed as:

$$W = W_o \exp\left[-\left(\frac{A}{\psi E_a}\right)^n\right] \tag{B.7}$$

where W is the quantity adsorbed at relative pressure p/p_o, W_o is the limiting micropore volume, E_a is the characteristic energy of adsorption for the reference vapour (benzene), ψ is the affinity coefficient and A is the adsorption potential. The value of n is selected to give the best linear regression fit and has a value usually between 1 and 3 and often near 2.

Hovarth-Kawazoe (H-K) method assumes that either micropores are full or empty according to type pressure of the adsorptive is greater or less than the value characteristic of a particular micropore size. Also assumed that the adsorbed phase behaves thermodynamically as a two dimensional ideal gas. The H-K method is based on the model of Everett and Powel which describes the potential energy of a single molecule between two parallel planes off atoms of graphitized carbon. The final form of the H-K equation is:

$$RT \ln\left(\frac{p}{p_o}\right) = N_A \left[\frac{(N_a A_a + N_{aa} A_{aa})}{\xi^4 (1-d)}\right] x$$
$$\left[\frac{\xi^4}{3(l-d/2)^3} - \frac{\xi^{10}}{9(l-d/2)^9} - \frac{\xi^4}{3(d/2)^3} + \frac{\xi^{10}}{9(d/2)^9}\right] \tag{B.8}$$

where ξ is the distance from a surface atom at zero interaction energy, N_A is the Avogadro number, $RTln(p/p_o)$ is the free energy change, l is the slit width, d is the diameter of the adsorbate molecule, N_a is the number of atoms per unit area of adsorbent, N_{aa} is the number of molecules per unit area of adsorbate, A_a and A_{aa} are constants in Lennard-Jones potential for the adsorbent and adsorbate, respectively.

APPENDIX C

Density Measurements

Various porosities were calculated from the bulk and apparent densities of the zeolite sample in this study.

In order to determine the wet and dry (bulk and apparent) densities of clinoptilolite, a specimen of rectangular prism in shape was cut. The volume of the specimen was calculated as 4.714 cm^3 ($V_{specimen}$). The specimen was placed was kept in the oven at 400°C for 24 hours and kept in a desiccator to cool down. After the weight was recorded as m_{dry}, the specimen was immerged in deionized water and vacuumed at -500 mmHg at room temperature until the exit of air bubbles stopped and dried with a tissue. The weight was recorded as m_{wet}. Knowing the volume of the specimen, the dry (ρ_{dry}) and wet (ρ_{wet}) densities of the clinoptilolite were calculated as follows:

$$\rho_{dry} = \frac{m_{dry}}{V_{specimen}} = \frac{5.26g}{4.714cm^3} = 1.240 \text{ g/cm}^3 \qquad \rho_{wet} = \frac{m_{wet}}{V_{specimen}} = \frac{7.08g}{4.714cm^3} = 1.502 \text{ g/cm}^3$$

Then, the bed voidage (ε) was calculated from the known dry clinoptilolite density and dry weight of the packed clinoptilolite regarding regeneration of the clinoptilolite before adsorption experiments as follows:

Volume of clinoptilolite packed into the column:

$$V_{\text{packed clinoptilolite}} \colon \frac{m_{packed\ clinoptilolite}}{\rho_{dry}} = \frac{1.389\ g}{1.240\ g/cm^3} = 1.120 \text{ cm}^3$$

$$\varepsilon\ \colon \text{Bed Porosity:} \frac{V_{column} - V_{packed\ clinoptildite}}{V_{column}} * 100 = \frac{1.661 - 1.120}{1.661} * 100 = 32.57\%$$

REFERENCES

1. Giddings, J.C., Chemistry, Man, and Environmental Change, Canfield, San Francisco, 1973.

2. Masters, G.M., Introduction to Environmental Engineering and Science, 2nd Edition, Prentice –Hall International Inc., USA, 1998.

3. Commoner, B., Making Peace with the Planet, New York, Pantheon, 1990.

4. Medical and Biological Effects of Environmental Pollutants–Carbon Monoxide, National Academy of Sciences, Washington, D. C., 1977.

5. Peavy, H.S., Rowe, D.R. and Tchobanoglous, G., Environmental Engineering, McGraw Hill, Singapore, 1995.

6. Decision Analysis Corporation, Measurement of Emissions: Greenhouse Gas Estimates for Alternative Transportation Fuels, unpublished final report prepared for the Energy Information Administration, Vienna, VA, December 1995.

7. Council of Environmental Quality: Twelfth Annual Report of the Council on Environmental Quality, Washington, D. C., 1982.

8. Multinational Monitor, Vol. 20, No.6, June 1999.

9. Bulletin on Green House Gases by State Institute of Statistics, 04.04.1999.

10. http://www.eia.doe.gov/cabs/turkey.html

11. Müezzioğlu, A., Hava Kirliliğinin ve Kontrolünün Esasları, Dokuz Eylül Üniversitesi, 1987.

12. Coe, C.G., Separation of Gases by Zeolites, Gas Separation Technology, Edited by E.F. Vansant and R. Dewolfs, Elsevier Science Publishers B.V., Amsterdam, 1990.

13. Breck, D. W. Zeolite Molecular Sieves, Wiley- Interscience, New York, 1974.

14. http://www.amzorb.com/uses.html

15. Dyer, ·A., An Introduction to Zeolite Molecular Sieves, John Wiley and Sons, Chichester, 1988.

16. Neuhoff, P. S. and Bird, D. K., Method of Characteristics Algorithms for Estimation of Apparent Standard Molar Thermodynamic Properties for Rock-Forming Zeolites, Department of Geological and Environmental Sciences, Stanford University, http://pangea.stanford.edu/~neuhoff/phil-agu97.html

17. Özkan, F., Ülkü, S., Amabalaj sanayinde nem tutucu olarak doğal zeolitlerin kullanılması, Ulusal Ambalaj Teknolojisi ve Yan Sanayi Kongresi ve Sergisi, p. 278, 1988.

18. Sirkecioğlu, A., Esenli, F., Kumbasar, I., Eren, R. H., Erdem - Şenatalar, A., Mineralogical and Chemical Properties of Bigadiç Clinoptilolite, Proc. International Earth Science Congress on Aegean Regions (IESCA), 1-6 Ekim 1990, Izmir, M.Y. Savascin, A.H. Eronat (ed.), Vol.1, 291-301, 1991.

19. Sirkecioğlu, A., Bigadiç Klinoptilolit Rezervinin NH_4^+ Değişimi ve CO_2 Adsorpsiyonu Yardımıyla Karakterizasyonu, Doktora Tezi, İTÜ, İstanbul, 1994.

20. Erdem-Şenatalar, A., Sirkecioğlu, A., Güray, I., Esenli, F., Kumbasar, I., "Characterization of the Clinoptilolite-rich Tuffs of Bigadic: Variation of the Ion-Exchange Capacity with Pretreatments and Zeolite Content" Proc. of the 9th International Zeolite Conference, 5-10 Temmuz 1992, Montreal, Kanada, R. von Ballmoos, J.B. Higgins, M.M.J. Treacy (ed.), Butterworth-Heinemann Ltd., Vol.2, 223-231,1993.

21. Gündoğdu, M.N., Ph.D. Thesis, Hacettepe Univ., Ankara, 1982; Göktekin, A., Istanbul Tech. Univ., YBYK-UYG-AR Projesi, 1989.

22. Tsitsishvili, G.V., Andronikashvili, T.G. and Kirov, G.N., Natural Zeolites, Ellis Horwood Limited, 1st Edition, New York, p.40, 1992.

23. Tsitsishvili, G.V. and Andronikashili, T.G., J. Chromatography, 58, 39, 1971.

24. Ackley, M.W., Giese, R.F., Yang, R.T., Zeolites, 12, 780, 1992.

25. Barrer, R.M. and Coughlan, B., Molecular Sieves, The Society of Chemical Industry, London, 141, 1968.

26. Smith, J.V., in J. A. Rabo (Editor), Zeolite, Chemistry and Catalysis, American Chemical Society, Washington, DC, 69, 1976.

27. Barrer, R.M., in F. Ramoa-Ribeiro, A. E. Rodrigues, L. Deane Rollmann and C. Naccache (Editors), Zeolites: Science and Technology, Martinus Nijhorf, The Hague, p. 227, 1984.

28. Barrer, R.M., J. Colloid Interface Science, 21, 415, 1966.

29. Gottardi, G. and Galli, E., Natural Zeolites, Springer-Verlag, Berlin, 1985.

30. Ackley, M.W. and Yang, R.T., Diffusion in Ion Exchanged Clinoptilolites, AIChE J.,Vol. 37, No. 11, 1645-1656, 1991.

31. Barrer, R.M., Hydrothermal Chemistry of Zeolites, Academic Press, London, 1982.

32. White, D.A. and Bussey, R.L., "Water sorption properties of modified clinoptilolite", Separation and Purification Technology, 11, 137-141, 1997.

33. Babaev, I.S., Rajabli, S.B. and Aliev, T. B., Technical Progress, 6, 45, 1976.

34. Babaev, I.S., Kasumova, S.M., Aliev, T.B. and Akhmedov, M. A., Proc. Az. Res. Inst. Water Problems, 8, 83, 1979.

35. Aliev, T. B. and Schvartzman, N. D., Proc. Az. Res. Inst. Water Problems, 8, 96, 1979.

36. Tarasevich, Y.I., Rudenko, G.G., Kravchenko, V.A. and Polyakov, V.E., Chem. and Techn. Water, 1, 66, 1979.

37. http://www.roskill.co.uk/zeolites.html

38. Kärger, J. and Ruthven, Ð.M., Diffusion in Zeolites and other Microporous Solids, John Wiley & Sons, New York, 1992.

39. Ruthven, D.M., Principles of Adsorption and Adsorption Processes, John Wiley and Sons, New York, 1984.

40. Haynes, Jr.,H. W. and Sarma, P.N., AIChE J., 19, 1043, 1973

41. Hyun, S.H. and Danner, R.P., Ind. Eng. Chem. Fundam., 24, 95, 1985.

42. Sarma, P.N. and Haynes, Jr.,H.W., Application of Gas Chromatography to measurements of Diffusion in Zeolites, Adv. Chem. Ser., 133, 205, 1974.

43. Hufton, J.R., Diffusion and Equilibrium of Alkanes on Silicalite Determined by Perturbation Chromatography, The Pennsylvania State University, Ph.D.Thesis, 1992.

44. Cunningham, R.E. and Williams, R.J.J., Diffusion in Gases and Porous Media, Plenum Press, New York, 1980.

45. Chapman, S. and Cowling, T.G., The Mathematical Theory of Non-Uniform Gases, 3rd Edition, Cambridge University Press, 1970.

46. Ranz, W. E. and Marshall, W. R., Chem. Eng. Prog. , 43, 173, 1952.

47. Deemter van, J. J., Zuiderweg, F. J. and Klinkenberg, A., Chem. Eng. Sci., 5, 271, 1956.

48. Kucera, E., J. Chromatogr., 19, 237, 1965.

49. Kubin, M., Collection Czech. Chem. Commun., 30, 1104, 1965.

50. Cerro, R.L. and Smith, J.M., AIChE. J., 16, 1035, 1970.

51. Ma, Y.H. and Mancel, C., Diffusion Studies of CO_2, NO, NO_2 and SO_2 on Molecular Sieve Zeolites by Gas Chromatography, AIChE J., Vol. 18, No. 6, 1972.

52. Van der Vlist, E. and Van der Meijden, J., Determination of the Adsorption Isotherms of the Components of Binary Gas Mixtures by Gas Chromatography, J. Chromatography, 79, 1-13, 1973.

53. Martin, A.J.P. and Syinge, R.L.M., Biochem. J., 35, 1358, 1941.

54. Haydel, J. J. and Kobayashi, R., Ind. Eng. Chem. Fundam., 6, 546, 1967.

55. Shah, D.B. and Ruthven, D.M., Measurement of Zeolitic Diffusivities and Equilibrium Isotherms by Chromatography, AIChE. J., Vol.23, No. 6, 1977.

56. Chihara, K., Suzuki, M. and Kawazoe, K., AIChE J., 24, 237, 1978.

57. Ruthven, D.M. and Kumar, R., Can. J. Chem. Eng., 57, 342, 1979.

58. Hsu, L.K.P. and Haynes, H.W. Jr., AIChE J., 27, 81, 1981.

59. Haynes, H.W.Jr., Chem. Eng. Sci., Vol. 30, 995-961, 1975.

60. Ruthven, D.M., Sorption of oxygen, nitrogen, carbon monoxide, methane, and binary mixtures of these gases in a 5A molecular sieve, AIChE J., 22, 753-759, 1976.

61. Hashimoto, N. and Smith, J. M., Ind. Eng. Chem. Fundam., 12, 353, 1973.

62. Ruthven, D.M. adn Kumar, R., Ind. Eng. Chem. Fundam., 19, 27-32, 1980.

63. Harper, R.J., Stifel, G.R. and Anderson, R.B., Adsorption of gases on 4A synthetic zeolite, Can. J. Chem., 47, 4661-4669, 1969.

64. Haq, N. and Ruthven, D.M. Chromatographic study of sorption and diffusion in 5A zeolite, J. Coll. Interface Sci., 112, 154-163, 1986a.

65. Haq, N. and Ruthven, D.M. Chromatographic study of sorption and diffusion in 4A zeolite, J. Coll. Interface Sci., 112, 164-169, 1986b.

66. Esenli, F. and Kumbasar, I., Thermal behaviour of Heulandites and clinoptilolites of Western Anatolian, Zeolite and Related Microporous Materials: State of the Art 1994, Studies in Surface Science and Catalysis, Weitkamp, J., Karge, H. G., Pfeifer, H., Hölderich, W. (Eds.), Elsevier Science, B.V., Vol. 84, 1994.

67. Özkan, F. and Ülkü, S., Enerji Depolama Sistemlerinde Yerel Doğal Zeolit Mineralinin (Klinoptilolit) Kullanılması, ULIBTK'97 11.Ulusal Isı Bilimi ve Tekniği Kongresi, Edirne, 17-19 Eylül 1997.

68. Altav, Y., Sirkecioğlu, A. and Erdem-Şenatalar, A., 1.Ulusal Kimya Mühendisliği Kongresi, ODTÜ, Ankara, 13-16 Eylül 1994.

69. Tezel, F.H. and Apolonatos, G., Chromatographic study of adsorption for CO, CH_4, and N_2 in molecular sieve zeolites, Gas Sep. Purif., 7, 11-17, 1993.

70. Triebe, R.W. and Tezel, F.H., Adsorption of Nitrogen, Carbon Monoxide, Carbon Dioxide and Nitric Oxide on Molecular Sieves, Gas Separation and Purification, 9, No. 4, 223-230, 1995a.

71. Triebe, R.W. and Tezel, F.H., Adsorption of Nitrogen and Carbon Monoxide on Clinoptilolite: Determination and Prediction of Pure and Binary Isotherms, Canadian Journal of Chemical Engineering, 73, 717-724, 1995b.

72. Emesh, I.T.A. and Gay, I.D., Adsorption and [13]C N.M.R. studies of ethene, ethane and carbon monoxide on Zn- and Cd-exchanged A Zeolites, J. Chem. Tech. Biotechnol. 35A, 115-120, 1985.

73. Ackley, M.W. and Yang, R.T., Ind. Eng. Chem. Res., 30, 2523-2530, 1991.

74. Sirkecioğlu, A., Altav, Y., Erdem-Şenatalar, A., Adsorption of H_2S and SO_2 on Bigadiç Clinoptilolite, Separation Science and Technology, 30, 13, 2747-2762, 1995.

75. Triebe, R.W., Tezel, F.H., Erdem - Şenatalar, A. and Sirkecioglu, A., Promising Air Purifications on Clinoptilolite, Zeolite Science 1994: Recent Progress and Discussions Studies Surface Science and Catalysis, Vol. 98, 1993.

76. Rukenstein, E., Vaidyanathan, A.S., Youngquist, G.R., Sorption by Solids with Bidisperse Pore Structures, Chem. Eng. Sci., 26, 1305, 1971.

77. Rakic, V.M., Hercigonja, R.V. and Dondur, V.T. (CO Interaction with Zeolites studied by TPD and FTIR: Transition-metal Ion-exchanged FAU-type Zeolites, Microporous and Mesoporous Materials, 27, 27-39, 1999).

78. Kamble, V.S., Gupta, N. M., Kartha, V.B., Iyer, R. M., J. Chem. Soc., Faraday Trans. 89, p. 1143, 1993.

79. Rao, C.N.R., Chemical Applications of Infrared Spectroscopy, Academic Press, New York, 1963.

80. Webb, P.A. and Orr, C., Analytical Methods in Fine Particle Technology, Micromeritics Instrument Corporation, Norcross, GA, USA, 1997.

81. Katz, E., Quantitative Analysis Using Chromatographic Techniques, Separation Science Series, John Wiley and Sons, Chichester, 1988.

82. Tsitsishvili, G.V., Andronikashvili, T.G., Sabelashvili, Sh.D. and Osipova, N.A., J. Chromatogr., 130, 13, 1977.

83. Tsitsishvili, G.V., Andronikashvili, T.G., Sabelashvili, Sh.D. and Osipova, N.A., in Sand, L. B. and Mumpton, F. A. (Editors), Natural Zeolites, Occurence, Properties, Uses, Pergamon Press, Oxford, p. 379, 1978.

84. Tezel, F.H., Tezel, H.O. and Ruthven, D.M., Determination of Pure and Binary Isotherms for Nitrogen and Krypton, Journal of Colloid and Interface Science, Vol. 149, No.1, March 1, 1992.

85. Farooq, S., Sorption and Diffusion of Oxygen and Nitrogen in Molecular Sieve RS-10, Gas Sep. Purif., Vol. 9, No. 3, 205-212, 1995.

86. Ülkü, S., Balköse, D., Baltacıoğlu, H., Özkan, K. and Yıdırım, A., Natural Zeolites in Air Drying, Drying Technology, 10, 2, 475-490, 1992.

87. Arcoya, A., Gonzalez, J.A., Llarbe, G., Seone, X.L., Travesio, N., Role of the Countercations on the Molecular Sieve Properties of a Clinoptilolite, Microporous Materials, 7, 1-13, 1996.

88. Flanigen, E.M., Khatami, H., Seymenski, H.A., in E. M. Flanigen, L. B. Sands (Eds.), Advances in Chemistry Series 101, American Chemical Society, Washington, DC, 201-228, 1971.

89. Bertsch, L. and Habgood, H.W., J. Phys. Chem., 37, 1621, 1963)

90. Rodriguez-Fuentes, G., Ruiz-Salvador, A. R., Mir, M., Picazo, O., Quintana, G., Delgado, M., Microporous and Mesoporous Materials, 20, 269-281, 1998.

91. Bish, D. L., Occurrence, Properties and Utilization of Natural Zeolites, 585, 1988.

92. Knowlton, G.D. and White, T.R., Thermal Study of Types of Water associated with Clinoptilolite, Clays and Clay Minerals, Vol. 29, No. 5, 403-411, 1981.

93. Meier, W.M., Proc. 7th Int. Zeolite Conf. Tokyo, 13, 1968.

94. Barrer, R.M. and White, E.A.D., J. Chem. Soc.: 1561, 1952.

95. Milton, R.M., U.S. Pat., 2, 996, 358, 1961.

96. Hirschfelder, J., Gurtiss, C.F., Bird, R.B., Molecular Theory of Gases and Liquids, Wiley, New York, 1954.

97. Sing, K.S.W., Everett, D.H., Haul, R.A.W., Moscou, L., Pierotti, R. A., Rouquérol, J., Siemieniewska, T., Reporting Physisorption Data for Gas/ Solid Systems with Special Reference to the Determination of Surface Area and Porosity, Pure and Appl. Chem., Vol. 57, No. 4, 603-619, 1985.

98. Lowell, S. and Shields, J. E., Powder Surface Area and Porosity, Chapman & Hall, 3rd Edition, London, 1991.

99. Sing, K.S.W., Adsorption, Surface Area and Porosity, Academic Press, London, 1982.

100. Sheikh, M.A.,Hassan, M.M., and Loughlin, K.F., Adsorption equilibria and rate parameters for nitrogen and methane on Maxsorb activated carbon, Gas Sep. Purif., Vol.10, No.3, 161-168, 1996.

101. Carleton, F.B., Kershenbaum, L.S. and Wakeham, W.A.,Chem.Eng.Sci.,33,1239, 1978.

102. Lapidus, L. and Amundson, N. R., J. Phys. Chem. , 56, 984, 1952.

103. Ülkü, S., Mobedi, M., Adsorption in Energy Storage, Energy Storage, Kluwer Academic Pub.,167, 487-507, 1989.

104. Ülkü, S., Mobedi, M., Zeolites in Heat Recovery, Studies in Surface-Science and Catalysis Zeolites, Elsevier Science Pub.,49, 511-518, 1989.

105. Ülkü, S., Çakıcıoğlu, F., Energy Recovery in Drying Applications, Int. J. Renewable Energy, 1, 5/6, 695-698, 1991.

106. http://www.malvern.co.uk/Laboratory/laser.htm